Development of a MEMS Device for the Determination of Cell Mechanics

by

Rachael Schwartz

Submitted in partial fulfilment of the requirements
for the degree of Master of Applied Science

at

Dalhousie University
Halifax, Nova Scotia
November 2012

DALHOUSIE UNIVERSITY

DEPARTMENT OF MECHANICAL ENGINEERING

The undersigned hereby certify that they have read and recommend to the Faculty of Graduate Studies for acceptance a thesis entitled “Development of a MEMS Device for the Determination of Cell Mechanics” by Rachael Schwartz in partial fulfilment of the requirements for the degree of Master of Applied Science.

Dated: November 26, 2012

Supervisor: _____

Readers: _____

_____

_____

DALHOUSIE UNIVERSITY

DATE: November 26, 2012

AUTHOR: Rachael Schwartz

TITLE: Development of a MEMS Device for the Determination of Cell Mechanics

DEPARTMENT OR SCHOOL: Department of Mechanical Engineering

DEGREE: MASc CONVOCATION: May YEAR: 2013

_____

Signature of Author

Table of Contents

List of Tables

List of Figures

Abstract

Cell mechanics are directly related to the biological functionality of a cell, and therefore have been extensively studied. Current understanding of the unique relationships associated with mechanical loading conditions and the biological outcomes of a cell is far from complete [1].

The main objective of this thesis work was the design of a device capable of determining mechanical properties including stiffness and Young's modulus of a biological cell. The device was implemented using micro-electro mechanical systems technology (MEMS), and the cell testing was limited to yeast cells for the purpose of this research.

The design consisted of a micro-gripper which performed controlled cell squeezing with a spring of known stiffness. Differential displacements were obtained allowing for the calculation of cell mechanical properties. The incorporation of spatially periodic structures on the moving components of the gripper enabled measurements with 10 nm precision based on discrete Fourier transformation and phase [2].

The operation of the initial design was negatively affected by stiction, and therefore modified and enhanced for the next fabrication iteration. Four yeast cells were successfully tested, with their stiffnesses ranging from 7 - 19 μN/μm, and with Young's moduli ranging from 14 - 41 MPa.

The device designed for this work has a higher functional range for force application than most previously reported techniques. The gripper contact area is between what is achieved with atomic force microscopy, and micro-plate compression techniques. The device was used to measure displacements in the 0.2 – 3 μm range, and cell compression forces in the 1 to 100 μN range

This work has established a starting point for future investigation in the Dalhousie MEMS Research Group. Furthermore, this work adds to the literature base for the measurement of whole cell mechanical properties, as the majority of yeast cell testing studies have been performed using nano-indentation.

List of Symbols and Abbreviations Used

1D	1 Dimensional
2D	2 Dimensional
3D	3 Dimensional
∅	Diameter
A	Area
AFM	Atomic Force Microscopy
BSAC	University of California's Berkley Sensors and Actuators Center
CC	Cell Comb
CMC	Canadian Microsystems Corporation
CS2	Cell Squeezer 2
CS4	Cell Squeezer 4
d	Chevron Height
DFT	Discrete Fourier Transform
F	Force
FFT	Fast Fourier Transform

IC	Input Comb
K	Stiffness
L	Beam Length
MEMS	Micro Electrical Mechanical Systems
MUMPs	Multi-User MEMS Processes
ROI	Region of Interest
T	Temperature
X	Displacement
y	Displacement of Chevron Center Point
α	Coefficient of Thermal Expansion
σ	Stress
ϵ	Strain

Acknowledgements

First and foremost, I would like to acknowledge and thank Marek Kujath. His encouragement and support in my senior year of engineering greatly influenced my decision to pursue a Master's degree. His ability to identify the wonder and beauty associated with science has touched me.

I would like to thank Ted Hubbard for his sincere and tireless guidance. He has been an invaluable mentor.

My parents; I cannot thank them enough. I was encouraged from an early age to make discoveries, think critically, and love learning. The endless love and support of my family has made this adventure possible.

Finally, many thanks, and much love to Dylan.

Chapter 1: Introduction

1.1 Objective

The main goals of this thesis work are the design of a device capable of determining cell mechanical properties such as stiffness and Young's modulus and the testing and advancement of the device.

1.2 Scope

The test device will be implemented using Micro-Electro Mechanical Systems (MEMS) technology, and cell testing will be performed on yeast cells.

A micro-gripping device will be designed to perform controlled cell squeezing with a spring of designed stiffness. The cell stiffness will be calculated using differential displacements obtained using a displacement measurement technique with resolution on the order of tens of nanometers.

This technique will have a functional range which is complementary to existing techniques. The contact area and the cell deformations achieved will lie between what is achieved with existing techniques. Therefore; the mechanical properties measured are expected to be between the experimentally determined properties from existing methods (nanoindentation techniques and micro-plate compression).

1.3 Background on MEMS

MEMS devices are some of the smallest functional machines engineered by humans [3], with features on the order of microns, and thicknesses measuring from 2 to 25 μm. MEMS technologies are derived from those of the micro-electronics industry. Sensors and actuators can be combined with measurement, control, and signal conditioning systems, all within a space not much larger than a quarter [3].

The uses of MEMS technology are wide spread, spanning the fields of aerospace and defence, medical and biomedical, optical communications, and consumer electronics. The importance of MEMS in the field of life science is growing rapidly with the potential for lab-on-a-chip technologies, minimally invasive operating and diagnostic tools, and in vivo monitoring [3]. MEMS have been integrated into eye surgery, dialysis, and patient monitoring systems.

1.3.1 Multi-User MEMS Processes

The Multi-User MEMS Processes, or MUMPs®, is a commercial program providing industry, universities, and government programs access to cost-effective, proof of concept MEMS fabrication worldwide [4]. MEMSCAP offers a standard processes, PolyMUMPs™, which is a three layer polysilicon micromachining process. Devices fabricated for this thesis work were made using the PolyMUMPs™ process.

1.3.2 PolyMUMPs™

The PolyMUMPs process was derived from work performed at the Berkeley Sensors and Actuators Center (BSAC) in the late 80s and early 90s [4]. The flexibility and versatility of the process has since been increased by modifications and enhancements.

The process begins with a silicon wafer. A silicon nitride layer is deposited as an electrical isolation layer. The two mechanical layers (Poly 1 and Poly 2, or P1 and P2) are comprised of polysilicon, and interlaced with layers of phosphosilicate glass film that are used for the sacrificial layers (Oxide 1 and Oxide 2, or Ox1 and Ox2). See Figure 1.3.1 for a cross section of the available layers in the PolyMUMPs process. The polysilicon layers (P1 and P2) are patterned by photolithography, and then etched in a plasma system. The sacrificial layers of phosphosilicate glass (Ox1 and Ox2) are removed at the end of the process to free the mechanical layers of polysilicon. This process has dimensional tolerance of approximately 200 nm. Detailed process steps are presented graphically in Appendix A [4] .

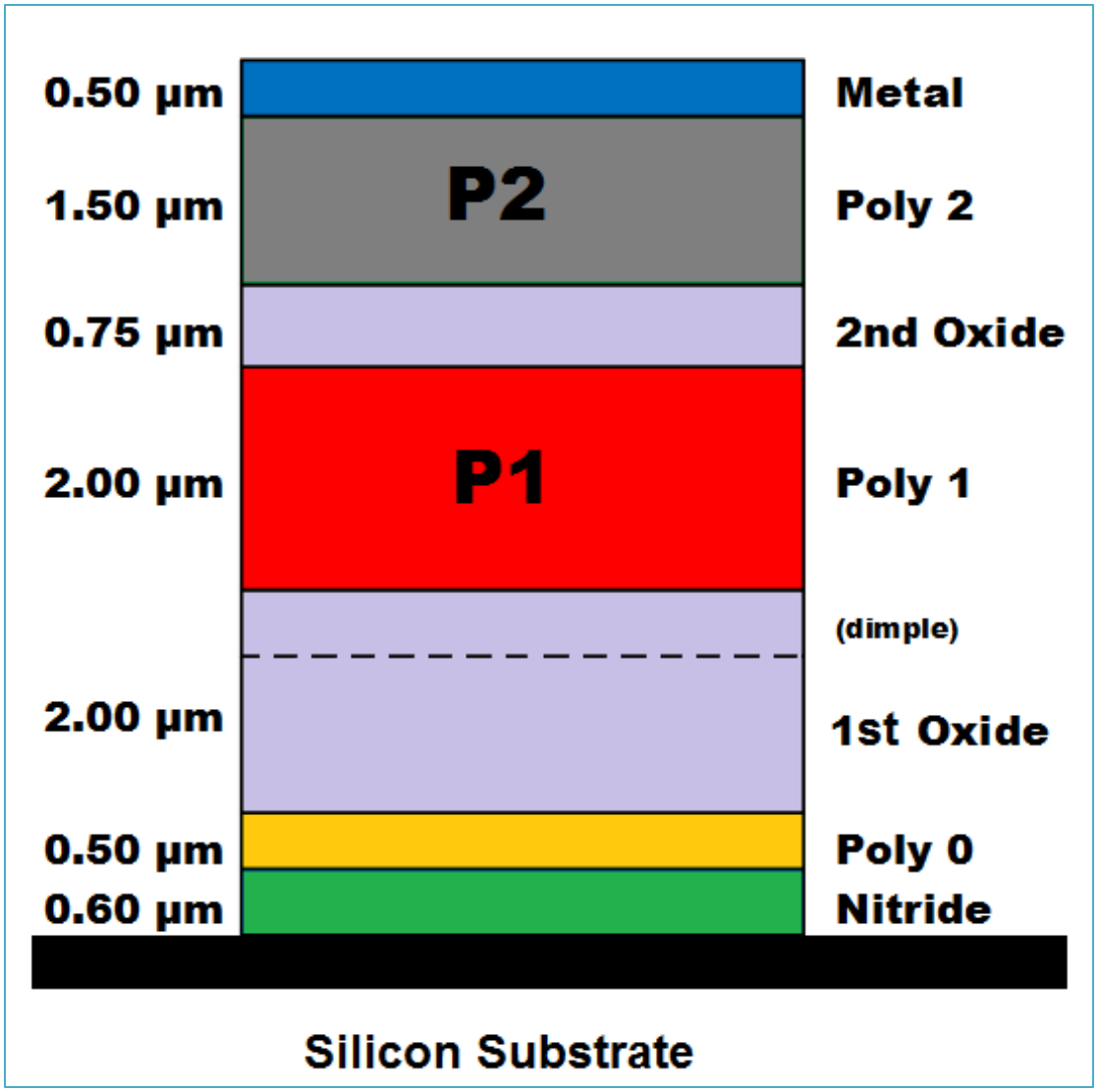

Figure 1.3.1: PolyMUMPs Layers Label (Note Structural Layers P1 and P2)

1.4 Why Use MEMS for Measurement of Cell Mechanics?

The aim of the following section is to explore how MEMS devices can advance the understanding of cellular mechanics. Existing techniques such as atomic force microscopy (AFM), micropipette aspiration, optical and laser trapping, and magnetic twisting cytometry (which will be described later) can exert forces on the order of femtonewtons, but generally cannot exert forces beyond a few

micronewtons [5]. The range of forces and displacements which can be achieved with MEMS devices is complementary to existing techniques. The force range for MEMS-based systems spans from 100s of nN to 100 μN, beyond the range which is possible with commonly used magnetic and optical tweezers, and most atomic force microscopy probes. The exploration of cell behaviour in response to higher forces in addition to the individual molecular forces previously characterized, will lead to a more complete understanding of cell mechanics.

Many MEMS measurement devices are based on compliant beam designs, incorporating micro-scale pillars, probes, and pullers. These devices are used in combination with optical microscopy to observe the beam deflection [5].

MEMS test apparatus lend themselves well to simulation, with well-defined loading and deformation techniques. These devices also naturally accommodate cellular and sub-cellular level mechanical testing [5]. MEMS devices are excellent interfaces between macro-scale tools, and micro or nano-scale biological systems.

Loh et al [5] have two particularly relevant statements that apply to the work presented here:

> "While promising, the application of MEMS to cell mechanics is relatively new. Accordingly, (cell testing) devices incorporating combinations of multiple MEMS sensors and actuators have yet to be demonstrated." [5]

“MEMS will clearly not replace existing techniques which already exhibit extremely fine force and displacement resolutions. However, the use of self-sensing, self-actuating MEMS devices will reduce reliance on external equipment, allowing conditions to be optimized for imaging cellular response.” [5]

These statements are relevant as this work will incorporate MEMS actuators, with optical displacement measurement systems, leading to the further integration of multiple actuators and sensors creating lab-on-chip devices. The devices developed for this work will allow testing complementary to that which has already been performed by allowing larger forces (up to 100μN) to be exerted on the specimen.

1.5 Stiction Problems with MEMS

Although relatively minor at the macro scale, at the micro scale stiction forces can be catastrophic. Stiction can cause adhesion between the surfaces of MEMS components, causing them to fail completely.

Stiction is often referred to in the literature as a short term for static friction. It is now, however, widely accepted that the correct definition of stiction is adhesion between two surfaces [6]. Stiction is a force which not only resists relative motion in addition to friction, but can actually increase the normal forces between surfaces, and in turn frictional forces [6]. These forces can be upwards of 100 μN depending on the specific device.

There are two types of stiction; in-use stiction, and fabrication stiction. In-use stiction is the result of four major adhesion mechanisms; capillary forces, Van der

Waals forces, hydrogen bridging, and electrostatic forces [6]. Fabrication stiction results from the use of wet etchants, and is a major failure mode. The evaporation of the wet etchant between two surfaces can draw them together causing them to permanently adhere.

In order to develop a measurement tool, the effect of stiction on the design must be minimised. It is expected that this will be a significant hurdle to overcome.

Dimples (see figure Figure 1.5.1) are used to prevent stiction during use by reducing the contact area between the device and the substrate. They therefore prevent the device from adhering to the substrate when the oxide release is performed as part of the fabrication process.

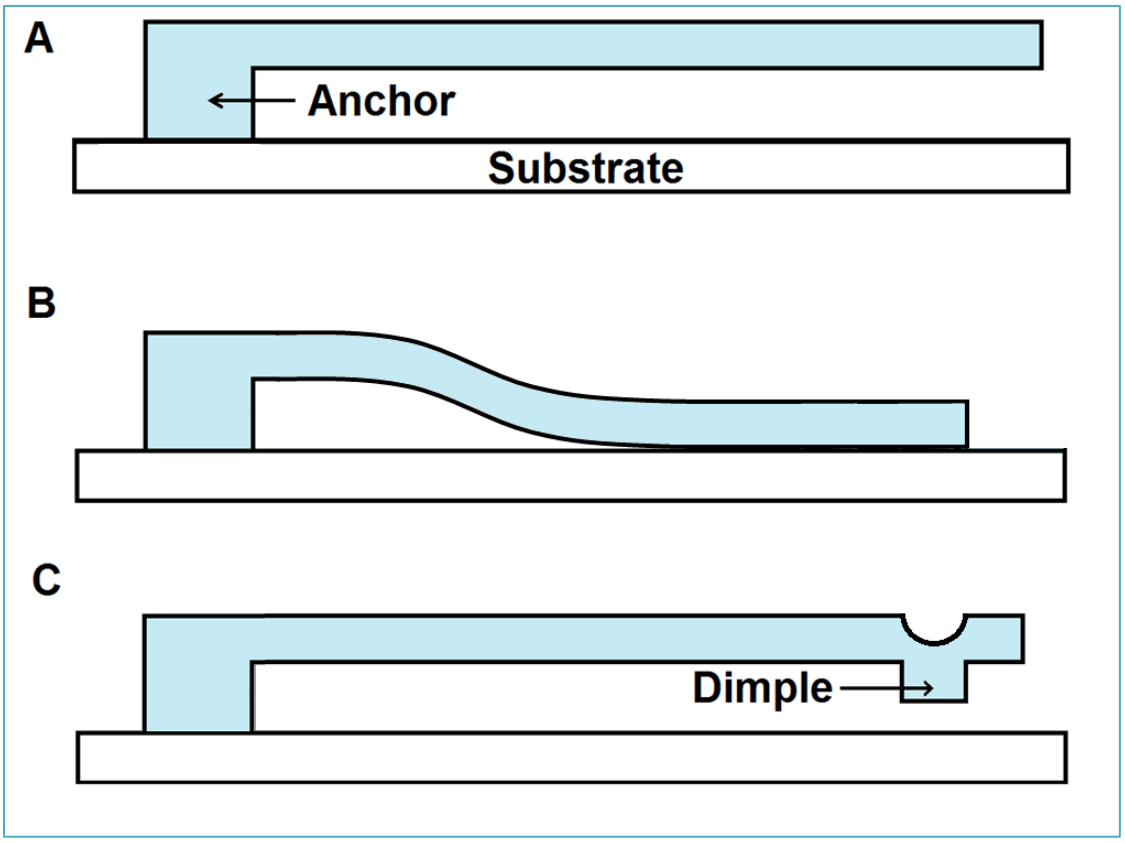

Figure 1.5.1: A- Simple Cantilevered MEMS Structure, B- Simple Structure Affected by Stiction, C- Incorporation of a Dimple to Prevent Stiction

Dimples are formed by partially etching the underlying sacrificial layer. This causes the structural layer deposited after this to be contoured to the etched indentation. Figure 1.5.1 presents a schematic of a simple cantilevered structure, illustrating the effect of stiction, and the incorporation of a dimple to reduce stiction.

1.6 Single Cell Manipulation

Single cell manipulation is well established, and commonly performed using glass capillary micropipettes. Negative pressure is applied to the capillary tube, controlling the aspiration of a desired cell while positive pressure dispenses the cell [7]. Micro-motion stages with multiple degrees of freedom are used to manually manipulate the micropipette and control its tip position with accuracy for micromanipulation or injection. Single cell manipulation by micropipette has been demonstrated to be reliable, but time consuming, labour intensive, and unsuitable for processing large numbers of single cells [7]. As the cell testing required for this work is as a proof of concept, processing of large number of single cells is not required. This means costly, automated systems for cell manipulation can be avoided. There are commercial options available including the Quixell, and TransferMan NK 2. The Quixell system allows for some degree of automation, by programming transfer destinations [7]. Other techniques exist for cell manipulation, such as optical trapping and acoustic wave manipulation, but dissipated power can potentially influence or damage biological material [8].

In order to perform cell testing, either the device has to move to the site of the cell, or the cell needs to be moved to the device. To reduce the complexity of the

device design, it was decided to use micropipette manipulation to move the cell to the test site.

1.7 MEMS in Aquatic Environments

To avoid the design challenges and time consuming testing associated with aquatic MEMS devices, for the purposes of this research, testing was performed on a dry chip. Nonetheless, implementation of an aquatic test environment will be addressed as following iterations will incorporate aqueous testing.

For aquatic designs, one has to consider the unique problems associated with underwater MEMS actuation. For example, there are large thermal losses to the surroundings as water has a thermal conductivity of about 20 times that of air [9]. This means that far more power is require to heat a structure underwater, than in air. A COMSOL simulation indicates that the jaw of the gripper design would see only a modest increase in temperature (10 - 20ºC) in air. This temperature would be greatly reduced in water, resulting in conditions appropriate for yeast cells.

Surface tension presents such complications that it was concluded that only complete submersion would eliminate stiction, and allow reasonable actuation [9]. It was experientially determined that water with dissolved materials left a film on the chip following evaporation, which was problematic when re-using devices. The residue of the dissolve materials caused devices to stick and sometimes the film could not be readily dissolved [9]. This means that distilled or deionised water, free of ions and therefore most impurities would prevent stiction due to film

buildup. Unfortunately, in order to maintain a ‘cell friendly’ testing environment, altering the ion composition is not suggested. This can cause cell lysis, resulting from interactions of solution ions with ions in the cell membrane [10].

Now having discussed the objective, scope and some background relating to this work, the following section will provide more detailed background relating to cellular mechanics.

Chapter 2: Cell Mechanics

Although this is a Mechanical Engineering thesis, the interdisciplinary nature of this work means that explanation of the associated cell biology, and existing tools for the measurement of cell mechanical properties is required. This chapter will provide a background on cell mechanobiology, and test apparatus currently used to determine cell mechanical properties. Furthermore, as testing will be performed on yeast cells, a section concerning yeast cytology will be presented.

Within the past decade, cellular investigations have been mainly focused on chemical and topographical properties such as cellular response to chemical signals, varied surface interface chemistry, and surface topography. Mechanical properties of cells have been less researched [11]. 'Cellular mechanobiology' is the study of the role of mechanical forces in cell biology. It stems into two main branches: the study of the mechanisms by which cells sense, transduce and respond to mechanical loadings, and the characterization of cellular mechanical properties [1]. This work is concerned will the latter branch, mechanical properties.

2.1 Cell Mechanobiology

One of the most incredible aspects of cell mechanobiology is mechanotransduction. Cells have the ability to sense mechanical forces and convert them into biological signals [1]. Cellular loading conditions can influence tissue and organ pathology, such as the processes associated with osteoporosis, atherosclerosis, and fibrosis [1].

In some cases, the mechanical properties of a cell have been related to the mechanism of disease development. Studies have been performed on red blood cells showing that the stiffness of the cells change with the onset of malaria [5]. Furthermore, the infectivity of the human immunodeficiency virus has been related to the mechanical structure of the virus [5]. On a sub-cellular level, loading has been demonstrated to alter protein expression, and even control differentiation in stem cells [11]. Cell based therapy can exploit cell response to mechanical effects, by means of remodelling and regeneration [1].

Understanding of the unique relationships associated with loading conditions and the biological outcomes of a cell is far from complete [1]. Further research in the field of cellular mechanobiology could potentially drive innovations in cell-based therapies and diagnostics.

2.1.1 Cellular Response to Substrate Stiffness

Cells interact physically, by sensing local stiffness, tension, and deformation within their surrounding extracellular matrix. They can in turn remodel the matrix and generate forces with long-range effects [12]. Living cells are extremely sensitive to substrate mechanics, and therefore require appropriate substrate stiffness to function properly [1]. Different cell types tend to function best at different matrix rigidities [1]. For example, myotubes, which form muscle fibres, differentiate optimally on gel substrates with stiffness comparable to that of normal muscle [1]. It appears that cells attempt to match their stiffness to that of the underlying substrate by a combination of altering the organization of the cytoskeleton and by strain stiffening [1].

2.1.2 Cellular Elements and Mechanotransduction

The cell is composed of a variety of mechanical elements which are responsible for its form and locomotive ability [11]. The main mechanical element of the cell is the cytoskeleton, which is a filamentous network of molecular components including actin filaments, microtubules, and intermediate filaments [11]. The cyctoskeleton is highlighted with respect to the other organelle in an animal cell in Figure 2.1.1 [13]. The below figure is a generalized schematic of a non-adherent cell, one which does not adhere to an inert surface.

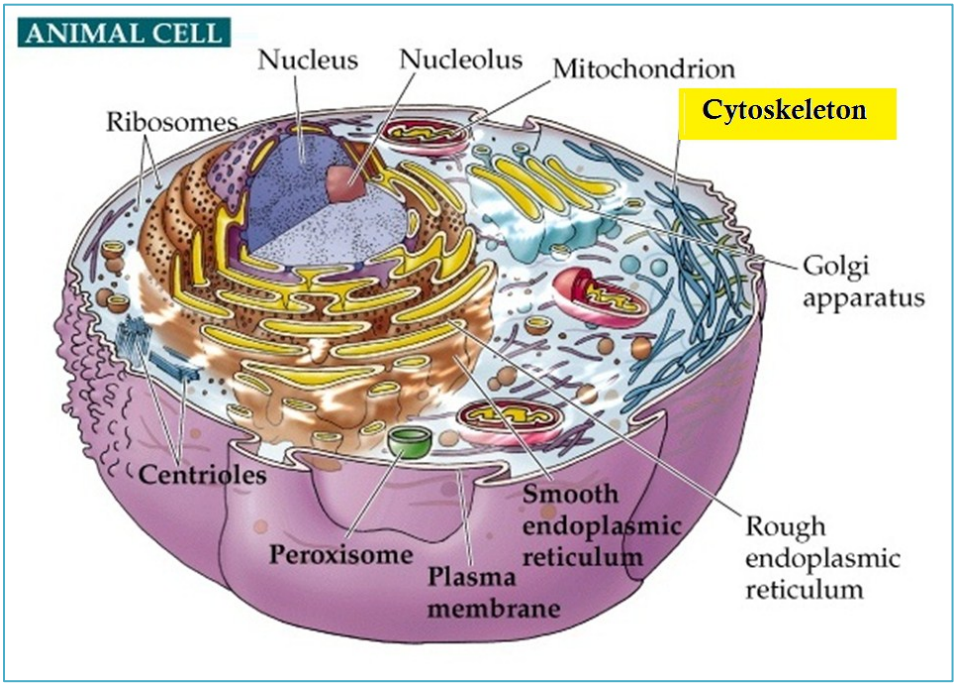

Figure 2.1.1: Cytoskeleton in an Animal Cell (Non-Adherent Cell) [13] (Reprinted with Permission)

A more truthful representation is presented in Figure 2.1.2 [14]. The two major mechanical cell components are highlighted with fluorescent markers. Actin filaments are marked red, and microtubules are labelled with green.

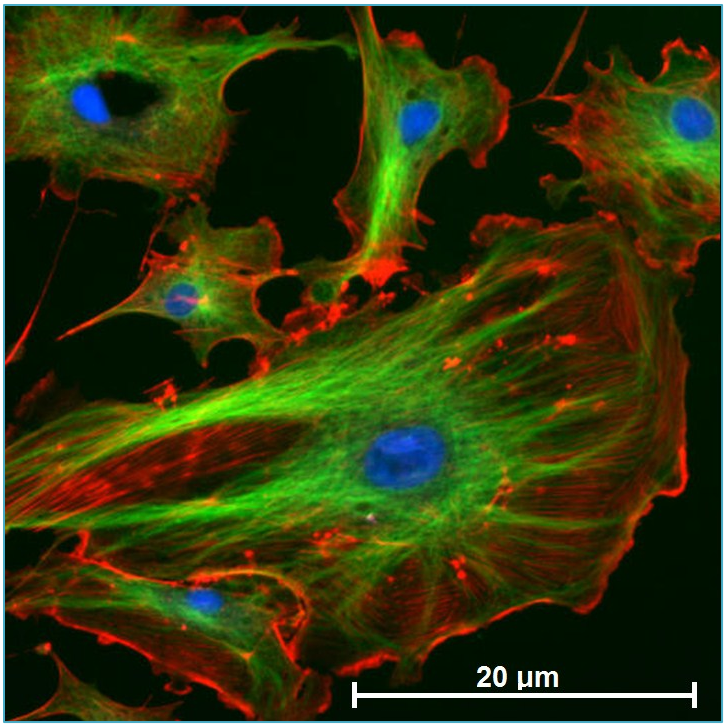

Figure 2.1.2: Components of Cytoskeleton Marked with Fluorescent Binders; Nuclei-Blue, Microtubules-Green, and Actin Filaments- Red, Bovine Tissue Cells [14]

Actin filaments migrate to positions below the cell membrane and within fibres in stress which span the cell [11]. The microtubules and intermediate filaments exist in a matrix which criss-crosses the cell. This contributes to the cytoskeletal matrix which couples the cell membrane to the nucleus and intermediate points [11]. Receptors called integrins, which mediate the attachment between the cell and cell tissues, physically link the external cell matrix to the cytoskeleton. This means the mechanical forces applied to the cell membrane are physically transmitted to the cytoskeleton via integrins inside the cell [11].

2.2 The Yeast Cell

A robust, easily handled cell was required for initial testing. In order to avoid using bio-hazardous animal cells, common baker's yeast was chosen. Yeast is

generally described as a unicellular fungus which reproduces vegetatively by budding or fission. Baker's yeast is of the species *Saccharomyces cerevisiae.* They are chemoorganotrophic, which means they require fixed, organic forms of carbon for growth [15]. Yeast rely on aerosols, animal and human activity for their natural dispersal. Yeast is an adherent cell, capable of adhering to inert surfaces, and soft tissues [15].

2.2.1 Yeast Cytology

Yeast is typical of eukaryotic cells as it contains the following organelles: nucleus, mitochondria, Golgi apparatus, secretory vesicles, endoplasmic reticulum, vacuoles and microbodies [15] . Its cell wall contains chitin, making it different from animal and eukaryotic cells .The cytoplasm contains ribosomes, occasional plasmids, and cytoskeletal components. The cytoskeleton is composed of actin, microtubules, and microfilaments. The yeast cell is represented schematically in Figure 2.2.1 [15].

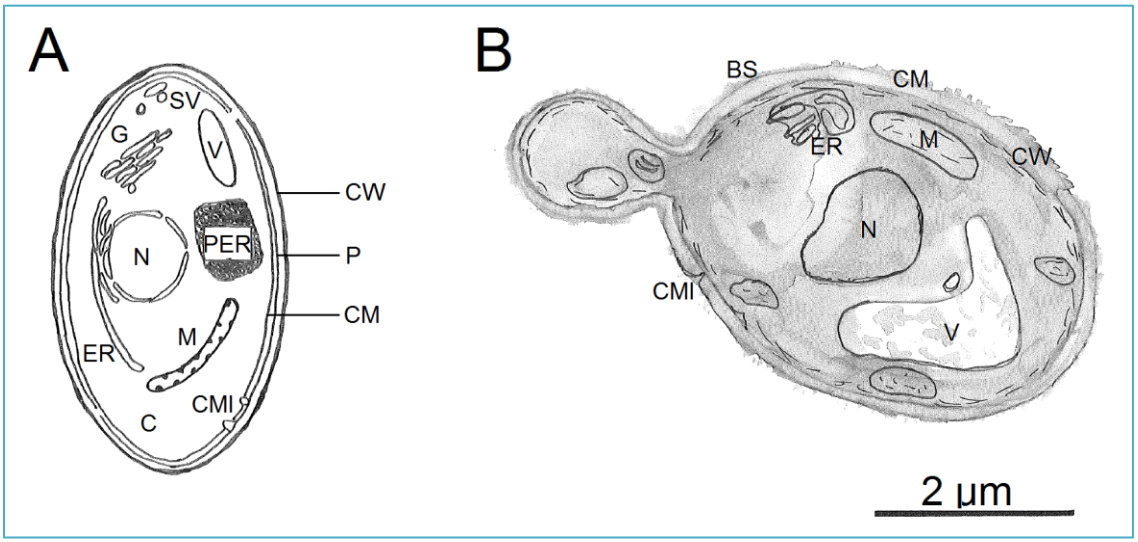

Figure 2.2.1: Yeast Sub-cellular Features; A: Idealized yeast cell. B: Candida albicans cell; CW - cell wall; P - periplasm; CM - plasma membrane; CMI - invagination; BS - birth scar; C - cytoplasm; N - nucleus; M - mitochondrion; ER - endoplasmic reticulum; G – Golgi apparatus(Adapted From [15])

The cell envelope surrounds and encases the yeast cytoplasm. It accounts for approximately 15% of the cell volume [15], and controls osmosis and cell permeability properties. It is comprised of the plasma membrane, the periplasm, and the cell wall.

The plasma membrane is the primary barrier against hydrophilic molecules, maintaining the yeast cytoplasm as separate from the aqueous surroundings. The *Saccharomyces cerevisiae* membrane is an approximately 7.5 nm thick lipid bilayer interspersed with globular proteins forming a fluid mosaic [15]. Selective permeability properties are mediated by specialized membrane proteins. The plasma membrane mediates signal transduction of external stimuli to internal biochemical reactions [15].

The periplasm is a thin 3.5 to 4.5 nm thick region between the plasma membrane and cell wall [15]. The periplasm contains secreted proteins which cannot permeate the cell wall. These proteins include invertase and acid phosphatase which catalyze the hydrolysis of substrates that do not cross the plasma membrane [15].

The yeast cell wall is generally 100 to 200 nm thick, accounting for 15 to 25% of the total dry mass of the cell [15]. The main structural components are polysaccharides, which comprise 80 to 90% of the cell wall [15] .The polysaccharides are mainly glucans and mannans, with a small proportion of chitin. The wall is layered, with the outermost section composed of cross-linked manoprotiens which are connected to the inner glucan network by covalent

bonds. Some glucans in the inner layer are cross-linked to chitin. Chitin is located in the cell wall and maintains osmotic and morphological integrity [15] . Bud scars, the ringed protrusions found on the mother cell surface after the birth of a daughter cell, are chitin-rich.

Saccharomyces cerevisiae reproduce by budding. Budding (Figure 2.2.2 [15]) is generally initiated when the mother cell achieves a critical size at a time coinciding with the onset of DNA synthesis [15] . Localized weakening of the cell wall, and tension exerted by turgor pressure, result in the extrusion of cytoplasm into an area bounded by new cell wall material. A chitin ring is formed at the junction between the mother and daughter cells. When mitosis is complete and the bud nucleus and other organelle have migrated into the bud, cytokinesis begins. During this cycle, cell growth is restricted to the developing bud. The cell sizes at division are asymmetric with the bud being smaller than the mother cell.

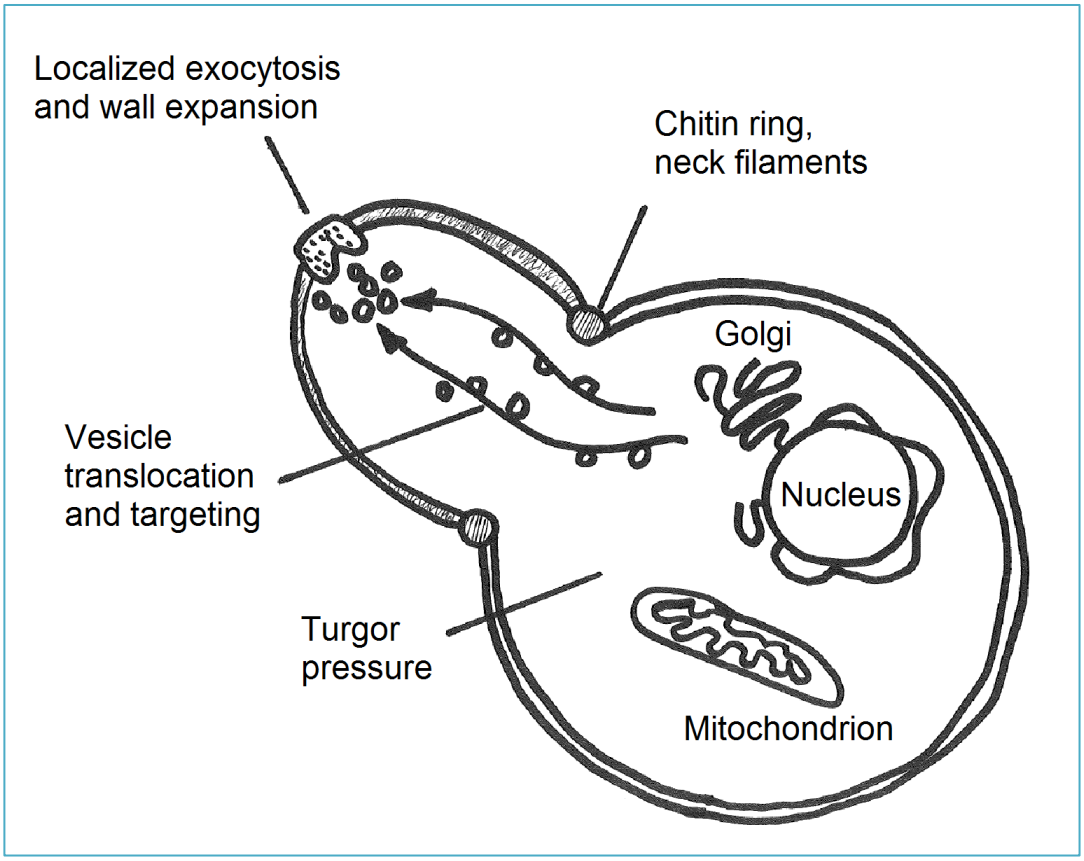

Figure 2.2.2: Budding of Yeast (Adapted From [15])

The typical growth of a yeast cell population is broken down into phases (Figure 2.2.3 [15]). The process consists of a lag phase of two to three cell divisions over a 5 hour period, followed by exponential growth for six more divisions, before they undergo a shift to ethanol respiration over approximately two more divisions as they enter stationary phase [16].

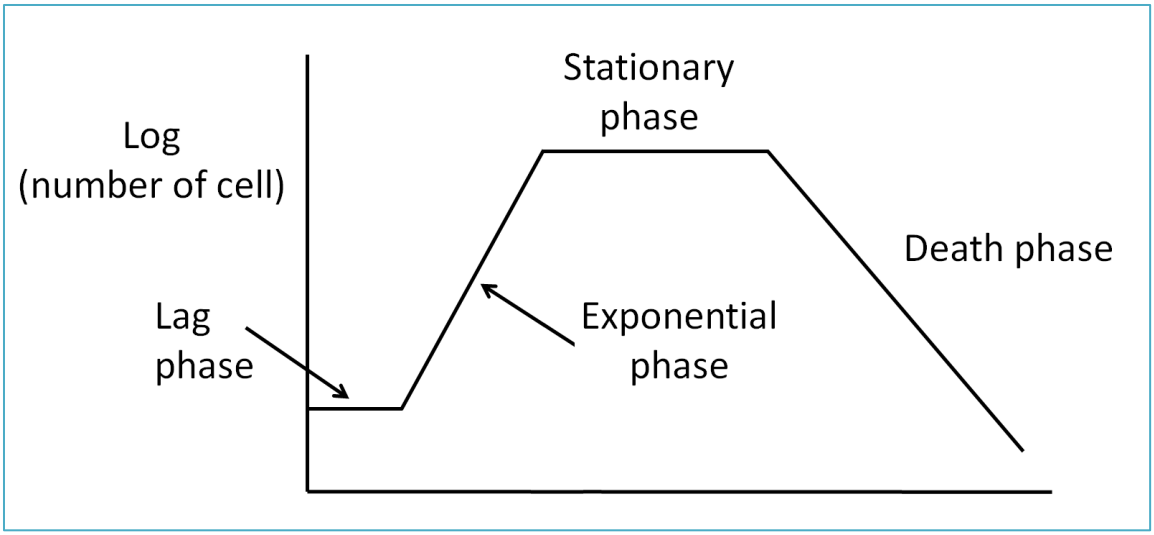

Figure 2.2.3: Yeast Growth Phase Diagram (Adapted From [17])

2.2.2 Mechanical Trends

Cell research has brought some insight into the mechanical properties and behaviour of *Saccharomyces cerevisiae*. The first is that cell stiffness is inversely proportional to cell diameter [18]. The second is that stiffness is also linked to the growth phase of the cell. Yeast stiffens during the exponential phase, and into the stationary phase [18]. This supports the conclusions of Smith and colleagues [19], that the yeast cell wall thickens and increases cell stiffness during stationary phase. As mentioned in the previous section, the bud scar region of the cell is high in chitin and it is stiffer than the surrounding cell [20]. The contact site on the cell influences the cellular spring constant [21] Furthermore, the internal osmotic pressure of the yeast cell is regulated in response to changes in the osmotic pressure of the external medium [22].

Chapter 3: Existing Test Apparatus for Determining Cell Mechanics

This section will present existing techniques for the measurement of cell mechanical properties. Both non-MEMS and MEMS based methods will be summarized. The functional ranges of these techniques will be discussed, and compared to the predicted achievable range for this work.

3.1 Non MEMS Methods

In order to later compare existing experimental techniques to MEMS based technique for determining cell mechanics, this section will summarize some common non-MEMS techniques. Some of these test methods are shown in Figure 3.1.1 [5].

The test methods shown below can be categorized based on their interaction with the cell: active, imposing a time varying mechanical stimulus; and passive, observing a response to a constant condition [5].

Some active techniques include: atomic force microscopy (AFM), micropipette aspiration,), optical or laser traps (tweezers), magnetic twisting cytometry, flow induced shear, and bending of flexible substrates. Passive techniques include multiple particle tracking microrheology, and the deformation of a compliant substrate.

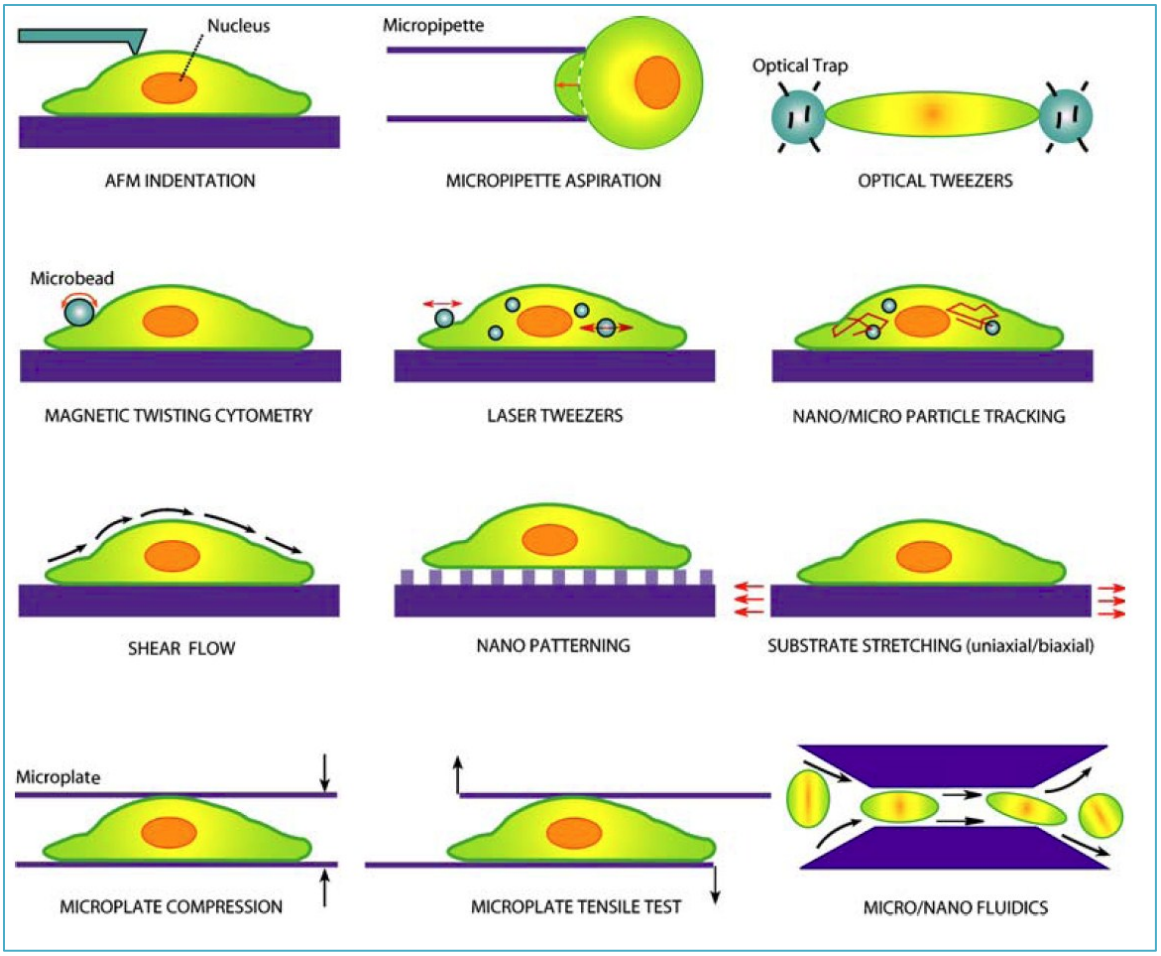

Figure 3.1.1: Test Set-ups for the Characterization of Cell Mechanics [5] (Reprinted with Permission)

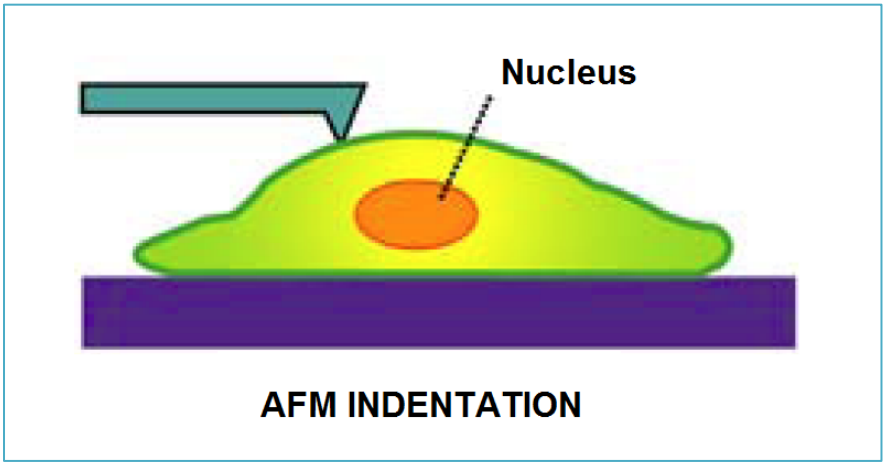

Figure 3.1.2: Atomic Foce Microscopy Indentation [5] (Reprinted with Permission)

Atomic force microscopy (Figure 3.1.2 [5]) determines cell stiffness by measuring the deformation of a micro-scale cantilever with a reflected laser beam, or optical microscope [23]. This technique is referred to as nano-indentation when the cell membrane displacements are on the order of nanometers. A stiffness map across the cell surface can be generated, providing insight into the cytoskeletal structure, and its response to environmental factors [11]. AFM is able to apply forces to the cell ranging from piconewtons to micronewtons, the widest force range of the devices compared here. Aqueous environments complicate operation by fluid-probe interaction, and reflection or refraction of the laser [5]. Difficulties also arise when testing non-adherent cells [24].

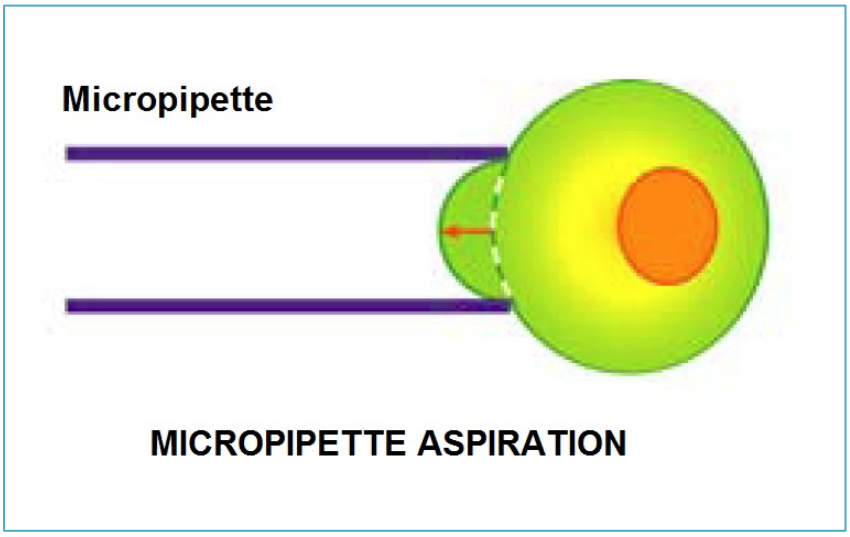

Figure 3.1.3: Micropipette Aspiration [5] (Reprinted with Permission)

Micropipette aspiration (Figure 3.1.3 [5]) utilizes a glass pipette with an internal diameter on the order of 10^{-6} m to deform the cell [11]. The pipette is placed close to the cell, and a known vacuum is applied, aspirating the cell partially into the pipette [11]. The loading pressure can be controlled to approximately 0.1Pa [5].

The functional range of force applied to the cell is from tens of piconetwons to approximately 100 nN [25].The force on the cell is determined using the length of aspiration into the pipette. This technique is generally used in combination with an optical microscope [5].

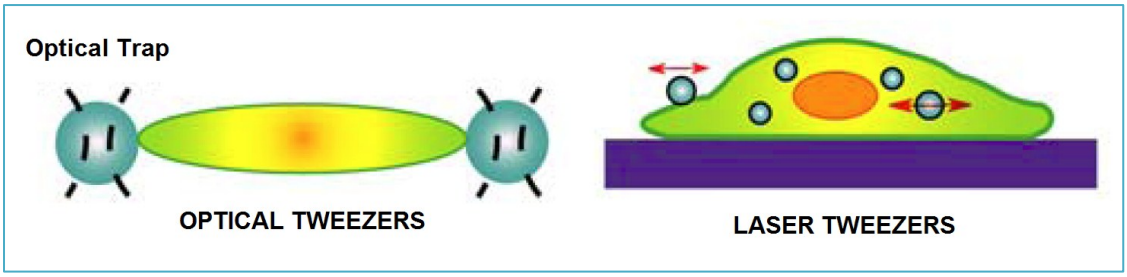

Figure 3.1.4: Optical and Laser Tweezers [5] (Reprinted with Permission)

Laser optical traps (Figure 3.1.4 [5]) utilize an optical potential well capable of trapping a small object within a defined region [11]. Optically functionalized beads are tethered to the object of interest (by means of a special procedure to induce cell binding to the beads) and used to manipulate it [26]. Bead displacements are quantified by tracking the refracted beam with photodiodes, or by analysis of optical images of interference patterns or by tracking the beads themselves [5]. This technique boasts the finest force resolution (10 fN), but is generally limited to experimentation with forces less than 0.1 nN [5].

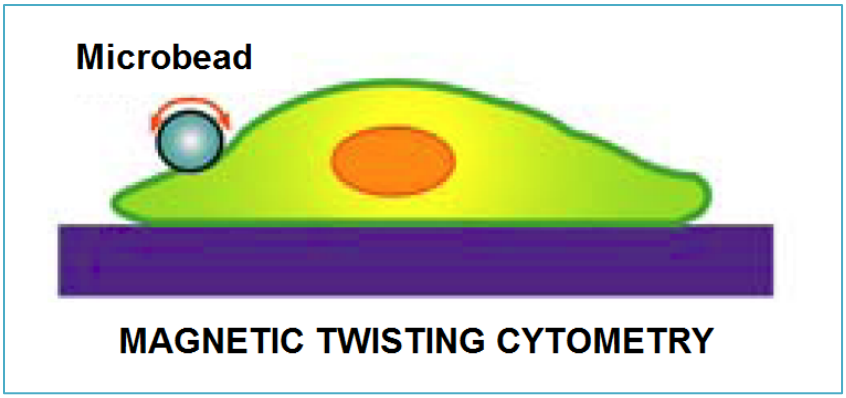

Figure 3.1.5: Magnetic Twisting Cytometry [5] (Reprinted with Permission)

Magnetic beads are used to manipulate the sample by means of an externally generated magnetic field (Figure 3.1.5 [5]). Translation and rotation of the external magnetic field results in variable force or torque applied to the sample [5].This technique has a force range of 10 fN to 5 nN [5]. The magnetic beads are attached to the cell sample using also using a special procedure to induce cell binding [27]. Unfortunately, magnetic forces scale poorly to small scales, with the magnetic force, F_m, being proportional to either the square or cube of length L ($F_m \propto L^2, L^3$), limiting the performance of these systems. This means the magnetic beads required must be large (2-8 μm) in comparison to the size of the sample [5]. By optically tracking the beads, stiffness can be computed by the ratio of pulling force to translation or from the ratio of twisting torque to bead motion (Figure 3.1.6 [23]).

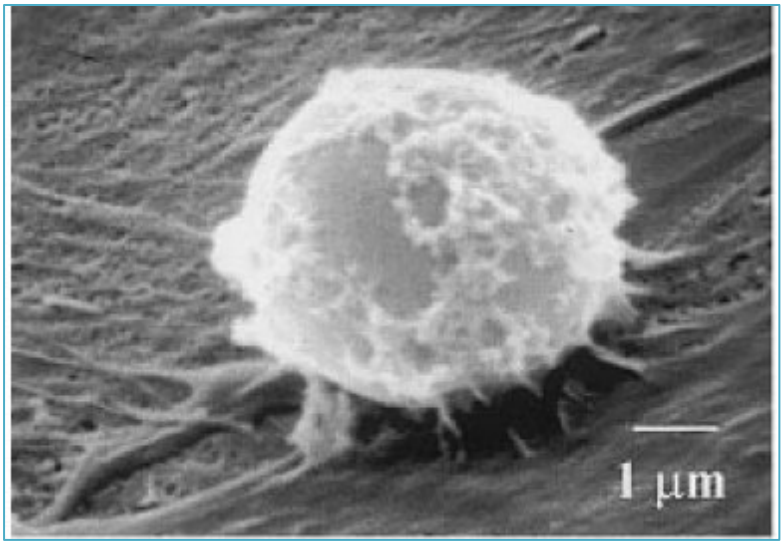

Figure 3.1.6: Electron Microscopy of Magnetic Bead Bound to Human Airway Smooth Muscle Cell [23]

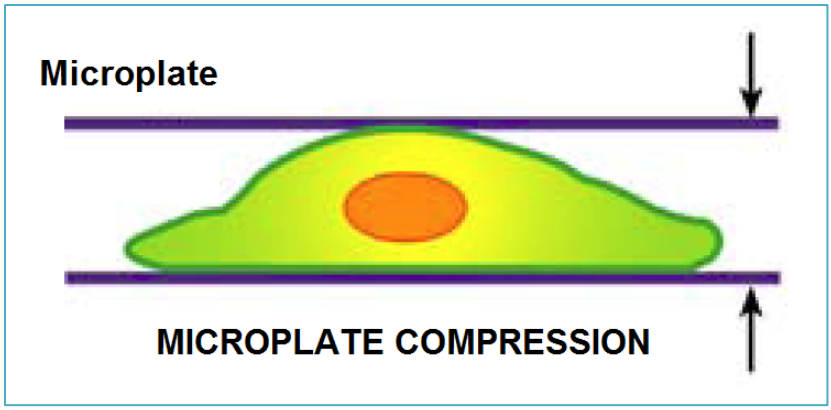

Figure 3.1.7: Micro-plate Compression [5] (Reprinted with Permission)

Micro-plate compression techniques (Figure 3.1.7 [5]) enable the force required to compress a single yeast cell between two parallel surfaces to be measured as a function of cell deformation [19]. Testing performed by Mashmoushy deformed a cell between a stationary glass plate, and the flat face of an optic fiber probe [24]. A micromanipulator with accuracy of $\pm$ 2 µm and a force transducer with a

response up to 490 μN with a resolution of 0.01 μN were used for measurements [24].

The functional ranges of the aforementioned techniques as well as a predicted range for this work are displayed later in Figure 3.2.2 [5].

3.1.1 Passive Non MEMS Techniques

Passive techniques must be carefully assessed as many of these methods are unable to measure cell mechanical properties.

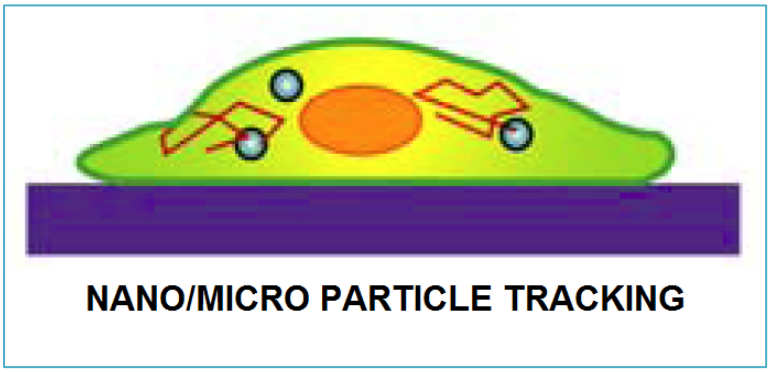

Figure 3.1.8: Nano/Micro Particle Tracking [5] (Reprinted with Permission)

Multiple-particle-tracking microrheology (Figure 3.1.8) is a passive technique involving the dispersal of micro and nano particles on the cell membrane and into the cytoplasm. The particles are tracked to map local displacements [5]. This technique is not valid for measuring cell mechanical properties as the particle are driven by the activity of the cell (adenosine triphospate hydrolysis cycle) as opposed to the Brownian motion suggested in Loh's [5] review article [30].

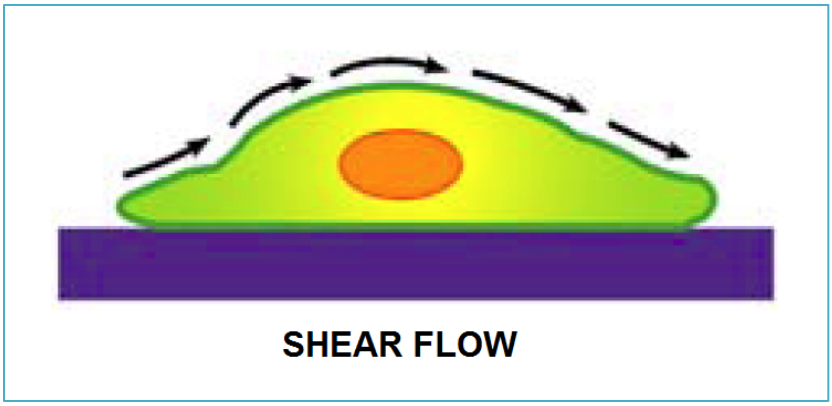

Figure 3.1.9: Shear Flow [5] (Reprinted with Permission)

Flow-induced shear techniques (Figure 3.1.9) load cells fixed to the walls of a flow chamber [5]. Like the previously discussed techniques, this is a cell-friendly test as it takes place in a fluid environment. The flow chamber can be designed to measure cell rolling velocity, deformation, and cell/substrate contact length, but not all mechanical properties.

3.2 MEMS Techniques

The potential of MEMS devices for advancing experimentation and modeling in cell mechanics has been explored by Loh and colleagues [5].There are many different categories of MEMS based devices for the investigation of cell mechanics.

Most MEMS based cell measurement techniques are based on the compliant beam. An assortment of probes, micro-pillars, and pullers are presented in Figure 3.2.1 [5]. Most of the designs allow optical measurement of displacement to be converted into forces based on the incorporation of a characterized beam [5].

The probe designs (both 1D and 2D) consist of probes suspended on single or pairs of compliant beams of known stiffness [5] .The designs are actuated by piezoelectrics, and applied force is calculated by observing deflection of the beam with an optical microscope.

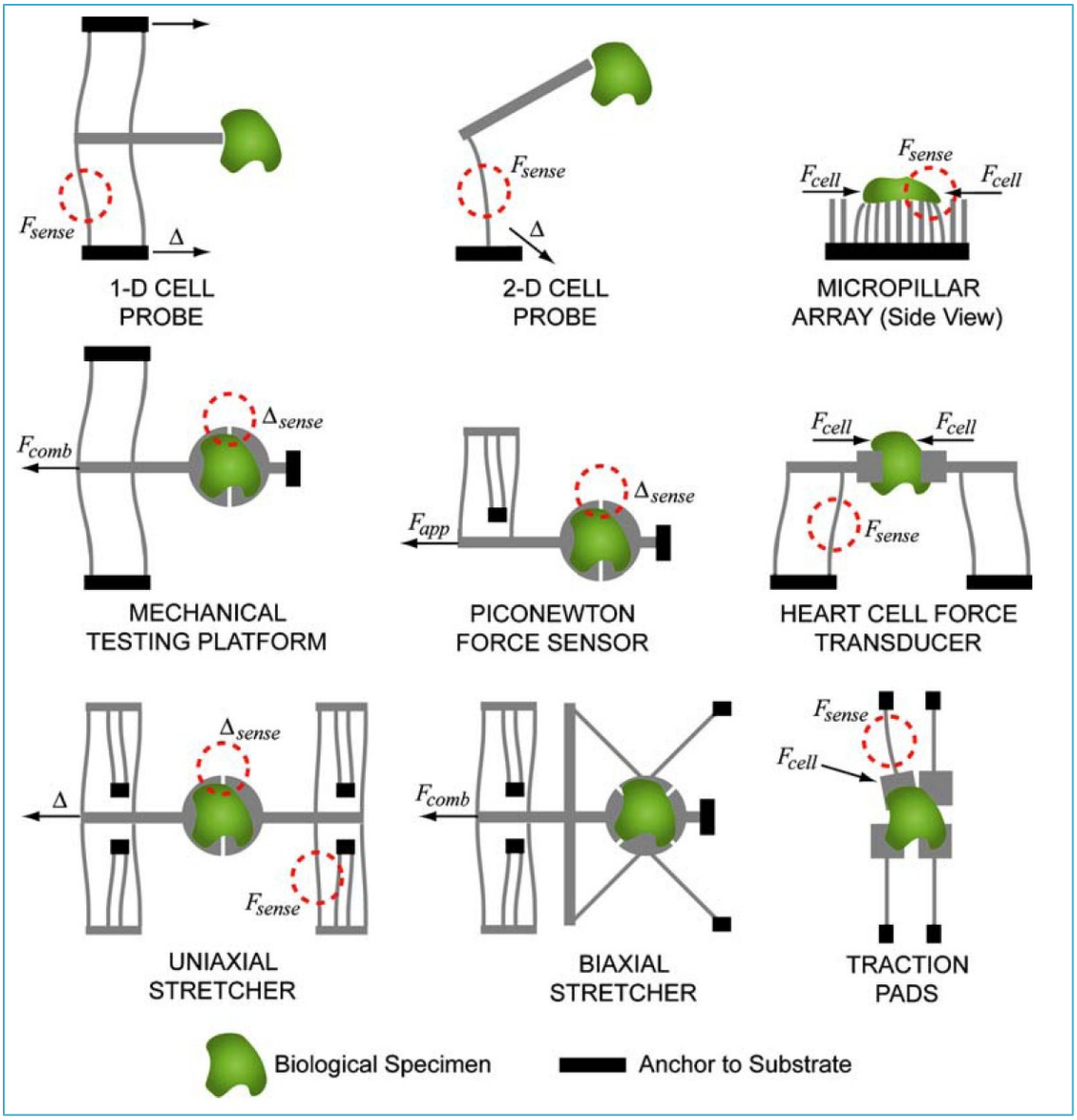

Figure 3.2.1: MEMS Devices for Cell Mechanics [5] (Reprinted with Permission)

Micro-pillar devices are comprised of arrays of closely spaced silicon or polymer pillars. The deformation of the pillars caused by the cell allows the study of interactions between the cell and its substrate [31].

Uniaxial and biaxial pulling devices (bottom left and center of Figure 3.2.1) are able to apply tensile loading to adherent cells. The platform is split down the center and coated in fibronectin to promote cell adhesion to the substrate [5]. The cell adheres across the platform, and then one half of the platform is pulled away from the other to strain the cell. The compliant beams in the systems are used as a load sensor to compute the applied force.

Traction pads have been developed to measure traction forces generated by fibroblasts [5]. A large array of square pads, which are fixed to the free ends of cantilevered beams, produce a surface for migrating cells. The cantilevered beams bend in response to traction forces produced by the cells. The motion of the pads is then used to determine the corresponding forces [5].

The functional ranges for the non-MEMS and MEMS based techniques are presented in Figure 3.2.2. Atomic force microscopy techniques allow the largest range of displacements, and midrange forces, while optical/laser trapping and magnetic bead cytometry enable the smallest force application. MEMS devices allow midrange to high displacements, and have some of the largest possible forces. Micro-plate compression has a high force and displacement range.

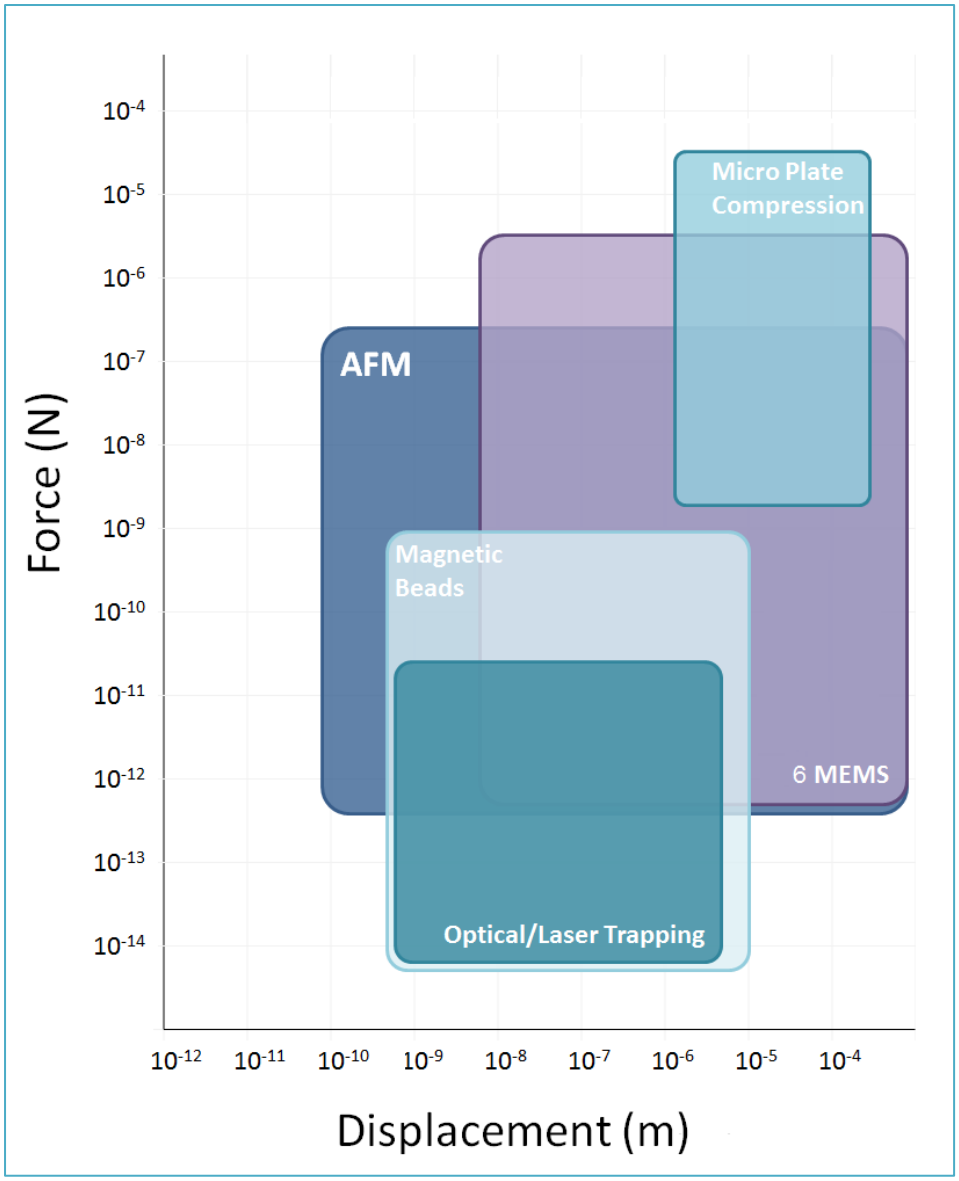

Figure 3.2.2: Functional Ranges of Existing Measurement Techniques (Adapted from [5]).

3.3 Technique Developed for This Research

The technique developed for this research is a compression technique, but does not incorporate full face contact between the cell and plate. Therefore, the technique is a cross between micro-plate compression, and indentation methods. The range of forces which can be applied to the cell are greater than those

achieved with AFM, optical/laser trapping, and magnetic cytomety (Figure 3.3.1). For the purpose of this research, results from nano-indentation (AFM) and micro-plate compression testing will be used as a basis for comparison.

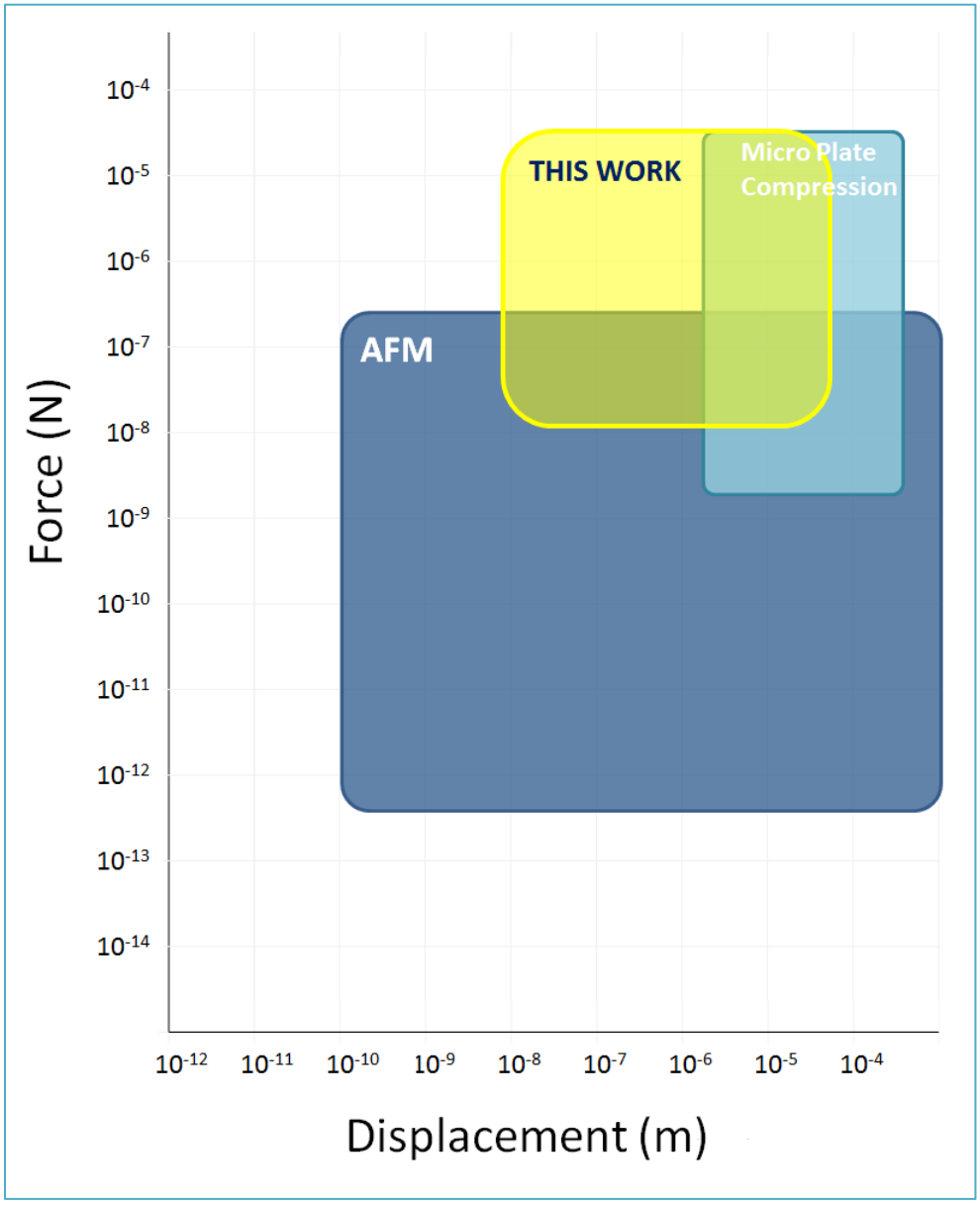

Figure 3.3.1: Functional Ranges of AFM, Micro-plate Compression, and prediction for this work (Adapted from [5]).

Chapter 4: Cell Squeezing to Determine Mechanics

Now that a brief background has been provided for the biology incorporated in this research, the mechanical side of this work will be explored.

4.1 Concept

The concept of squeezing a cell to determine its mechanical properties was derived from previous work by Shay (2007). Shay's work incorporated a spring of known stiffness, and used differential displacement to determine cell stiffness (Figure 4.1.1). Unfortunately, the Wentworth™ Probestation microscope was diffraction limited at around 250 nm, so cell displacement measurements were difficult to measure, and meaningful results could not be obtained.

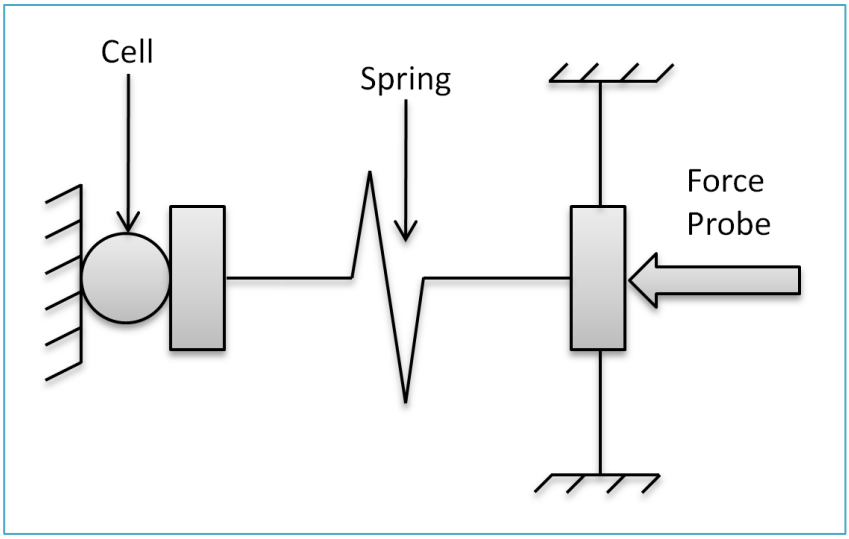

Figure 4.1.1: Cell Squeezing Concept Schematic [32]

A design incorporating a displacement measurement technique by Yamahata [2], was developed to enable measurement of cell mechanical properties. A schematic of the design is presented in Figure 4.1.2.

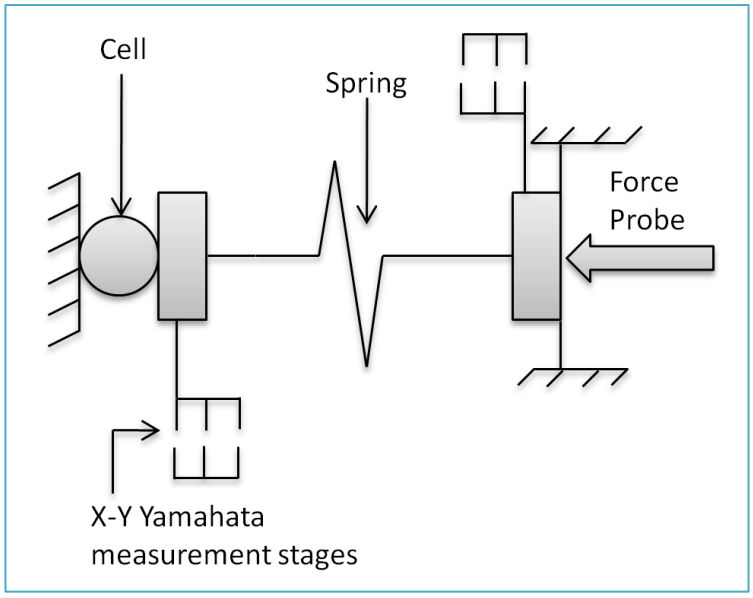

Figure 4.1.2: Cell Squeezing Concept Schematic with Improved Displacement Measurement Technique (Yamahata)

Using the Yamahata technique, the displacements of a periodic Cell Comb (CC) and a periodic Input Comb (IC) are determined using FFT, allowing much better resolution. The force observed by the spring is the same as observed by the cell as they are in series. Therefore, using the displacement measurements, the stiffness of the cell can be calculated as follows (Figure 4.1.3):

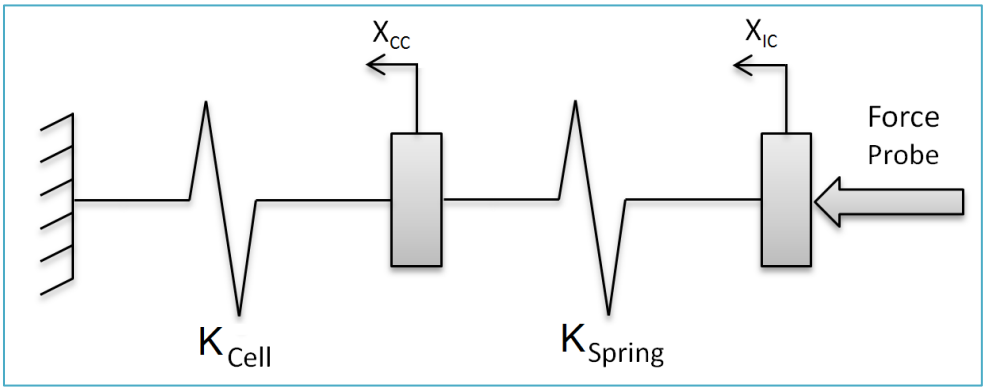

Figure 4.1.3: Spring System Schematic for Cell Squeezer

$$K_{cell} = \frac{K_{Spring}(X_{IC-}X_{CC})}{X_{CC}}$$

Equation 4.1.1

Where X_{IC} , input comb displacement, is the displacement at the interface of the S-spring and the chevron, and X_{CC}, cell comb displacement, is the displacement of the jaw deforming the cell.

Following this, the force observed by the cell can be calculated from the calculated cell stiffness, K_{cell}, and the measured cell comb displacement, X_{CC}:

$$F_{cell} = K_{cell}X_{CC}$$

Equation 4.1.2

The stress undergone by the cell is calculated as the force observed by the cell divided by an assumed constant cross-sectional area, A_{CS} of 4 μm^2. In reality the cell is deforming during squeezing, so the cell cross sectional area is increasing. This would result in a non-linear stress strain relationship. The chosen area of 4 μm^2 is equivalent to the cross-sectional area of the cell at a midway point where the diameter is 2.25 μm.

$$\sigma_{cell} = \frac{F_{cell}}{A_{CS}}$$

Equation 4.1.3

The strain is calculated as the change in cell diameter divided by the original cell diameter:

$$\epsilon_{cell} = \frac{\Delta \emptyset_{cell}}{\emptyset_{cell}}$$

Equation 4.1.4

4.2 Electrothermal Actuation

In order to drive the jaws of the microgripper closed, electrothermal actuation was utilized. This technique relies on joule heating induced thermal expansion. Joule heating is an increase in temperature of a conductor as a result of resistance to electrical current flowing through it [33]. The conductive material then expands proportionally to the change in temperature and the coefficient of thermal expansion as defined below:

$$\varepsilon = \alpha \Delta T$$

Equation 4.2.1

Where ε is the strain, α the material specific coefficient of thermal expansion (K^{-1}), and ΔT is the temperature change (K).

Chevron actuators (Figure 4.2.1) are driven by thermal expansion. They consist of two arms at a small angle θ, from their alignment, resulting in geometric amplification of the arm's expansion. Therefore, when thermal expansion takes place, linear motion occurs parallel to the line of symmetry of the actuator in the direction in which the chevron is pointed [33]. The displacement of the chevron is proportional to the voltage squared [27]. This style of actuator, with two hot arms, is more efficient that other designs which include both hot and cold arms. A single chevron (θ = 15º) has stiffness on the order of 100 μN/μm [28]. The stiffness increases with increasing θ and increasing number of chevron arms.

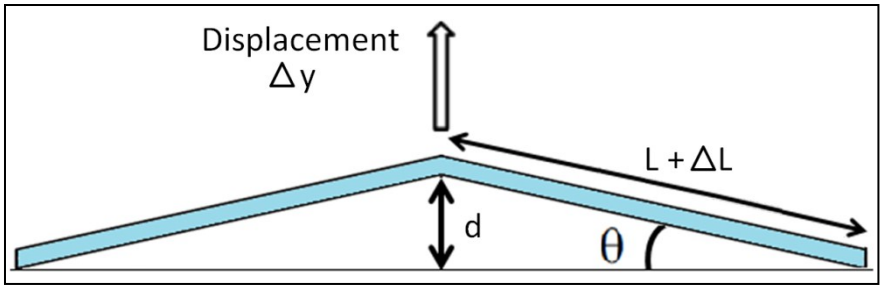

Figure 4.2.1: Electrothermal Chevron Actuator

The chevron actuators implemented in this work are presented in Figure 4.2.2.

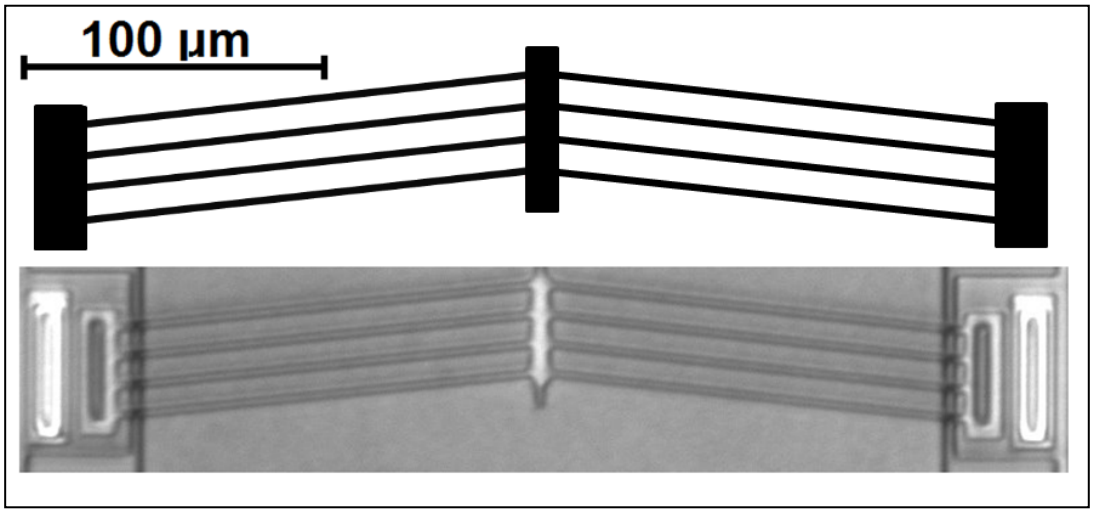

Figure 4.2.2: Chevron Actuator, L-Edit layout (Top) and Micrograph (Bottom)

The geometric advantage of the chevron actuator is simply $\frac{\Delta y}{\Delta L}$ [33]. Chevrons can be used in parallel to increase force produced and amplified to produce the desired displacement [27].

The displacement of the center point of the chevron actuator is described by Luo as [29]:

$$\Delta y = \frac{L\Delta L}{d} = \frac{\Delta L}{sin\theta} = \frac{\alpha L \Delta T}{\theta}$$

Equation 4.2.2

In the above, α is the thermal expansion coefficient of the material, d the height of the chevron device, and L is the beam length, see Figure 4.2.1. Chevron actuators used in this research are about 250 μm in length, producing approximately 100-200 μN of force and displacements up to 6 μm.

4.3 Yamahata Technique for Displacement Measurement

In order to determine the properties of micro-objects, it will be necessary to resolve sub-micron displacements. As mentioned above, the optical resolution of the Wentworth™ Probestation microscope is diffraction limited at around 250 nm. Previous attempts to measure cell properties with pattern matching techniques were unsuccessful. Pattern matching techniques allow for resolutions of about 100 nm. Yamahata [2] was able to achieve sub-nanometer resolution, using very fine periodic structures, by phase-shift comparison of the FFT of a moving image to a static image. Yamahata's technique incorporates a moving comb and static (or reference) comb to account for shift in the camera or table. In this work, reference combs were included for initial designs only. The work of Yamahata and colleagues [2] has been experimentally tested in the Dalhousie MEMS lab achieving resolution of 5 – 10 nm [30].In our particular setup, a pixel is 0.298 μm, and regions of interest (ROI) are typically 150 by 250 pixels. Based on a 10 nm precision, our lab has achieved 1/30th of a pixel precision. Yamahata's sub-nanometer resolution was not achieved in our lab as the pitch of the periodic

structures incorporated was not as fine as in Yamahata's work, in addition to this the optical microscope used was also different.

Figure 4.3.1 shows the steps in Yamahata's process. This technique requires periodic patterns with many repeated cycles to be implemented on the dynamic and static structures. The first step (A) in this measurement process is selecting the region of interest (ROI) on the dynamic or reference structure, in the image. The intensity profile is then calculated by column averaging the grey-scale value across the periodic structure (B). This produces a 1D line profile. Following this, the intensity profile is truncated to an integer number of wavelengths.

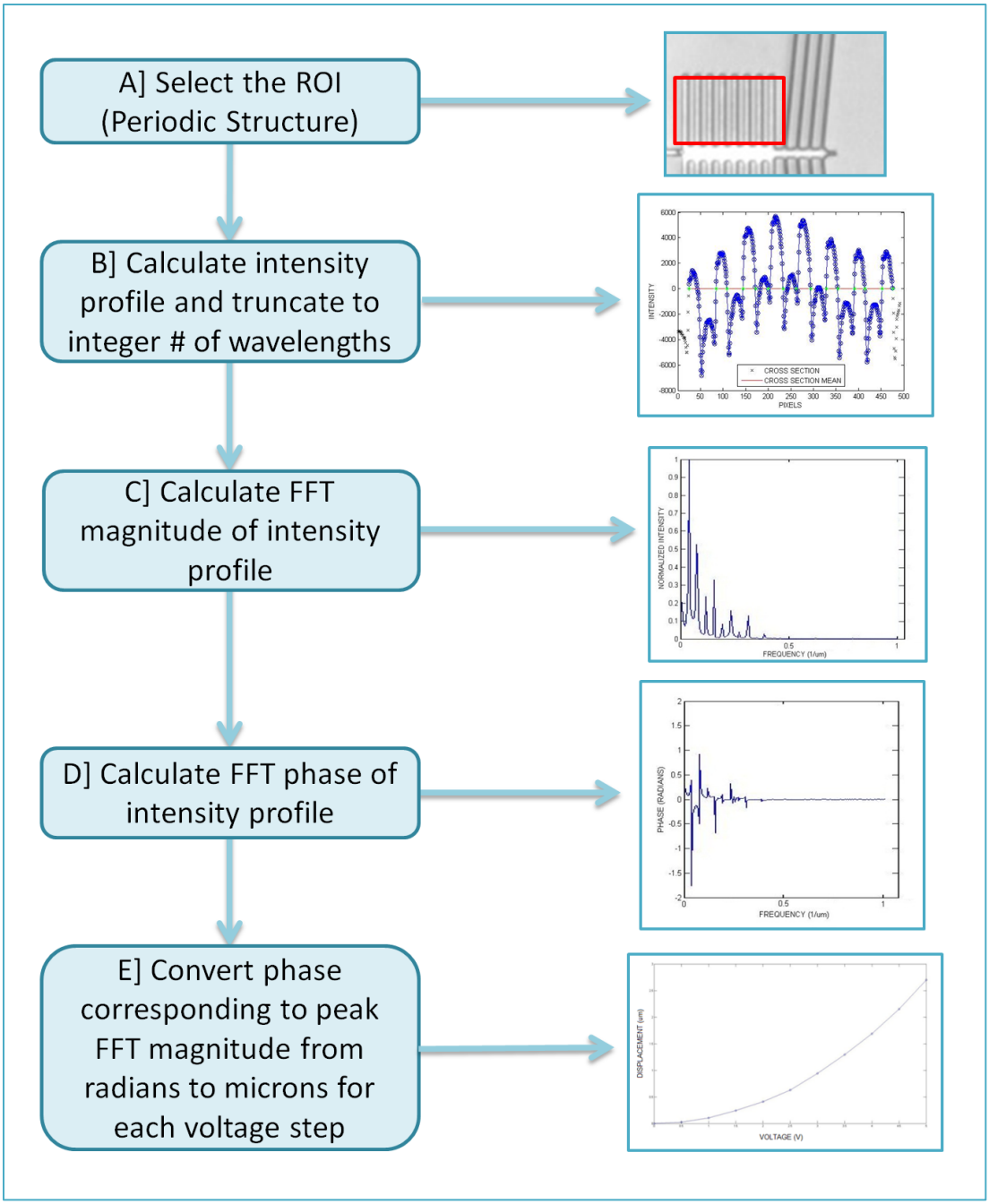

Figure 4.3.1: Yamahata Process Flowchart

Next, the Fast Fourier Transformation of the intensity is calculated (C and D). The value and location of the peak value of FTT magnitude is determined (C). The phase corresponding to this peak FFT magnitude is found for each voltage

step (D). The phase value corresponding to the peak magnitude is converted from radians to microns using the known pitch of the periodic structure in microns (E). The final result is a plot of voltage versus displacement in microns.

An example case for a periodic comb structure, with a pitch of 10 μm, driven from 0 to 5 V will be presented below. The comb structure showing the selected ROI is shown in Figure 4.3.2.

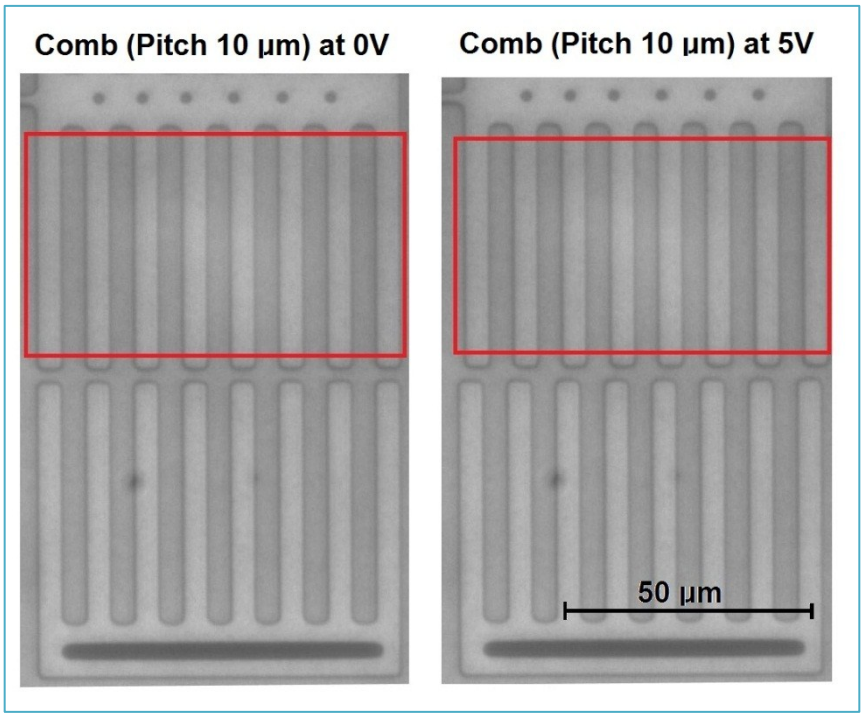

Figure 4.3.2: Sample Images for Combs at 0 V and 5 V (ROI in Red)

The intensity profile for a static image of the comb is presented in Figure 4.3.3. The profile is not a perfect sinusoid due to the shadowing in the regions between combs. It is also observed that the peak grey level values increase to the right as the light is not evenly distributed across the device.

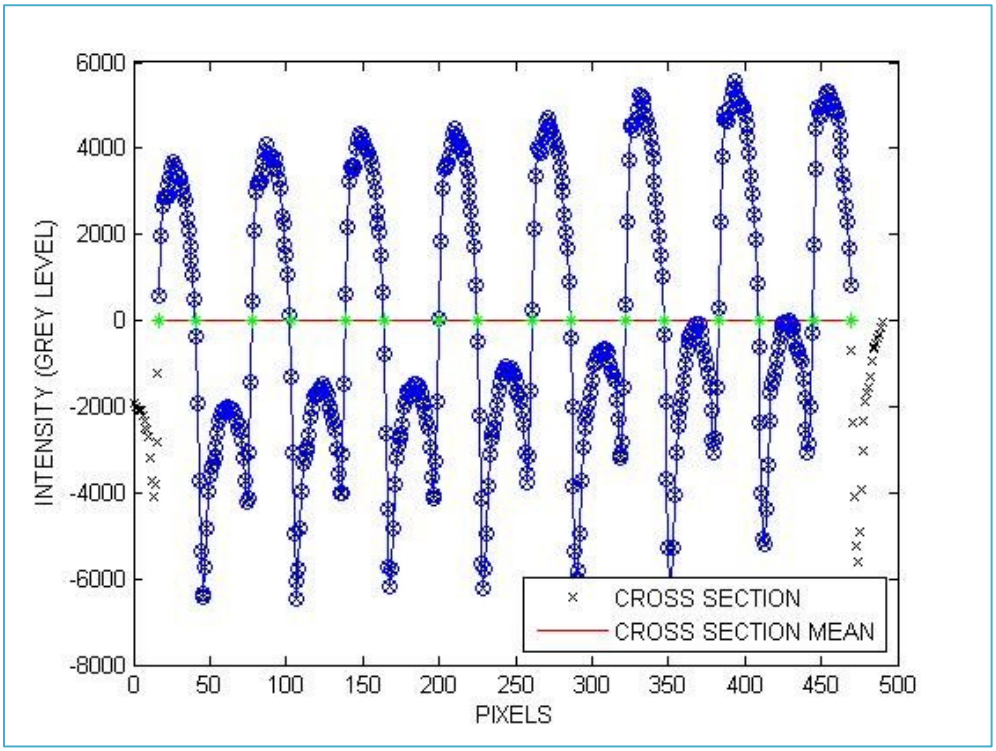

Figure 4.3.3: Sample Intensity Profile (Chevron Driven Comb P=10 μm)

FFT magnitude (Figure 4.3.4), and FFT phase (Figure 4.3.5) for this case are also presented below. The phase associated with the peak magnitude is converted to microns as the wavelength in microns is known. This is done for each voltage step resulting in a plot of displacement versus voltage (Figure 4.3.6).

In the example case presented in Figure 4.3.4 the peak magnitude occurs at a wavelength of 1/0.1 or 10 μm. The phase in Figure 4.3.5 at the peak magnitude is 1.7 radians, so the initial position is 1.2/2π*10 μm, or 1.91 μm. This process is

performed for each voltage step allowing one to plot displacement with respect to voltage.

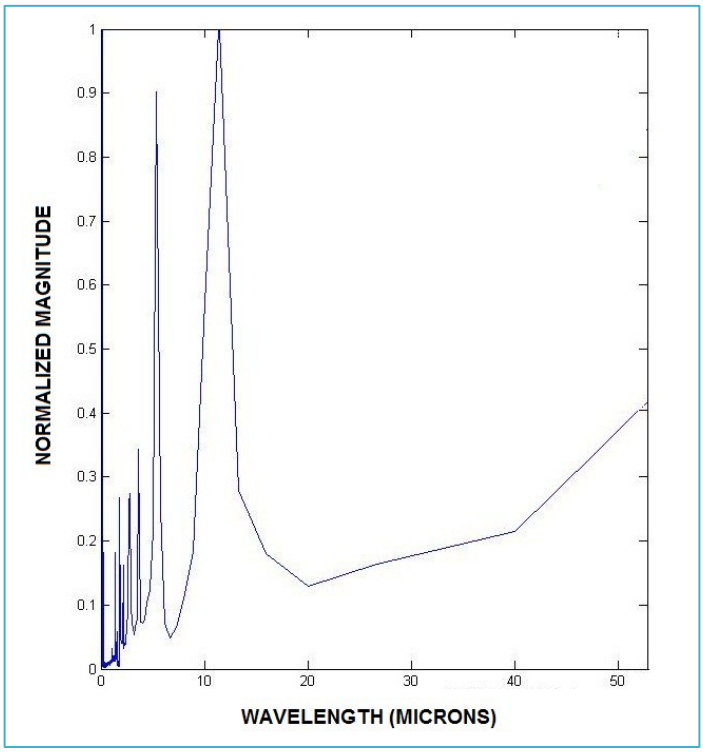

Figure 4.3.4: Sample FFT Magnitude (Chevron Driven Comb P=10 µm) Note Fundamental 10 µm

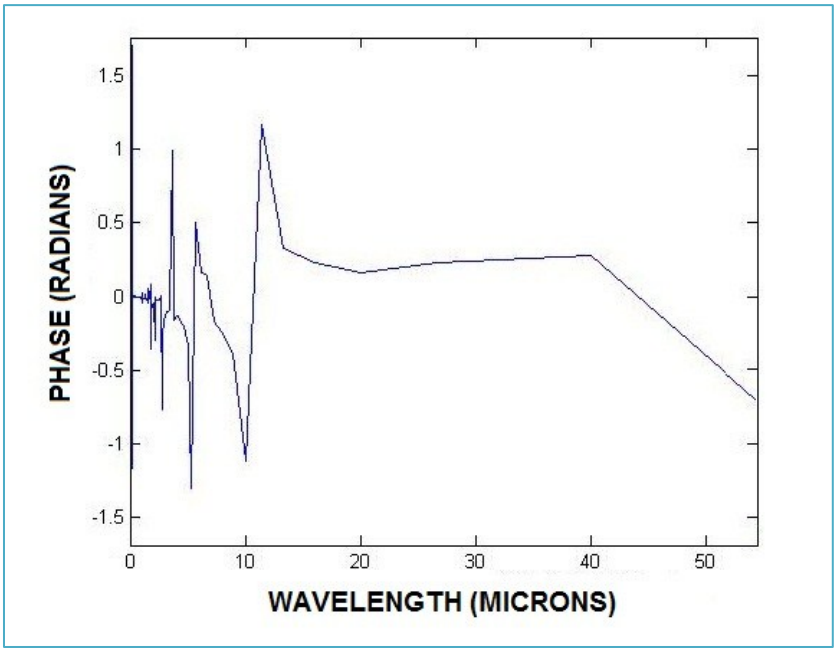

Figure 4.3.5: Sample FFT Phase (Chevron Driven Comb P=10 µm) Note Fundamental at 1.2 rad

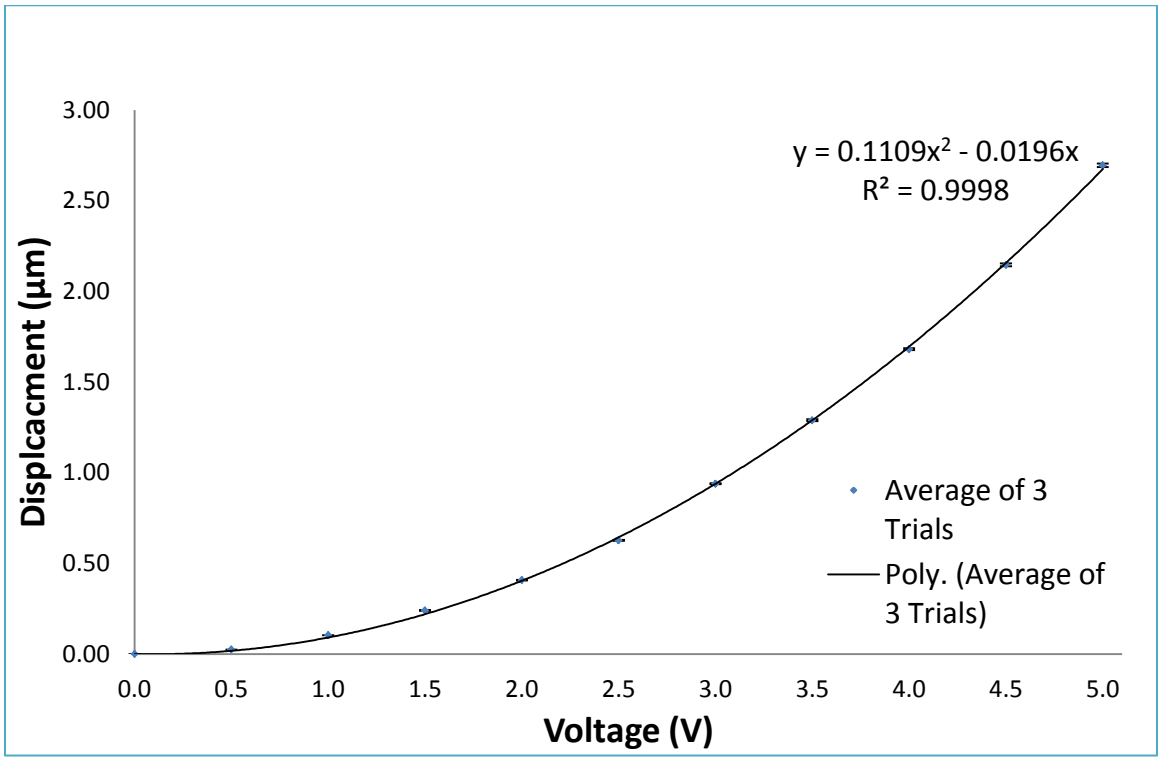

Figure 4.3.6: Sample Displacement vs Voltage Using Yamahata (Chevron Driven Comb P=10 µm)

The graph of displacement with respect to voltage (Figure 4.3.6) is presented as a polynomial representation, with the standard deviation of three trials marked as the error bounds. The standard deviation is approximately 10 nm.

The precision of this measurement technique is therefore approximately 10nm for displacement and approximately 0.3 degrees for phase.

Table 4.3.1 presents the displacement measurements acquired for a chevron device from 0 – 5 V, as well as the average and the standard deviation for the three trials. The resultant precision of the applied forces will be discussed later.

Table 4.3.1: Average and Standard Deviation of Three Trials

Voltage (V)	Trial 1 Displacement (μm)	Trial 2 Displacement (μm)	Trial 3 Displacement (μm)	Average (μm)	Standard Deviation (μm)
0.000	0.000	0.000	0.000	0.000	0.000
0.500	0.025	0.024	0.025	0.025	0.000
1.000	0.104	0.104	0.104	0.104	0.000
1.500	0.242	0.240	0.241	0.241	0.001
2.000	0.410	0.407	0.407	0.408	0.002
2.500	0.629	0.626	0.625	0.627	0.002
3.000	0.943	0.938	0.937	0.939	0.003
3.500	1.295	1.287	1.287	1.290	0.005
4.000	1.688	1.678	1.678	1.681	0.006
4.500	2.155	2.142	2.141	2.146	0.008
5.000	2.706	2.690	2.689	2.695	**0.010**

For comparison, pattern matching using National Instruments Vision Assistant was implemented in the Dalhousie MEMS lab by Arthur achieving a precision of approximately 0.160 μm [38], an order of magnitude worse than achieved with Yamahata's technique at Dalhousie.

Chapter 5: Implementation of Cell Squeezing Concept (CS2)

The cell squeezing devices were designed in Tanner EDA L-Edit v15.0, a computer assisted design software specifically for MEMS design. The L-Edit Layout of one of the devices, and its comparison to the actual fabricated device are presented in **Figure 5.1.1**. Illustrated in the figure are four key components; the location of the cell, the cell Combs (CC), the spring, and the Input Combs (IC). These components are denoted in the below figure.

The devices were implemented using the Poly 1 structural layer which is 2 μm from the substrate, and 2 μm thick. Dimples were placed along the length of the device, and on the spring to prevent it from adhering to the substrate during fabrication. A close up of the gripper and combs is presented in Figure 5.1.2.

5.1 Sensitivity and Stiffness Matching

In order to make the gripper design a sensitive measurement tool to determine cell stiffness, one needs to evaluate the effect of the spring stiffness on the sensitivity of the measurement device. In order to determine the optimum stiffness for the spring, the ratio of output (cell) displacement to input (comb) displacement was examined.

$$\frac{X_{CC}}{X_{IC}} = \frac{K_{Spring}}{K_{Cell} + K_{Spring}}$$

Equation 5.1.1

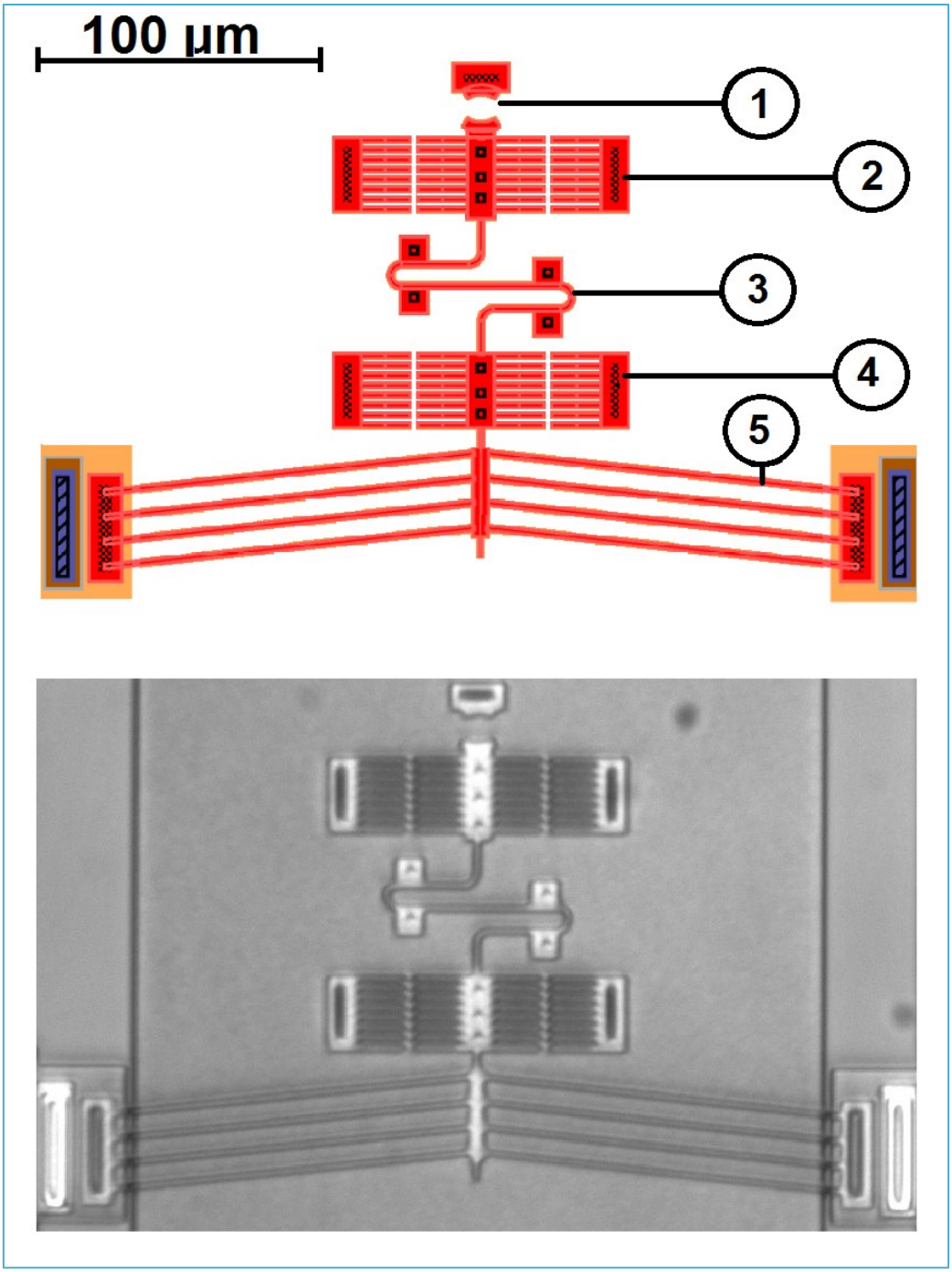

Figure 5.1.1: Cell Squeezing Device L-Edit Layout (Left) and Actual Device (Right), Micrograph of Fabricated Structure (Bottom): 1- cell location, 2- cell Yamahata combs (CC), 3 - spring, 4- input Yamahata combs (IC), 5- chevron actuator

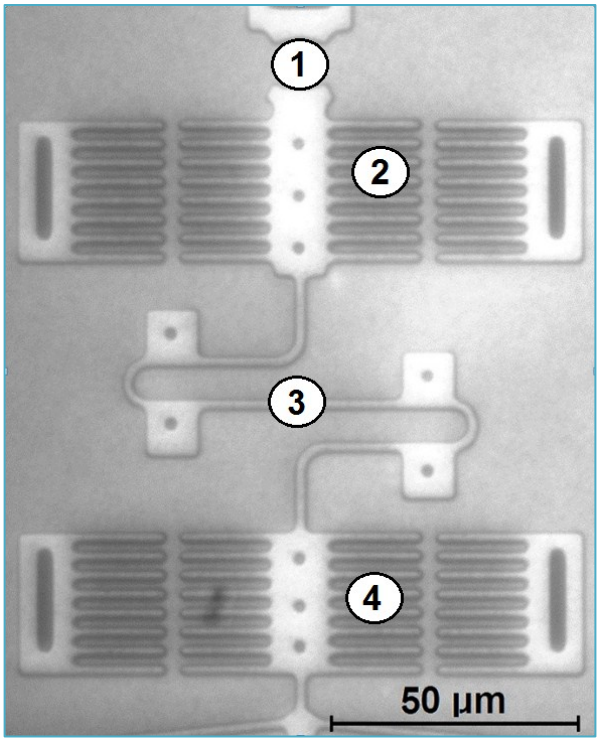

Figure 5.1.2: Cell Squeezing Device Micrograph Close up: 1- cell location, 2- cell Yamahata combs (CC), 3 - spring, 4- input Yamahata combs (IC)

The output, or cell, displacement was determined for different spring stiffnesses where the input displacement X_{IC} was 1 µm. In order to find the spring stiffness that makes the system most sensitive to small changes in cell stiffness, one looks at the difference in the cell displacement for small changes in cell stiffness. The larger this displacement is, the more sensitive the system is to changes in cell stiffness. The difference between the output cell displacements for a small change in cell stiffness was normalized and plotted against the spring stiffness (Figure 5.1.3). The largest difference occurred when the spring stiffness was equal to the cell stiffness.

From this exercise it is apparent that the greatest system sensitivity is achieved when the spring stiffness is equal to the cell stiffness. However, designing the

spring to be stiffer than the cell is better than softer than the cell. This is because the sensitivity decreases more gradually when the spring stiffness is increased beyond the cell stiffness than when it is lowered from the cell stiffness.

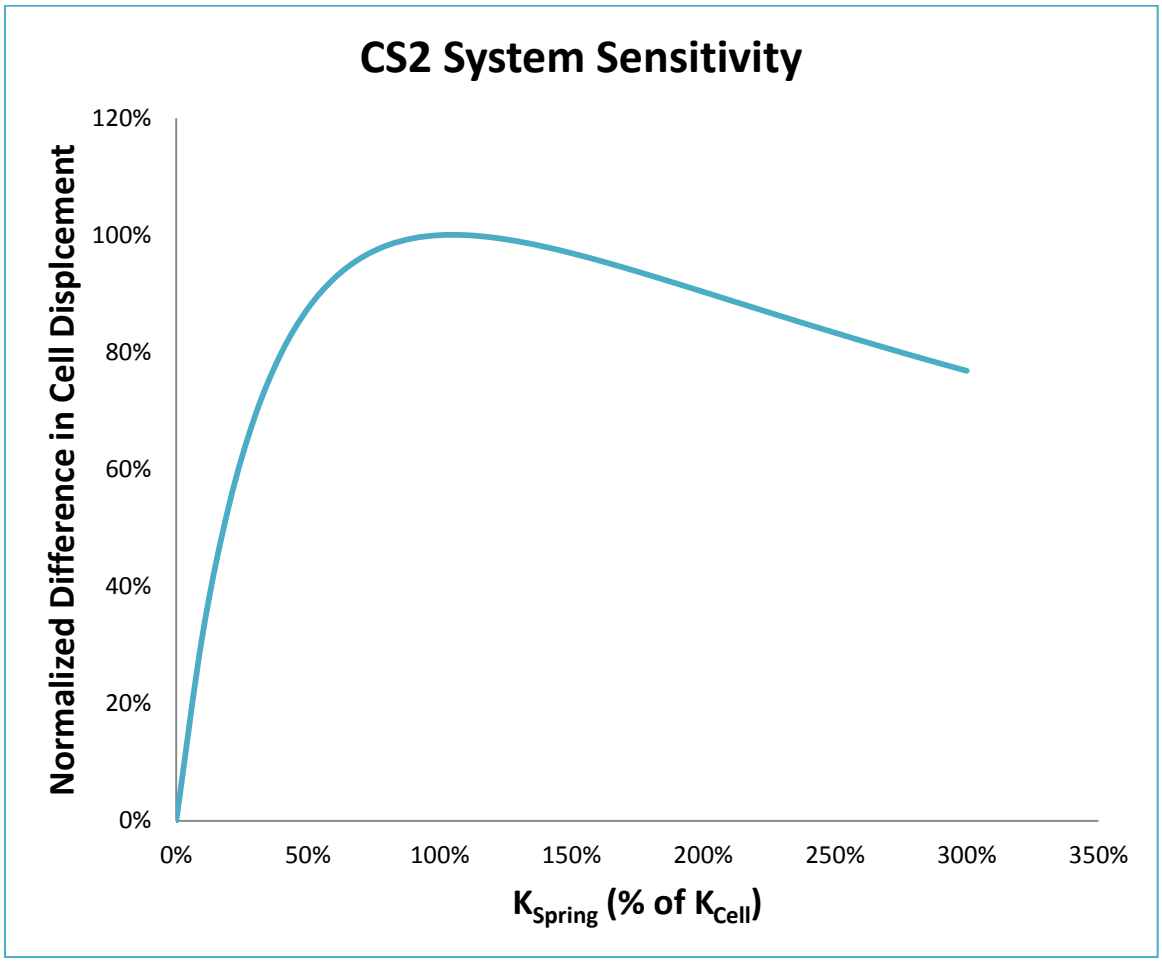

Figure 5.1.3: Cell Squeezer System Sensitivity

In order to match the spring stiffness appropriately, the approximate stiffness ranges for yeast cells must be known.

The mechanical properties of yeast, experimentally determined in literature, are presented in Table 5.1.1. The yeast cell stiffness is not a commonly reported property, and is reported around 1 μN/μm for AFM nano-indentation methods, and 10 μN/μm for an optic fibre probe compression technique. Tests performed with larger cell deformation or indentations resulted in higher values of Young's modulus.

Table 5.1.1: Mechanical Properties of Yeast Cells from Literature (*Max Indentation Values Were Interpreted from Graphs and Figures As Not Explicitly Stated in Literature)

Stiffness, (μN/μm)	Young's Modulus, (Mpa)	Bursting Strength (μN)	Technique	Max Indentation (μm) *	Source
-	-	55-175	Optic fiber probe compression	~5	Mashmoushy et al, 1998 [24]
-	0.6 ± 0.4	-	Nano-indentation Technique Aquatic Test	~0.055	Touhami et al, 2003 [20]
	0.73		Nano-indentation and Oscillation Aquatic Test	~0.007	Pelling et al, 2004 [32]
-	2.0 ± 0.2	-	Nano-indentation Technique Aquatic Test	~0.06	Lanero et al, 2006 [33]
~1	3.53 ± 0.83	-	Nano-indentation Technique	1	Ahmad et al, 2008 [34]
~11	112 ± 6	-	Optic fiber probe compression Aquatic Test	~4	Smith et al, 2009 [19]
-	14.3±10.4	-	Thermodynamic modeling of hyper-osmotic shock	NA	Schaber et al, 2010 [35]
~1	3.24 ± 0.09	-	Nano-indentation Technique		Fukuda, Nakajima, and Ahmad, 2011 [18]
-	12-46		Pressurised Elastic Shell	NA	Vella et al, 2011 [22]

As the reported yeast cell stiffness is a range from ~1-10 μN/μm, the springs in the gripper were designed to range from 0.5 to 240 μN/μm, as presented in the following section.

5.2 Spring Design

The s-springs in the gripper system were designed following formulas by Lai and colleagues (2005). The dimensions were chosen based on an effective length calculated for a chosen stiffness. A schematic of the design dimensions is presented in Figure 5.2.1 [36].

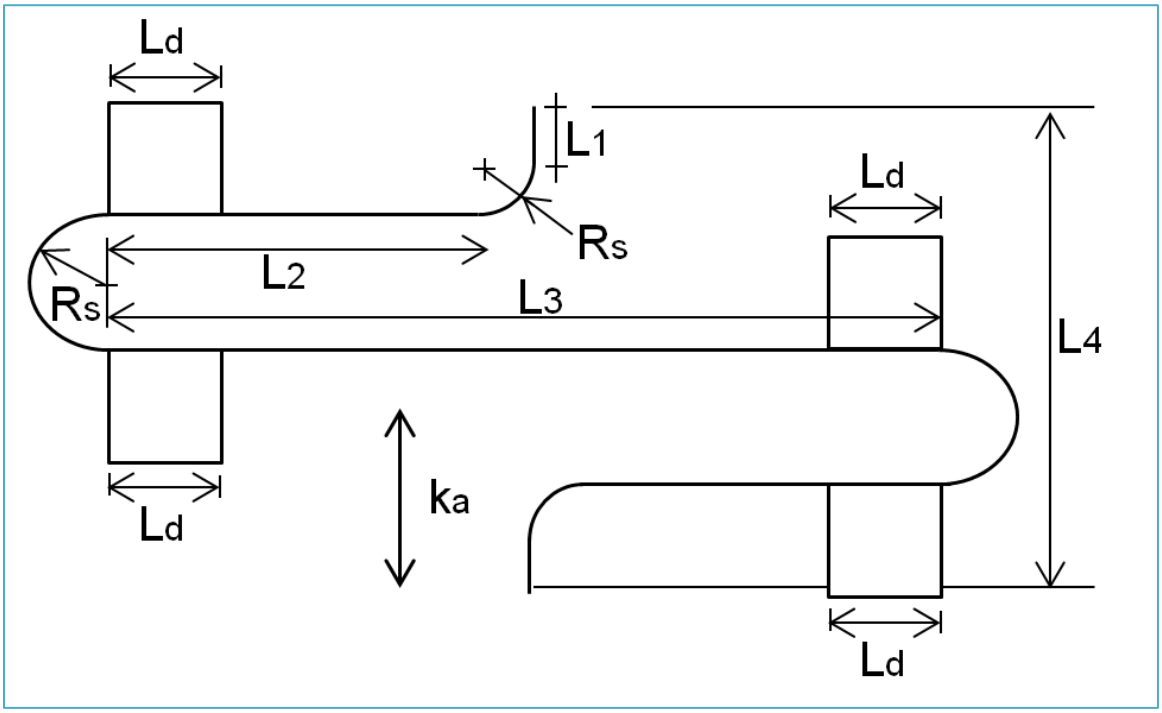

Figure 5.2.1: S-Spring Schematic Showing Dimensions (Adapted from [36])

The axial stiffness of the spring k_a is as follows [36]:

$$k_a = 0.83\left(\frac{250}{L_\propto}\right)^{3.19} \mu N/\mu m$$

Equation 5.2.1

Where $L_\propto$ is the effective length in microns:

$$L_\propto = L_{total} - 4L_d - \pi R_s - \pi R_L$$

Equation 5.2.2

Six s-springs were implemented on CS2; K0.25, K2, K4, K6, K8, and K10. This naming convention is related to spring stiffness. K10 is the stiffest spring while K0.25 is the least stiff. The stiffness of these springs predicted from the formulations by Lai (2005), and the actual stiffness modeled in COMSOL is presented in Table 5.2.1. See Appendix B for a summary of the COMSOL model. Micrographs of the springs are displayed in Figure 5.2.2.

Table 5.2.1: CS2 Spring Stiffness for S-springs

	K0.25	K2	K4	K6	K8	K10
Lai Formulas (μN/μm)	0.5	10	34	70	140	243
COMSOL (μN/μm)	4.1	40	92	140	154	175

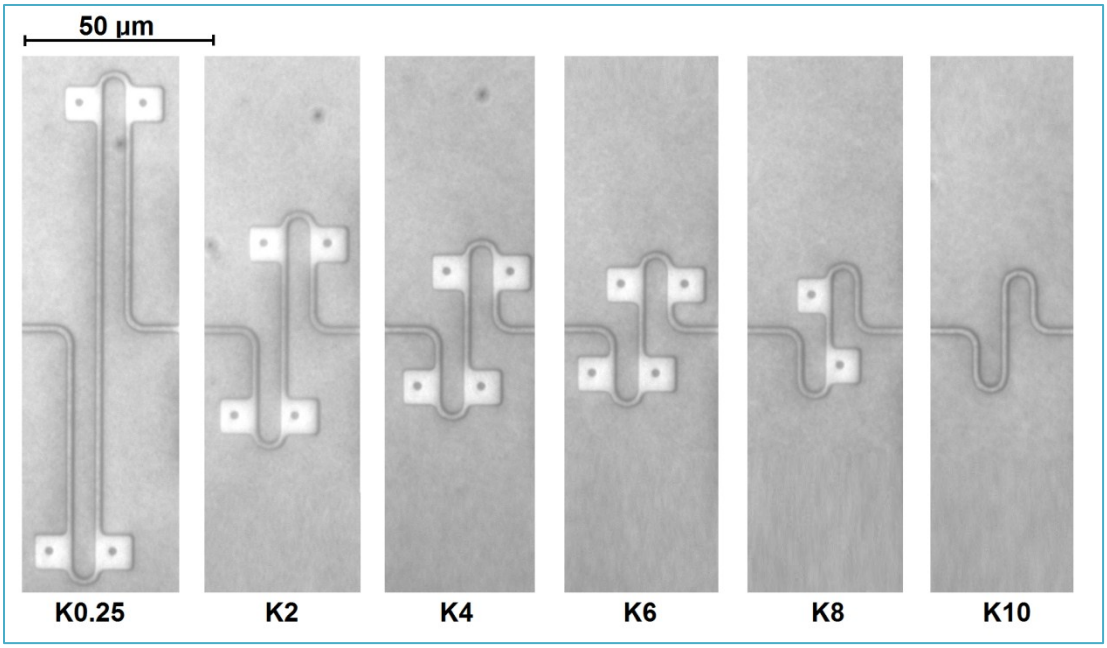

Figure 5.2.2: Micrograph of Fabricated Springs

5.3 U-Spring Design

In order to validate the measurement technique, 'pseudo cells' were tested. The 'pseudo cells' were U-springs with known stiffness. The chip was designed with some gippers having empty jaws allowing for biological cell testing, and some grippers having U-springs connecting the jaws of the device for validation (Figure 5.3.1). The U-springs in the gripper system were designed following formulas by Lai and colleagues (2005). Similarly to the S-spring design, the dimensions were chosen based on an effective length calculated for a chosen stiffness.

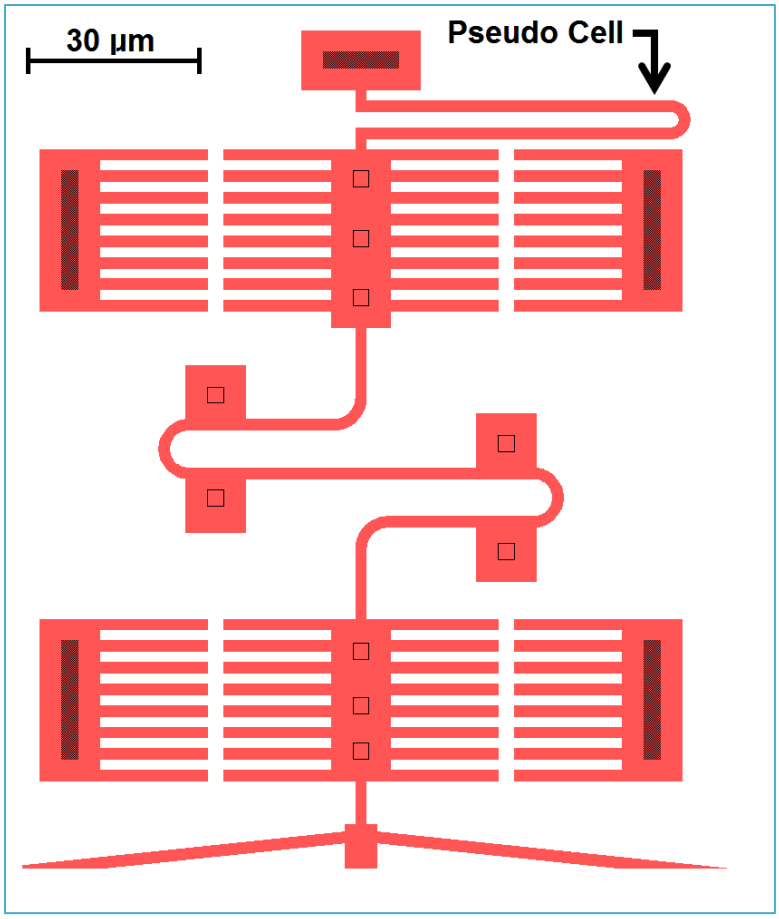

Figure 5.3.1: CS Device with Pseudo Cell

The axial stiffness of the U-spring k_{au} is as follows [36]:

$$k_{au} = 1.66\left(\frac{250}{L_{\propto}}\right)^{3.19} \mu N/\mu m$$

Equation 5.3.1

Two U-springs were implemented, KS and KL (K small and K large). The stiffness of these springs predicted from the formulations by Lai (2005), and the actual stiffness modeled in COMSOL is presented in Table 5.2.1. See Appendix

B for a summary of the COMSOL model. Micrographs of the springs are displayed in Figure 5.2.2.

Table 5.3.1: CS2 Spring Stiffness for S-springs

	KS	KL
Lai Formulas (μN/μm)	0.2	2.0
COMSOL (μN/μm)	2.1	17

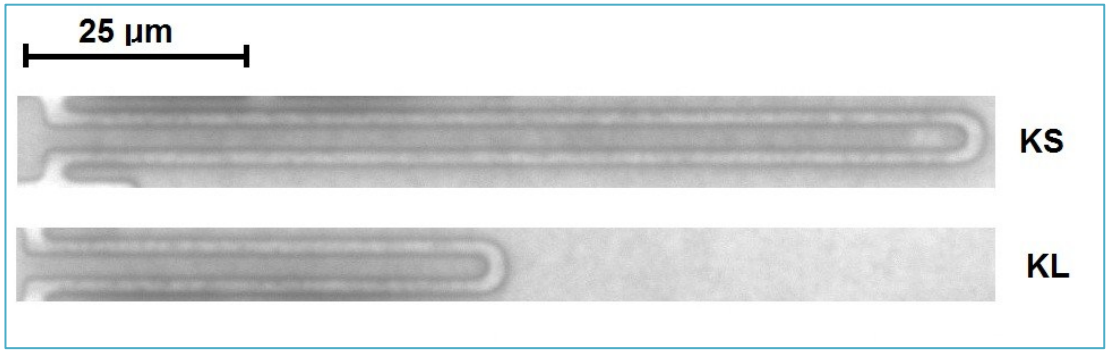

Figure 5.3.2: Micrograph of Fabricated U-Springs

The formulas developed by Lai were for springs with a cross section of 2 by 2 μm. The springs designed for this thesis work were of dimensions 3 by 2 μm, and 3 by 3 μm, therefore the equations were used only for estimating spring dimensions. The actual spring stiffnesses were higher than estimated using Lai's formulas due to the larger cross section. Spring stiffness was determined in COMSOL, and all calculations for cell mechanical properties used the COMSOL values.

5.4 Finite Element Model of Spring Designs

Finite Element Analysis was used to determine the stiffness of the springs in the gripper systems. COMSOL Multiphysics, MEMS Module was used. As the springs are planar, with a constant thickness, a two dimensional modeling approach was used. Poly-Si from the MEMS Module was used for the material.

5.4.1 Constraints and Loading

During operation, the springs undergo axial loading. When modeled, one end of the spring was fixed, and an axial boundary load applied to the other end. The load applied was 10 μN.

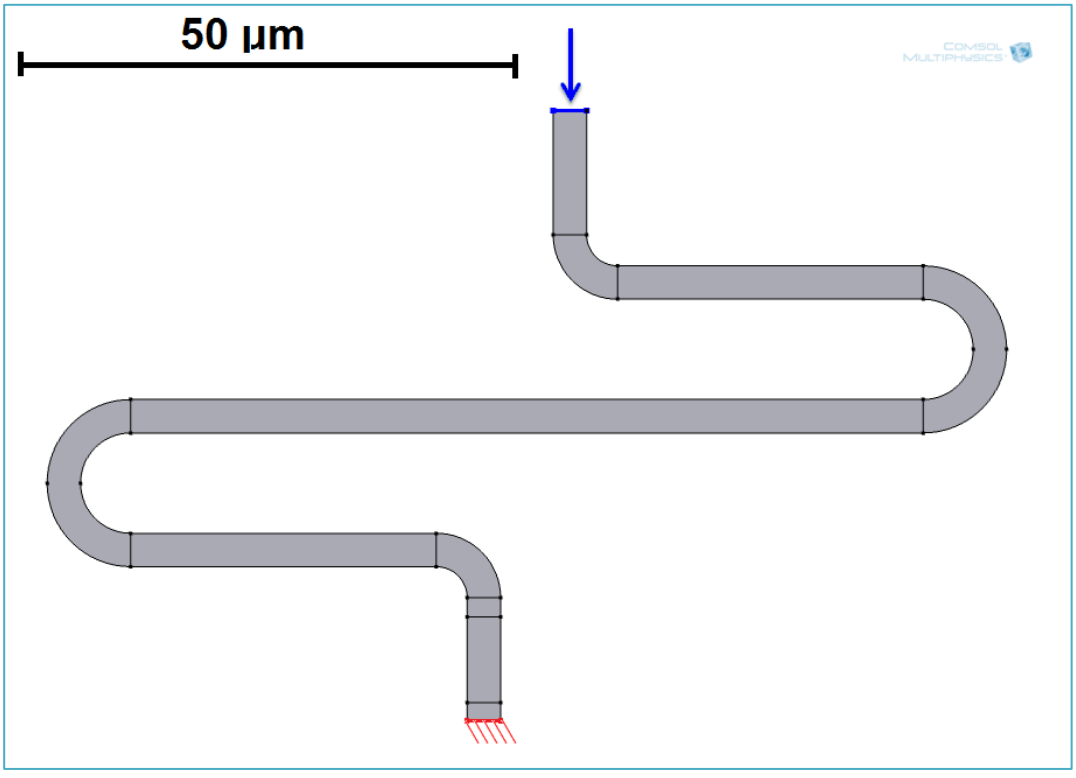

Figure 5.4.1: Schematic of Spring Model Showing Constraints (Fixed Constraint Shown in Red, Boundary Load Shown in Blue)

5.4.2 Element Type

Two dimensional quadrilateral elements were chosen. Generally the use of quadrilateral elements avoids constant stress and artificially stiff members which can be encountered with triangular elements.

5.4.3 Material Properties

The material properties of Poly-Si implemented for this model are presented in Table 5.4.1. The model is Hookean, or linear elastic as the relationship between stress and strain is linear(constant Young's modulus).

Table 5.4.1: Model Material Properties (Poly Silicon)

Property	Name	Value	Unit
Coefficient of thermal expansion	alpha	2.6e-6	1/K
Heat capacity at constant pressure	Cp	678	J/(kg*K)
Relative permittivity	epsilon	4.5	1
Density	rho	2320	kg/m^3
Thermal conductivity	k	34	W/(m*K)
Young's modulus	E	160e9	Pa
Poisson's ratio	nu	0.22	1

5.4.4 Mesh Convergence Study

Care was taken to ensure the smallest dimension, the width of the spring (approximately 3μm), had an appropriate number of elements across it. It is a general rule that a minimum of 3 elements is required across such a component.

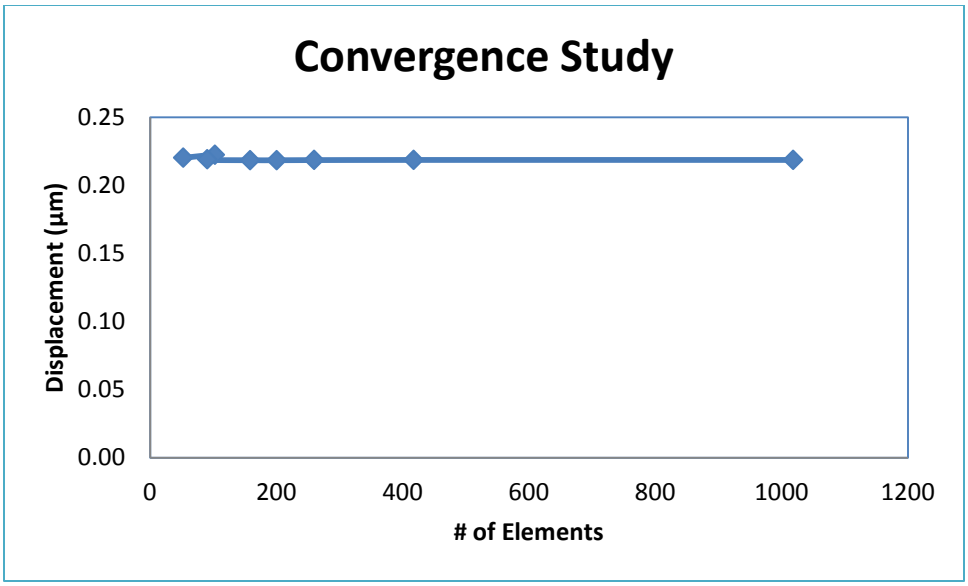

Figure 5.4.2: Convergence Study

Convergence was achieved even with relatively coarse meshes with only one element across the width of the spring. The finest mesh, with 1019 elements was selected. It had 4 elements across the width of the spring, and required less than 5 seconds of computation time.

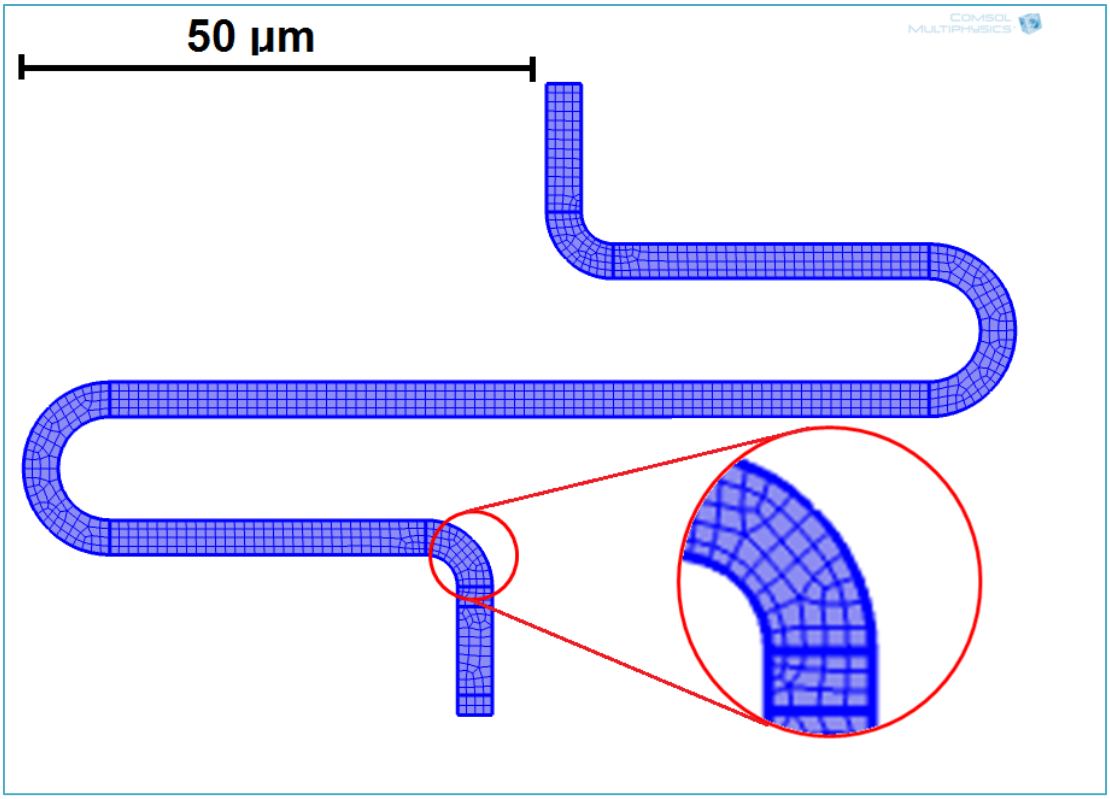

Figure 5.4.3: Schematic of Selected Mesh with Detail (Note 5 Elements Across Spring Width)

5.4.5 Verification of Model

The work of Fettig [44] was used to validate the COMSOL model used in this work. Fettig's thesis documented the simulation and experiments of various micro-joints, including the S-spring used in this work. The spring geometry from Fettig's work was simulated in the COMSOL model developed for this work. See Appendix B for validation geometry.

Experimental testing performed by Fettig compared favourably to his simulations. The measured values of stiffness were lower than the FEA predictions, but generally within 10 – 30% (Table 5.4.2). The COMSOL model implemented for

this work predicted stiffness slightly closer to the experimental values than that of Fettig, falling in the low range of experimental stiffness measured (Table 5.4.2).

Table 5.4.2: Comparison of Fettig's FEA and Experimental Results to COMSOL Results for this Work

S-Spring Variation	**Fettig's Experiments and Simulations [44]**		**This Work**
	Axial Stiffness FEA (μN/μm) [44]	Axial Stiffness Exp. (μN/μm) [44]	Axial Stiffness COMSOL (μN/μm)
X_Std_01	0.63	0.59 ± 0.12	0.48

5.5 Yamahata Combs

In order to determine an ‘optimum’ pitch for the periodic structures, combs with pitches of 2, 3, 4, 5, 6, 8 and 10 μm were implemented on CS2. It was expected that a smaller pitch would produce better displacement measurements, but the imperfect fabrication of the small features, and the shadows cast by the structures may limit the measurements. The results of these tests will be presented later.

5.6 Summary

Cell squeezer 2 (CS2) was developed as an initial investigation into cell testing (Appendix C). The designs include Yamahata combs with pitches ranging from 2 to 10 μm, S-springs with stiffness ranging from 4.1 to 174.5 μN/μm, U-springs (pseudo cells) with stiffness ranging from 2.1 to 17 μN/μm, and both chevron and probe actuated designs. See Appendix D for a summary table of the CS2 chip.

In Figure 5.6.1 an assortment of devices on the CS2 chip are presented. Notice the grippers designed with pseudo cells (A in Figure 5.6.1), those for biological cell testing (B in Figure 5.6.1), and periodic structures for investigation of different pitches (C in Figure 5.6.1).

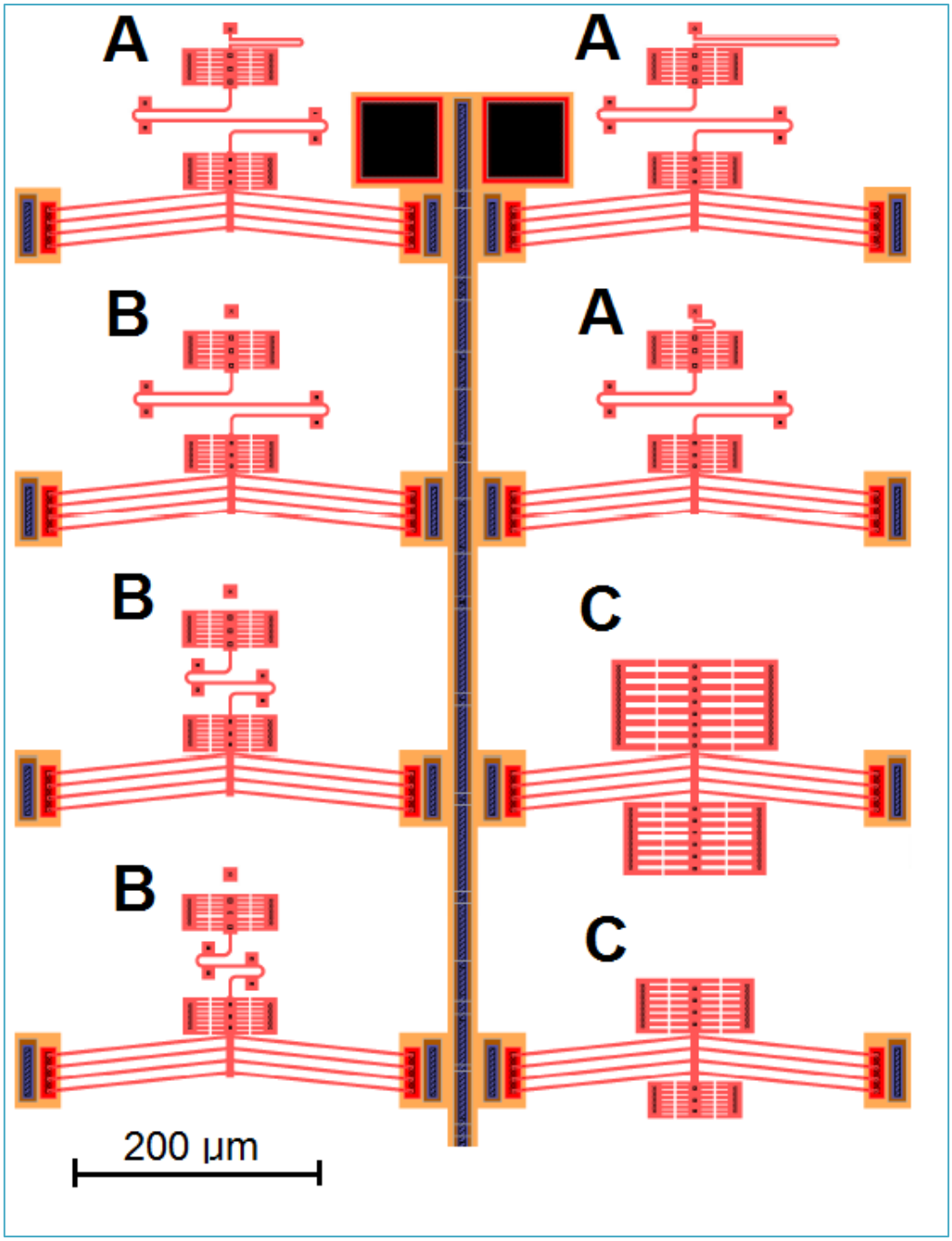

Figure 5.6.1: Assorted Designs on CS2: A-CS with Pseudo Cells, B-CS for Biological Cell Squeezing, and C-Periodic Structures for Pitch Investigation

Chapter 6: Experimental Set-up

6.1 CS Actuation and Imaging

The cell squeezer actuation and imaging will be described in the following section. The outcome of process can be summarized as follows: Voltage steps of 0.5V from 0-8V are sent to the chip. At each voltage step, an image is acquired and saved for processing. MatLab is used to determine a voltage versus displacement curve which is output as an Excel file. The overall flow of software and hardware required for this process is presented in Figure 6.1.1.

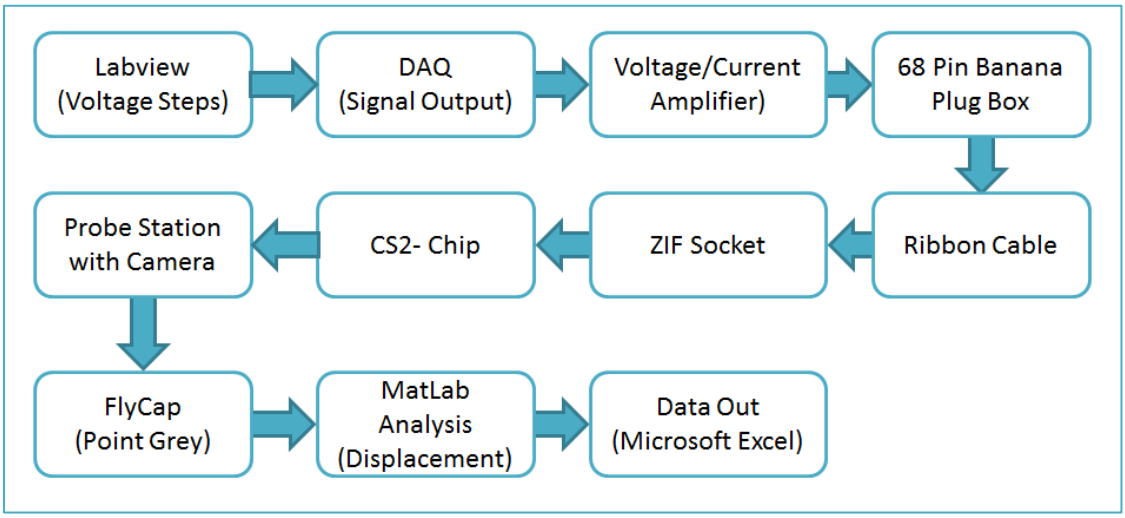

Figure 6.1.1: Cell Squeezer Testing Flow Chart

6.1.1 Hardware

The hardware used to drive the cell squeezer included a PC, a National Instrument PCI-MIO-16E Data Acquisition Card (DAQ), a current and voltage amplifier with a voltage gain of 2. The CS2 and CS4 chips were held in a ZIF

socket which was mounted on a Wentworth™ Probestation Model 901 microscope. The microscope was wired to a 68PGA connection box via a pair of ribbon cables.

Images were captured using a Point Grey™ camera model GRAS-14S3M-C: a 1.4MP B&W 1394b Firewire CCD camera with a maximum resolution of 1280 × 960 pixels, 16 bit grayscale, connected to the Wentworth™ Probestation microscope, 25X objective. In our particular setup, a pixel is 0.298 μm, and regions of interest (ROI) are typically 150 by 250 pixels. Based on a 10 nm precision, our lab has achieved 1/30th of a pixel precision. This camera was connected to the computer via a Firewire cable.

6.1.2 Software

National Instruments™ Labview was used to create a virtual instrument (VI) which sent voltage steps of 0.5V from 0-8V to the chip (via a RS232 cable), acquired, and saved an image for each voltage step. FlyCap, a software application by Point Grey Research was used to stream the camera images to the computer for positioning and cell placement. MATLAB V7.11.0.584 (R2010b) was used to implement the Yamahata technique to determine the voltage versus displacement curves, and Microsoft Office Excel 2007 was used to determine cell mechanical properties.

Chapter 7: Proof of Concept Testing with CS2

7.1 Yamahata Combs

In order to determine the effect of changing the pitch for the periodic structures, pitches of 2, 3, 4, 5, 6, 8 and 10 µm were tested. The effect of the selected region of interest (for grey scale averaging) on the displacement measurement was tested using three different crop areas Figure 7.1.1. Ideally the ROI selected should not affect the results.

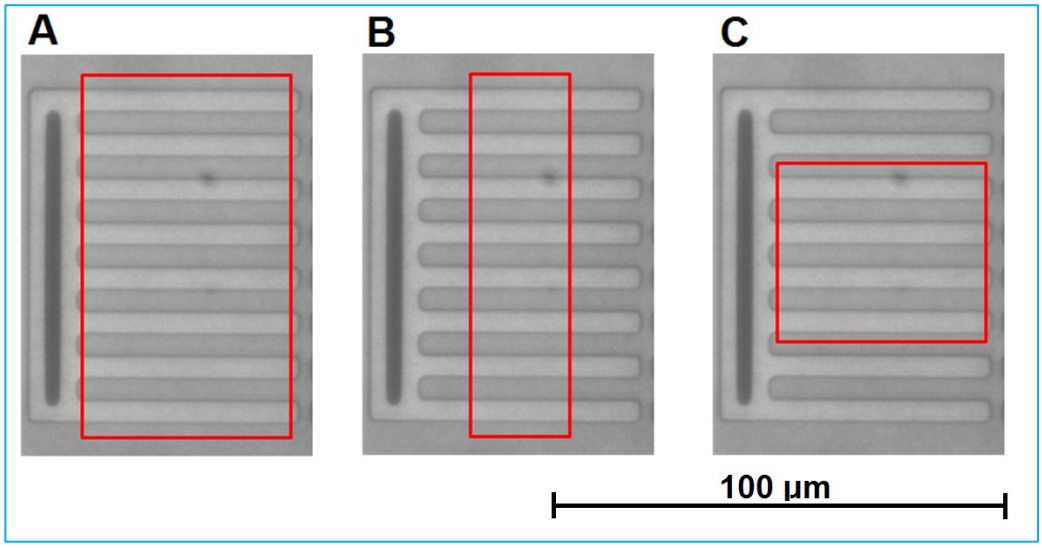

Figure 7.1.1: Different ROIs; A) Full Comb, B) Half Width C) Half Height

The combs with the larger pitch were least sensitive to the chosen region of interest (ROI), producing similar displacement measurements for the different ROIs. This means the larger the pitch, the more robust the measurement system is to different ROIs. Presented in Table 7.1.1 is the percentage error of displacement measurements based of the pitch of the periodic structures. The first column of the table presented the various pitches tested. The second column

contains the total percentage error across one trial, analyzed using three different crop boxes. The third column contains percentage error across three different trials, all analyzed using the same full crop box.

Table 7.1.1: Percentage Error for Displacement Measurements (Across 3 Different ROIs, and Across 3 Trials with Normal Crop boxes)

Pitch (µm)	Percentage Error (Across 3 Different ROIs for one trial)	Percentage Error (Full Crop Box, 3 trials)
4	86	38
6	19	15
8	10	0.1
10	4	0.4

In theory, the smaller the pitch the better the resultant resolution, as resolution is proportional to √Pitch [2]. Results of testing indicate that a larger pitch provided clearer, more accurate displacement measurement. The unexpected results regarding the pitch are likely due to the fabrication process which results in rounded edges on the combs. The smaller combs have very little flat surface, and make it hard to find phase change from the averaged grey scale values. Figure 7.1.2 and Figure 7.1.3 illustrates the difference between a pitch of 10 µm and a pitch of 4 µm. For all following designs, a pitch of 10 µm was used to ensure good resolution, and accurate displacement measurement.

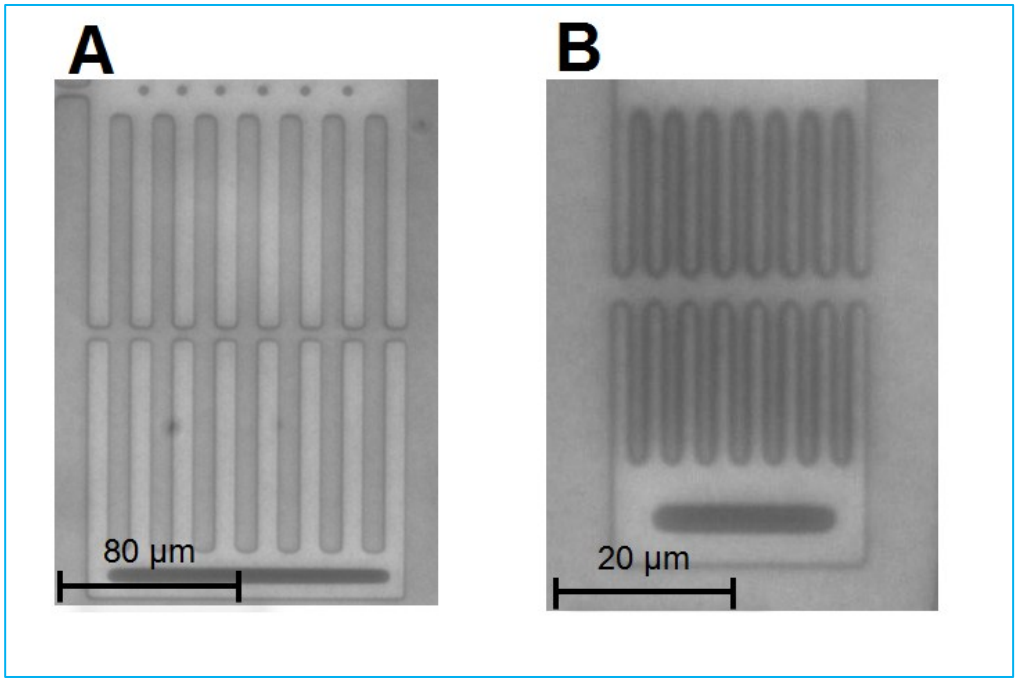

Figure 7.1.2: Different Pitches; A) Pitch= 10 µm, B) Pitch = 4 µm

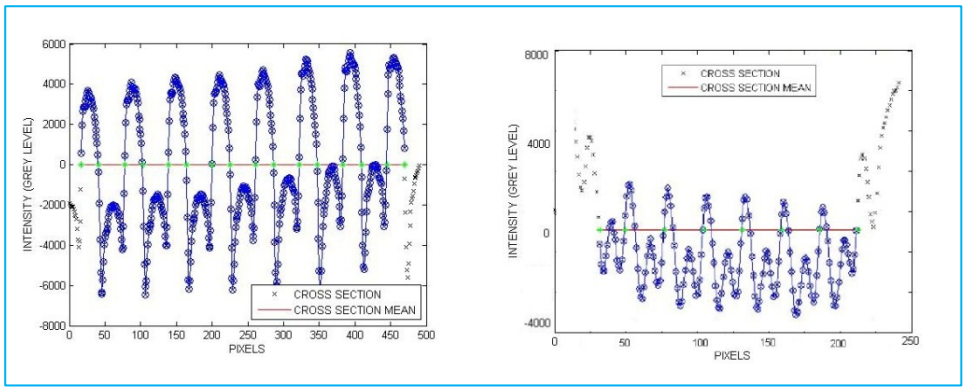

Figure 7.1.3: Intensity Profiles for Different Pitches; A) Pitch= 10 µm, B) Pitch = 4 µm

7.2 CS2 Testing

Testing was performed on IMUDTCS2. Initially, CS devices were tested with no cells present. Following this, tests were performed on the grippers with U-springs, or pseudo cells.

7.2.1 No Cell

A CS system with no cell present should behave as a rigid body, measuring the same displacement at the Input Comb (IC) as the Cell Comb (CC). The cantilevered structure formed by the empty gripper (Figure 7.2.2 and Figure 7.2.4) was subject to stiction forces which pulled it down to the substrate. Tests showed that the CS did not behave as a rigid body. It was assumed the squeezing end of the gripper was 'drooping' down and sticking to the substrate. The cantilevered structure of the gripper design, see cross section (Figure 7.2.1), allows it to be easily effected by stiction forces pulling the end of the beam toward the substrate.

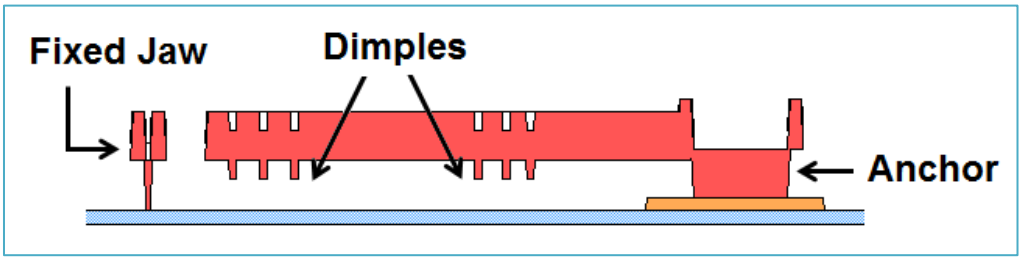

Figure 7.2.1: Cross Section of Gripper (Not to Scale, 10-20 times longer in reality)

This is illustrated in Figure 7.2.3 and Figure 7.2.5. It is observed that the input comb (IC) and cell comb (CC) initially move as a rigid body, but then the displacement of the CC is reduced by stiction forces.

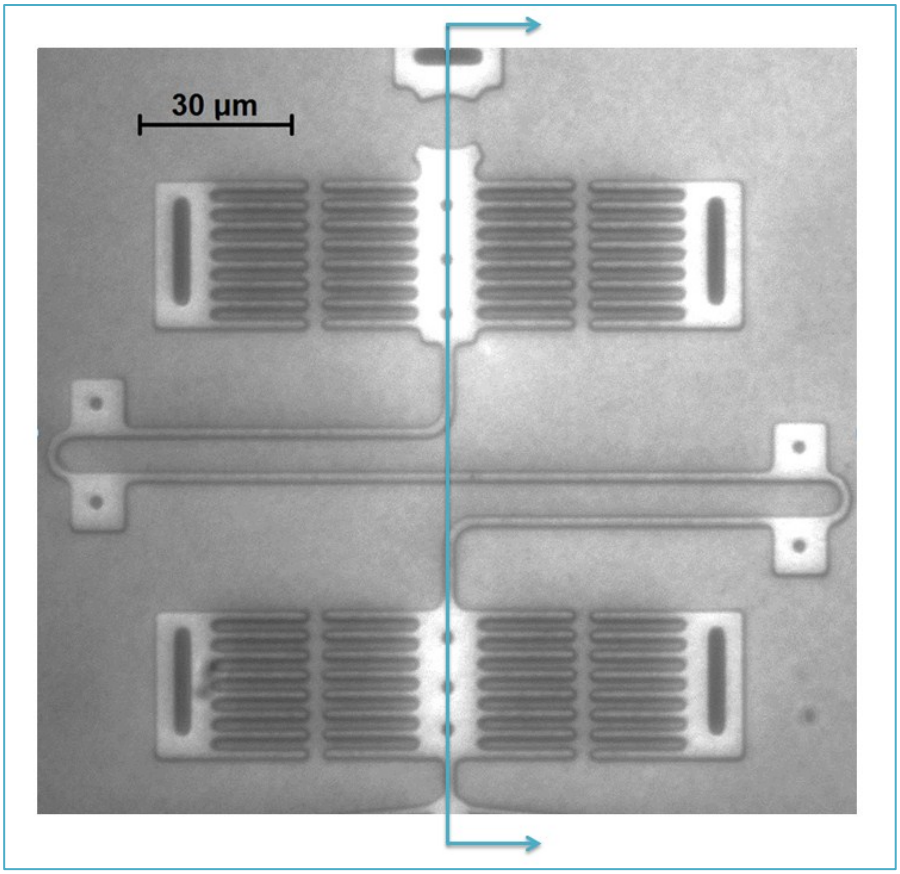

Figure 7.2.2: CS2 (with Spring K=4.1 µN/µm) Cross Section Line Marked in Blue

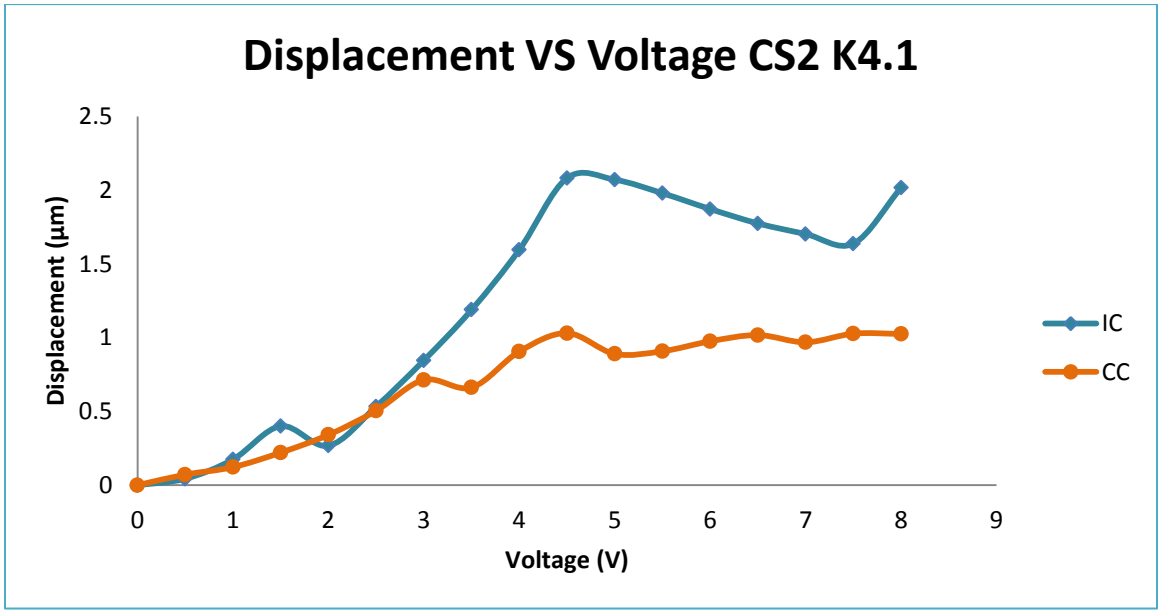

Figure 7.2.3: Displacement vs Voltage for IC and CC (K=4.1 µN/µm)

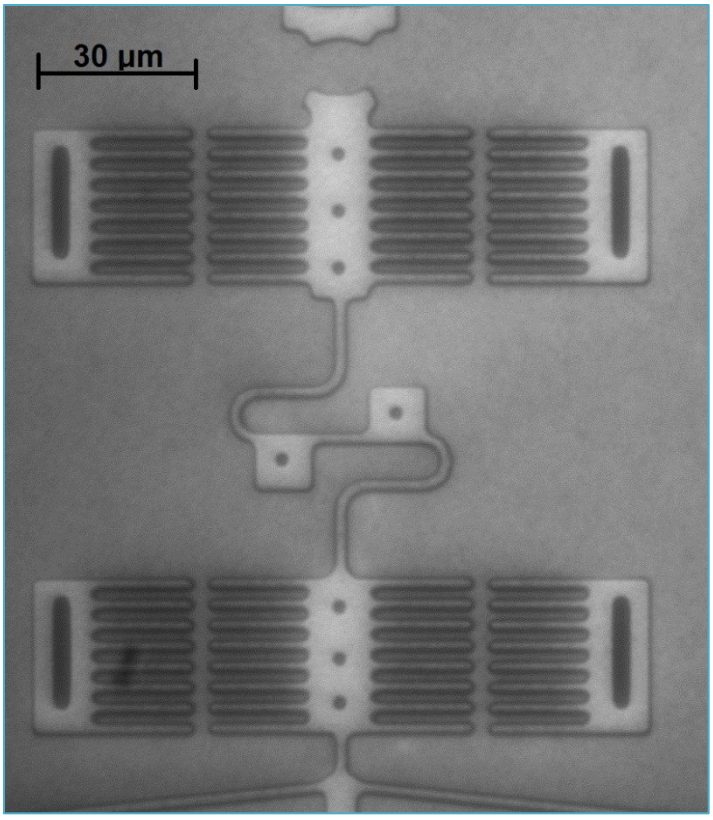

Figure 7.2.4: CS2 (with Spring K=154 µN/µm)

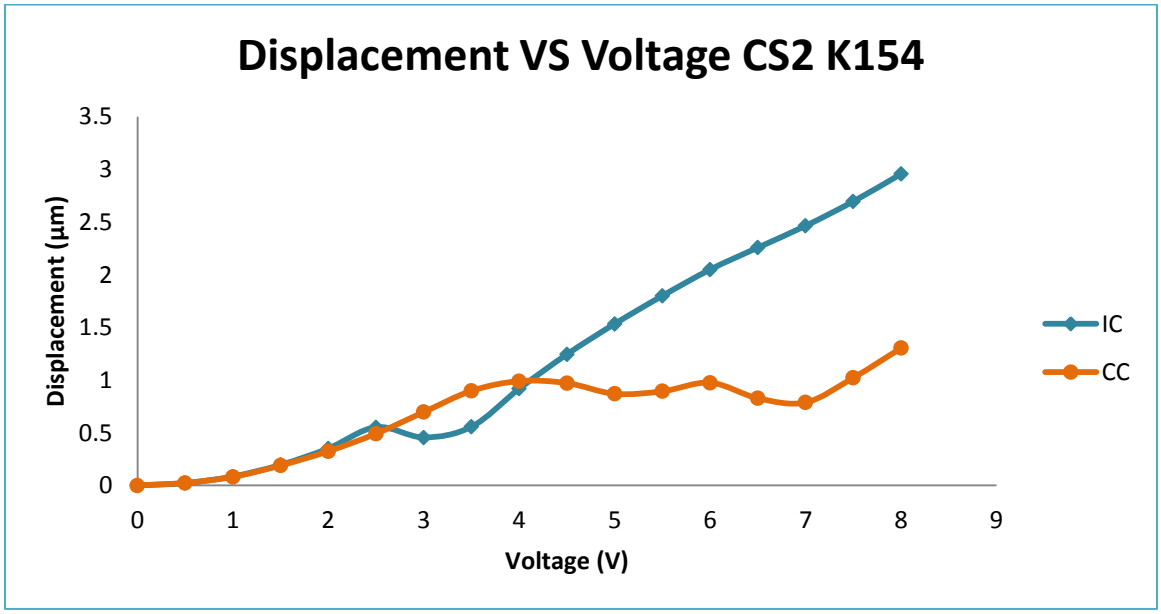

Figure 7.2.5: Displacement vs Voltage for IC and CC (K=154 µN/µm)

7.2.2 Spring Cells

The initial testing indicated that the CS designs of IMUDTCS2 do not behave as rigid bodies in the case with no cell present. Therefore, these CS2 designs cannot be used as meaningful measurement tools. Measurements of cell stiffness and in turn, Young's modulus will be exaggerated by the stiction forces.

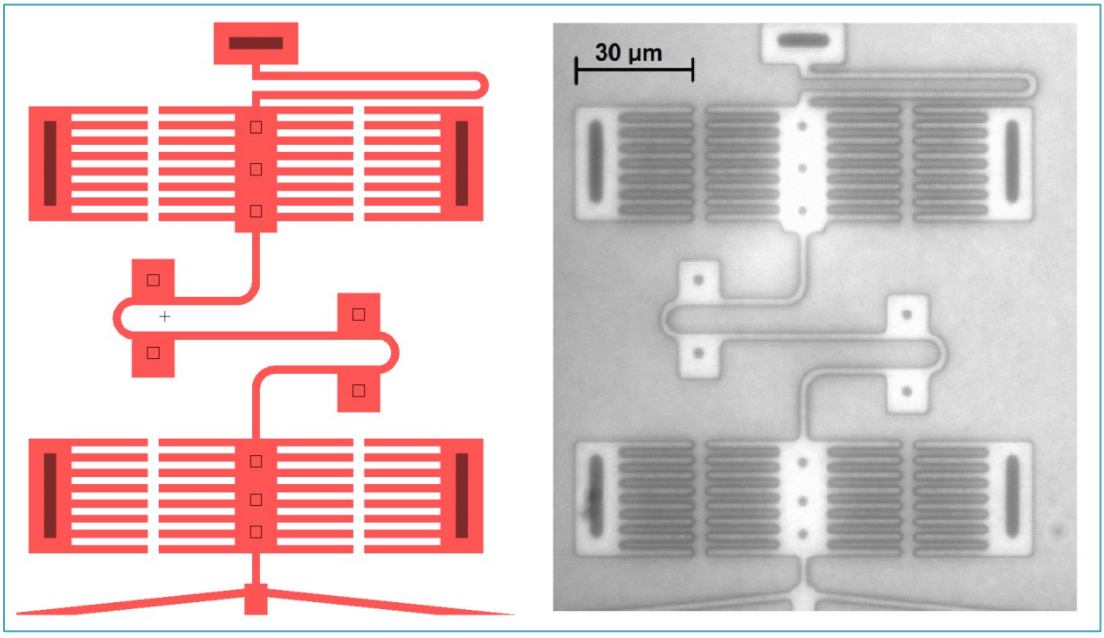

Figure 7.2.6: CS2 (with Spring K= 40 µN/µm and U-Spring =17 µN/µm): L-Edit Layout (Left) and Micrograph (Right)

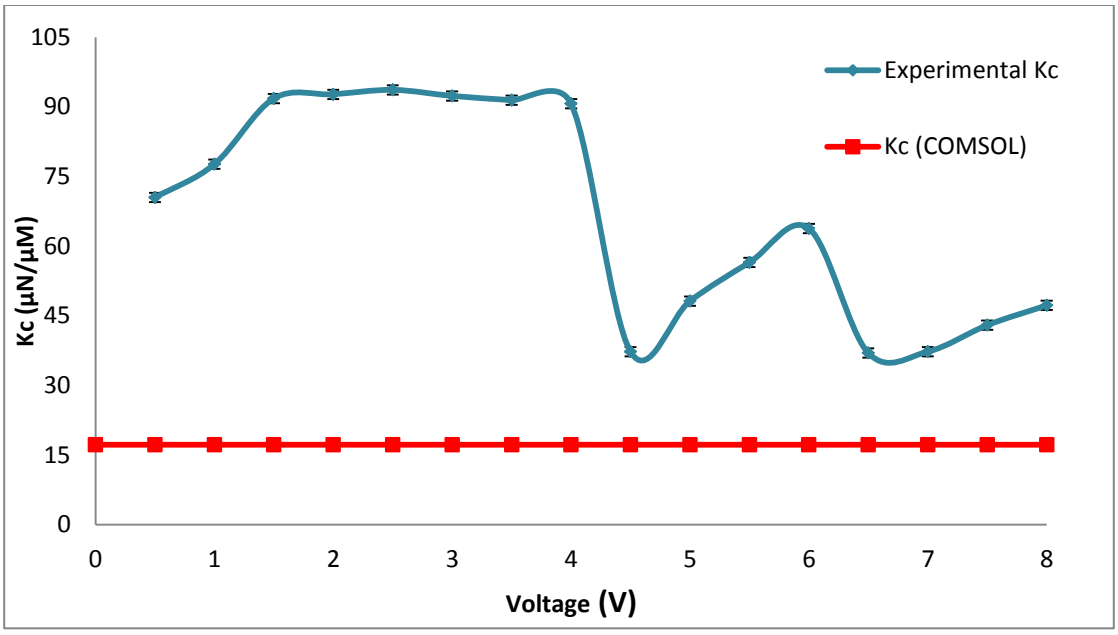

Figure 7.2.7: CS2 (with Spring K= 40 µN/µm and U-Spring =17 µN/µm): Kc vs Voltage

In the above figure, the experimental measurements for the pseudo cell (Figure 7.2.6), or U-spring, stiffness was inconsistently affected by stiction, and much higher than the actual stiffness of 17.2 µN/µm (Figure 7.2.7).

Chapter 8: Redesign to Avoid Stiction: IMUDTCS4

The CS2 structures were cantilevered, and susceptible to being pulled down to the substrate. As presented in previous sections, stiction was observable in many cases of experimental testing on CS2. The following design, CS4 (see Appendix E), incorporated modifications and enhancements to overcome the stiction related issues.

The grippers on IMUDTCS4 have been designed in two categories (Figure 7.2.1). Type A designs are the simple cantilevered structure from IMUDTCS2 and Type B designs have been anchored on the cell squeezing end, with the three springs in a triangular configuration.

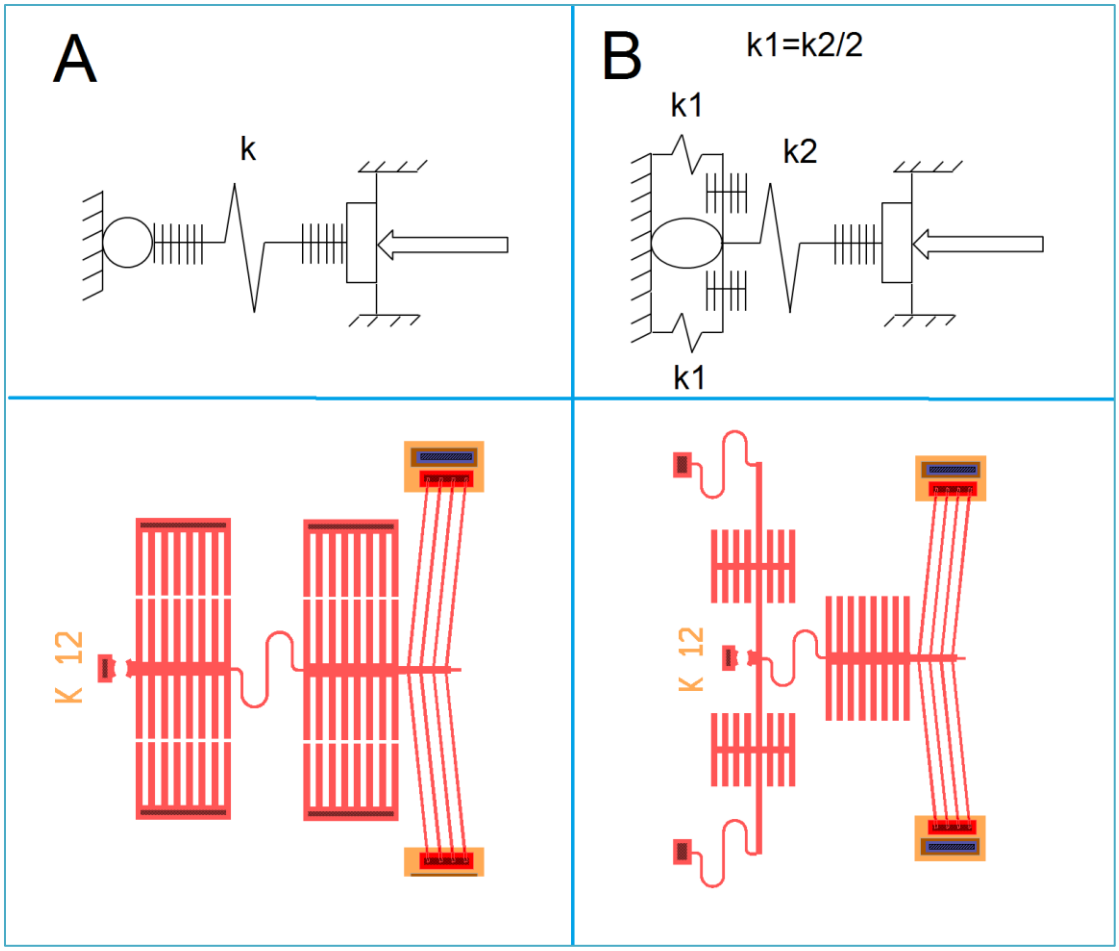

Figure 7.2.1: Schematic of A and B Type Designs (Top), L-edit Designs (Bottom)

The first modification to the gripper designs is the incorporation of double height structures. This improvement increased the thickness of the structure from 2.0 μm to 3.5 μm (Figure 7.2.2). This made the device about 5.5 times stiffer (cube of thickness ratio) in the vertical direction, to prevent stiction, while only increasing the axial stiffness of the device by about 1.8 times (linear thicknes ratio). Type A and Type B grippers were implemented in both single and double height designs.

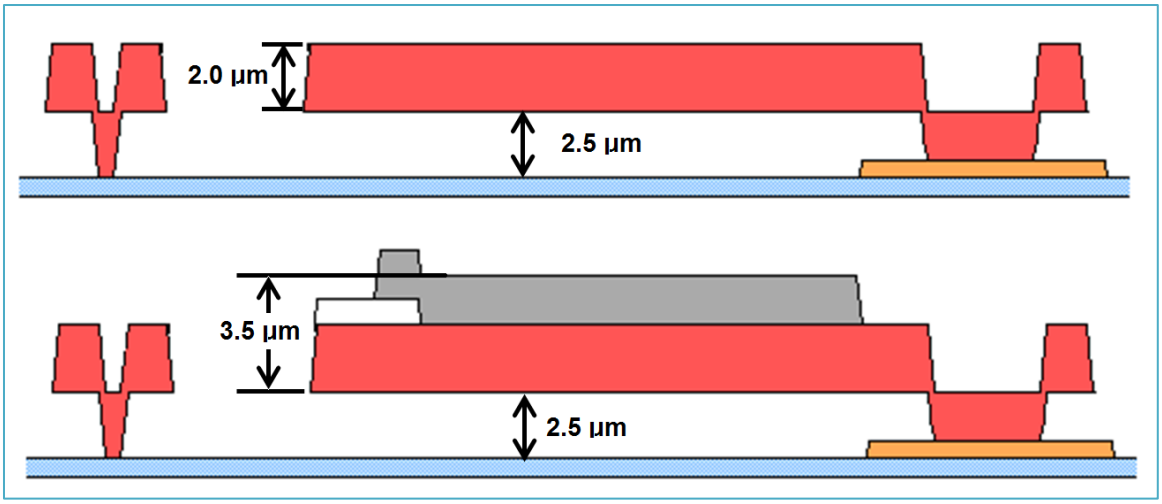

Figure 7.2.2: Single Height (Top) and Double Height (Bottom) Gripper Structures

The jaw design was implemented in single and double height structures as shown in Figure 7.2.3 and Figure 7.2.4.

These two designs enable axial squeezing of cells with diameters of 7 µm and 8.5 µm with the force application at the exact center of the cell.

The second modification was the elimination of the cantilevered gripper. Type B designs have been anchored on the cell squeezing end, with the three springs in a triangular configuration axial stiffness. By having the gripper anchored to the substrate on both ends, stiction due to drooping should be greatly reduced. See Appendix F for a summary table of chip CS4.

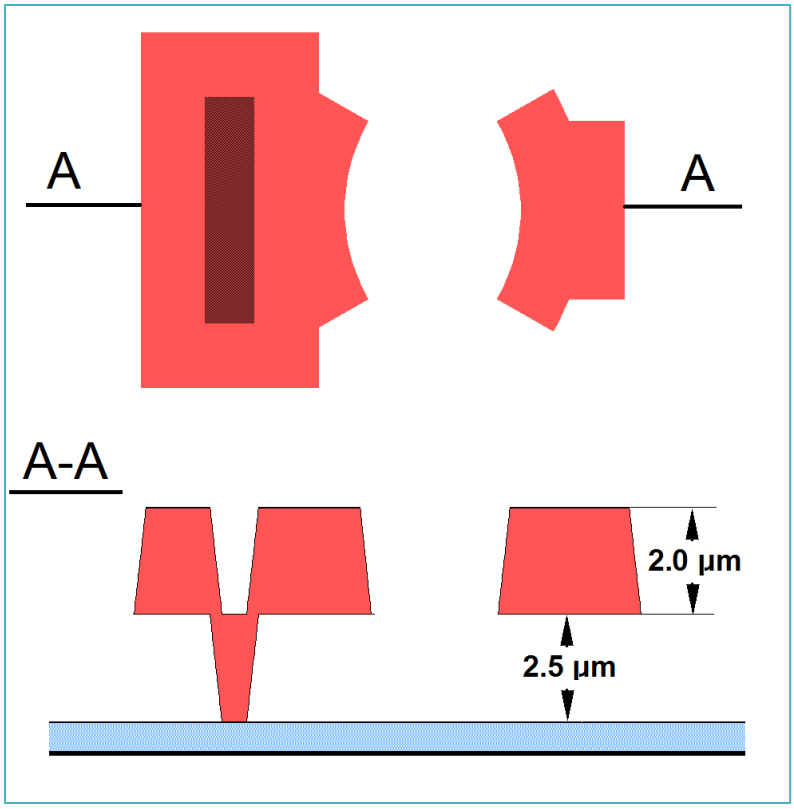

Figure 7.2.3: Single Layer Jaw Design (Not to Scale)

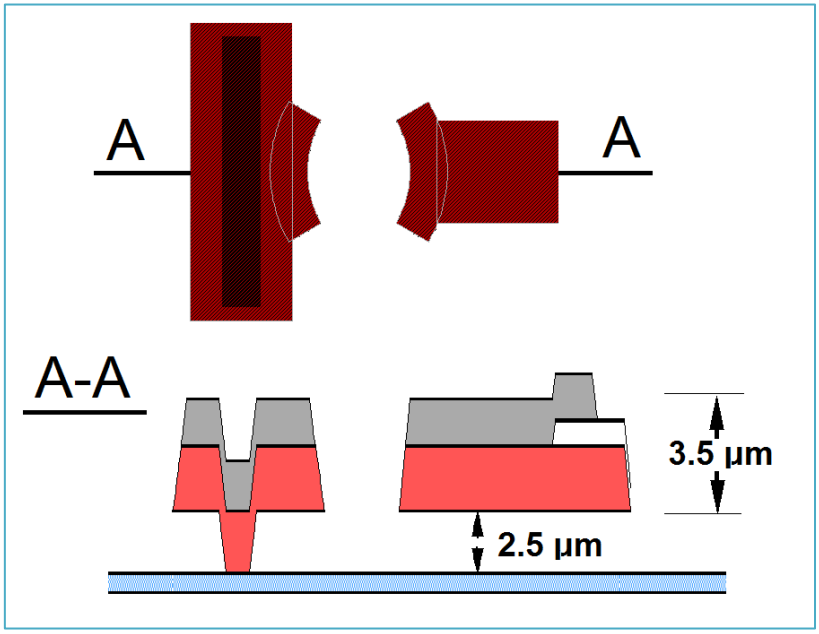

Figure 7.2.4: Double Height Jaw Design (Not to Scale)

All Yamahata combs on CS4 were designed with a pitch of 10 μm. The reference combs use in the CS2 designs did not affect the displacement measurement unless the camera or table was moved during testing. For this reason, on the CS4 designs, the reference combs were not included on all devices.

The cell stiffness can be calculated for Type B grippers similarly to the calculation for Type A grippers. Using the Yamahata technique, the displacements of the CC and IC are determined. Using these displacement measurements, the stiffness of the cell can be calculated as follows for a B Type Gripper (Figure 7.2.5):

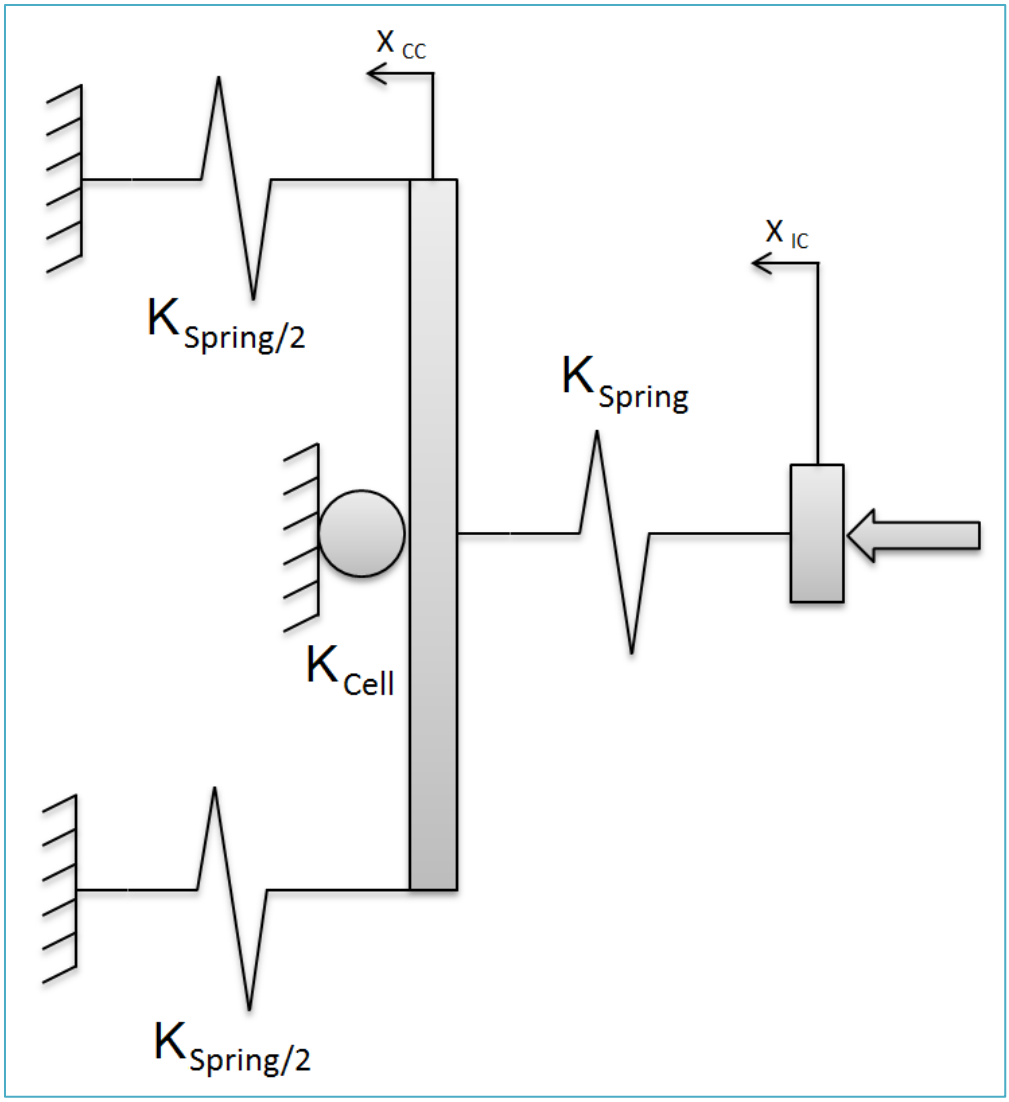

Figure 7.2.5: Spring System Schematic for B Type Cell Squeezer

$$K_{cell} = \frac{K_{Spring}(X_{IC} - 2X_{CC})}{X_{CC}}$$

Equation 7.2.1

8.1 Double Height Spring Design

The double height S-springs in the gripper system were designed following the formulas by Lai just as in the single height case. The S-springs designed for CS4

did not incorporate dimples. The use of dimples prevents the devices from getting stuck to the substrate during fabrication, but dragging of the dimples on the substrate during cell squeezing would falsely increase the measured value of cell stiffness. Increasing the thickness of the spring would make it less likely to adhere to the substrate during fabrication so dimples were not used in this design. The stiffness of these springs predicted from the formulations by Lai (2005), and the actual stiffness modeled in COMSOL is presented in Table 8.1.1. See Appendix B for a summary of the COMSOL model. Micrographs of the springs are displayed in Figure 8.1.1.

Table 8.1.1: CS2 Spring Stiffness for S-springs

	K2A	K2B	K7A	K7B	K12A	K12B
Lai Formulas (μN/μm)	0.2	0.5	1.0	2.3	1.8	4.3
COMSOL (μN/μm)	8.1	15.4	26.9	51.3	45.8	83.4

The formulations created by Lai apply to springs with a 2 by 2 μm cross section. The springs designed for this work had 3.5 by 3.5 μm cross sections. This accounts for the discrepancy between predictions with Lai's formulas, and the COMSOL results.

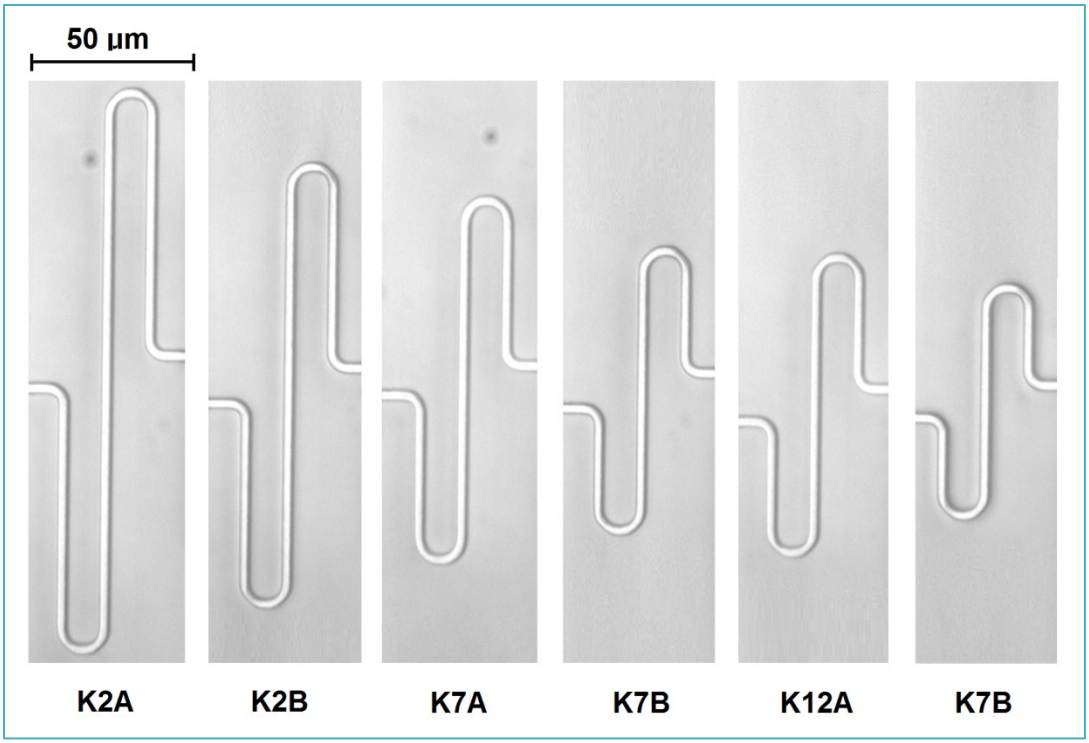

Figure 8.1.1: Micrograph of Fabricated Double Height S-Springs (Note No Dimples)

8.2 U-Spring Design

The U-springs were designed as in the single height case. Two U-springs were implemented, KDS and KDL (K double height small and K double height large). The stiffness of these springs predicted from the formulations by Lai (2005), and the actual stiffness modeled in COMSOL is presented in Table 8.2.1. See Appendix B for a summary of the COMSOL model. Micrographs of the springs are displayed in Figure 8.2.1.

Table 8.2.1: CS2 Spring Stiffness for S-springs

	KDS	KDL
Lai Formulas (µN/µm)	5.7	29
COMSOL (µN/µm)	29	103

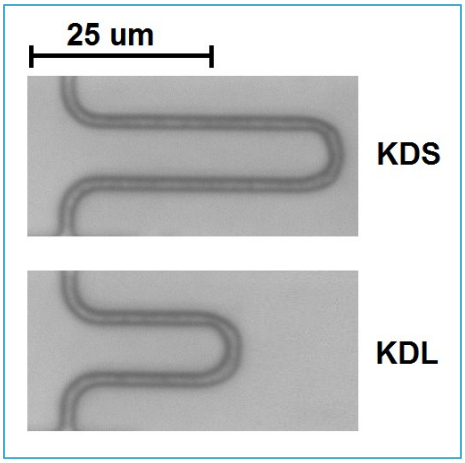

Figure 8.2.1: Micrograph of Fabricated Double Height U-Springs

As mentioned in the single height spring section, all calculations for cell mechanical properties used the values determined with COMSOL.

8.3 CS4 Testing of A and B Type Grippers

Initial testing of CS4 devices indicate that many of the devices had suffered from fabrication stiction. Neither single layer Type A or Type B designs were usable due to low yield (see Appendix G). Increasing the thickness of the Type A grippers from single layer to double layer resulted in an improvement of almost 4 times in the number of working devices, but stiction rendered the measurement devices useless Figure 8.3.1.

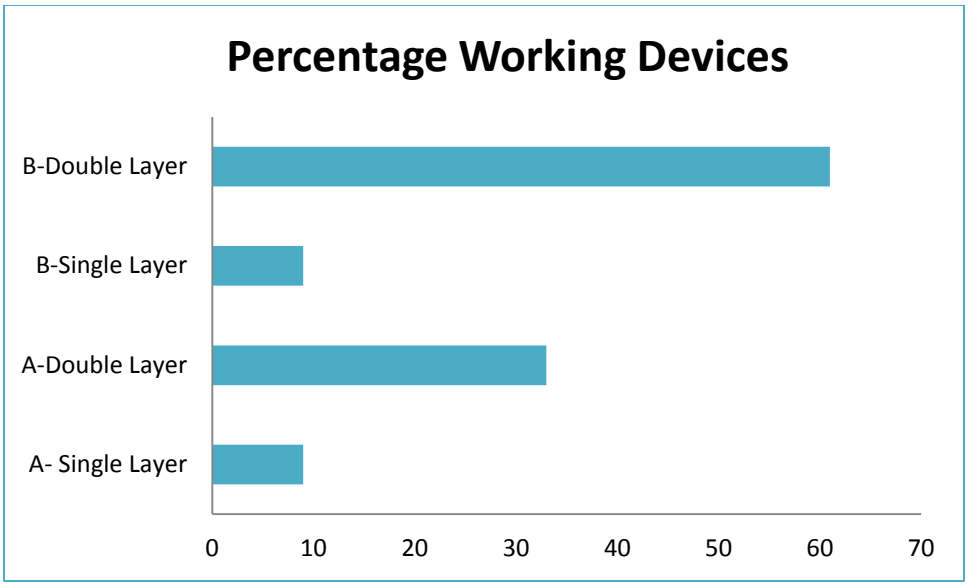

Figure 8.3.1: Percentage of Working Devices Based on Device Type

Increasing the thickness of the Type B grippers from single to double layer resulted in an improvement of almost 7 times in the number of working devices. Approximately 60% of double layer Type B designs were usable across all 15 chips.

CS4 testing was performed on double height Type B structures, initially with no cell present, then with pseudo cells (U-springs), and finally with yeast cells.

8.3.1 No Cell

Testing of the Type B designs with no cell present (Figure 8.3.2) resulted in motion closer to that of a rigid body than CS2 designs (Figure 8.3.3). The offset between the Input Comb (IC) and Cell Comb (CC) final displacement ranged from 0.2 μm to 0.4 μm. It is possible that some of this discrepancy is a result of the end of the gripper 'drooping' toward the substrate. If the gripper was at an

angle of even 0.05˚-0.1˚ below horizontal, this would be enough to result in a loss of 0.2 to 0.4 µm across the 214 µm cantilevered length of the system.

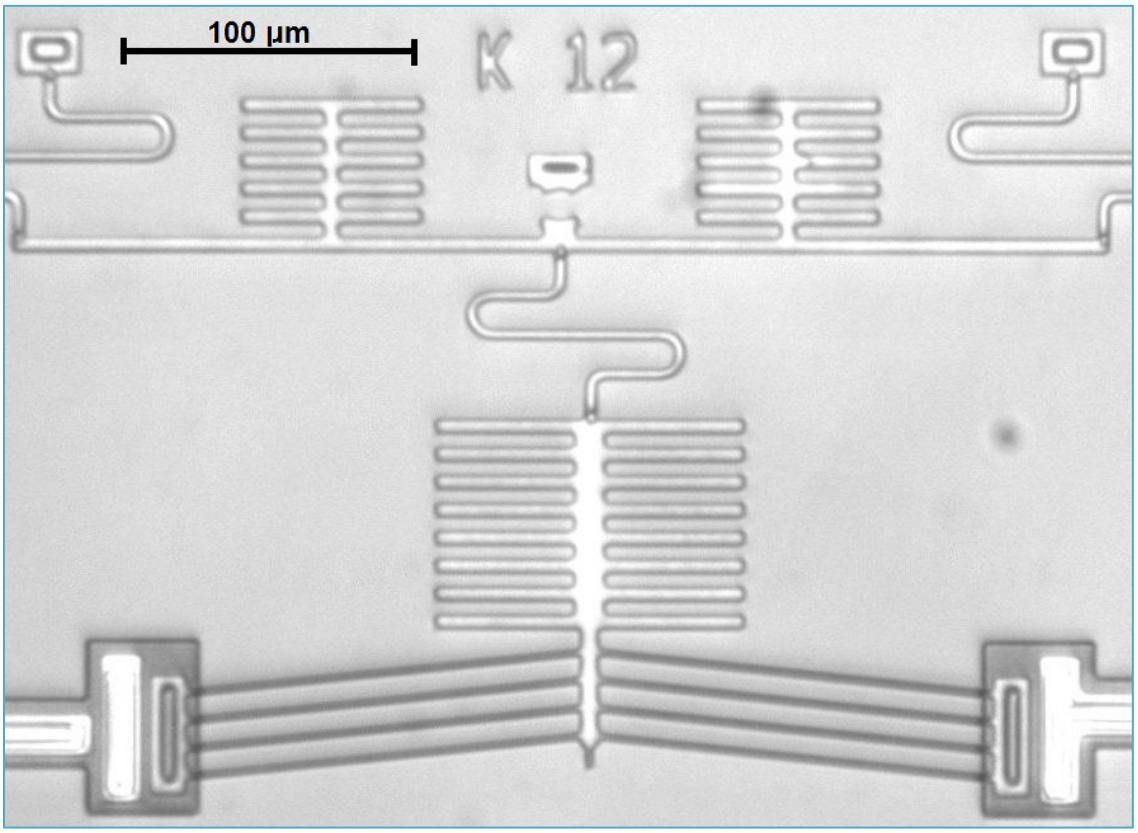

Figure 8.3.2: CS4 (B-Type Double Height with Spring K=104 µN/µm)

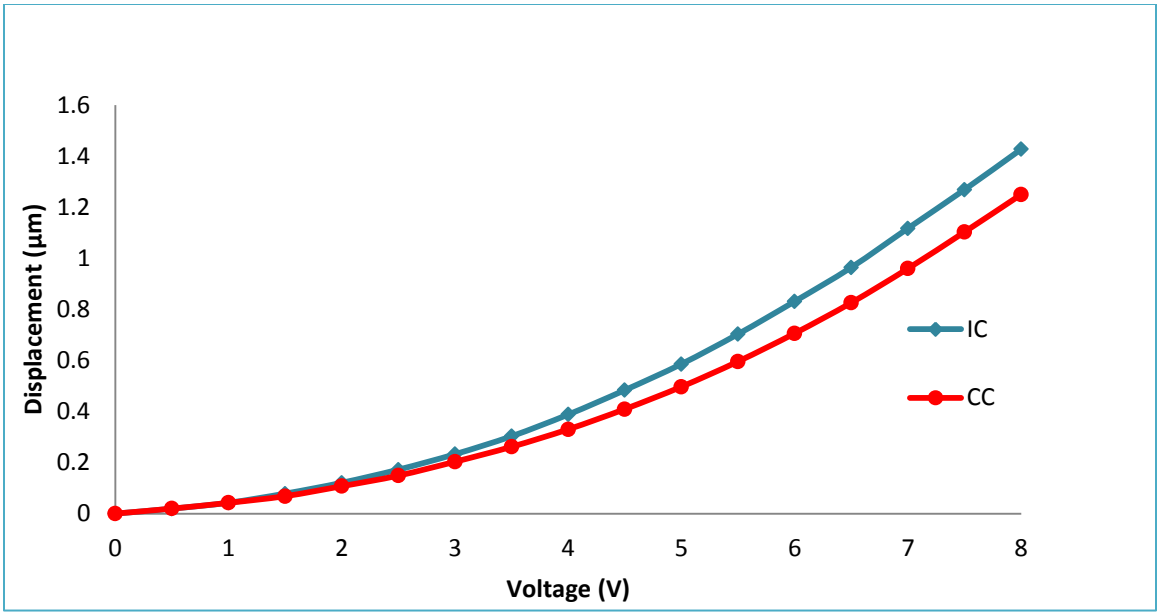

Figure 8.3.3.: CS4 (B- Type Double Height with Spring K=104 µN/µm): Displacement vs Voltage for IC and CC

8.3.2 Spring Cells

Double height Type B grippers with U-springs (pseudo cells) of 29 µN/µm and 103 µN/µm were tested, and the values calculated for the pseudo cells based on the displacement measurements.

The first case was for the U-spring with a stiffness of 29 µN/µm (Figure 8.3.5). Data was collected from 4 chips. Each chip was tested 3 times, and each set of data analysed for 3 different ROIs resulting in 36 values for each data point (Figure 8.3.6).

Residual stress from manufacturing resulted in preload forces within the springs. This is observed in Figure 8.3.4, which shows the initial position of the moving and reference comb. The slight offset of the combs indicates residual stresses were present.

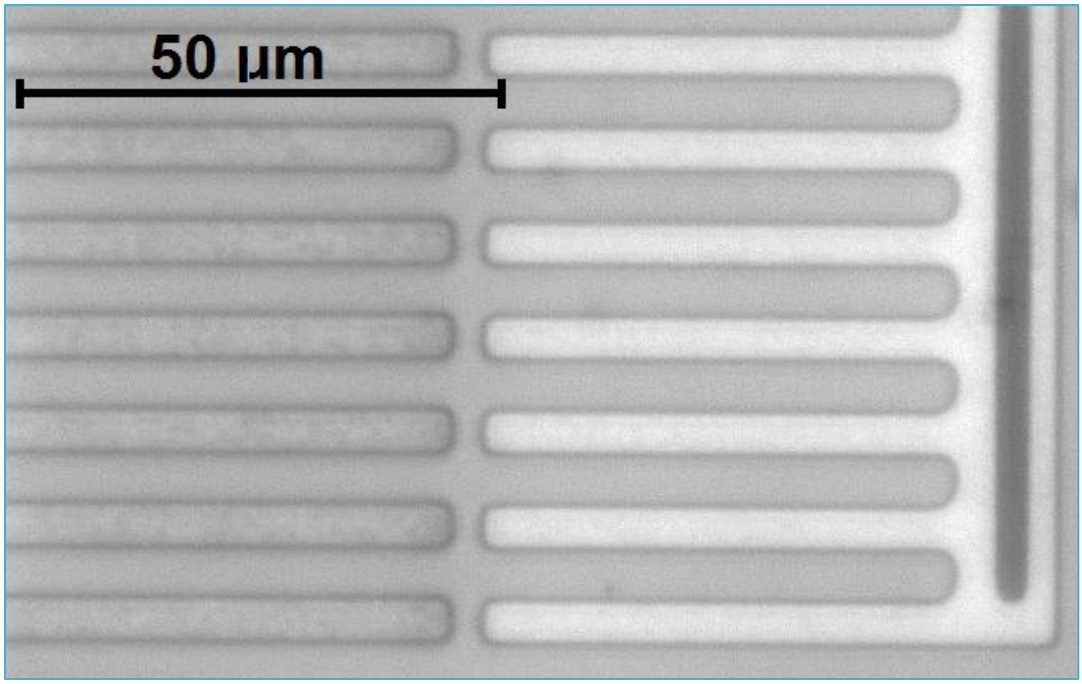

Figure 8.3.4: Initial Comb Position (0V)

The residual preloads existing in the springs following fabrication likely caused some error in the cell stiffness measurements at small voltages and displacements (See Appendix H). Therefore, data below 2 volts is disregarded in all cases for the stiffness calculations (from figure 8.3.5 this corresponds to a displ of about .2 um). At larger displacements, the small preload displacement has less of an effect on the measured stiffness, resulting in an error of approximately 4 -7 % at final displacements. The calculated value of stiffness (averaged from 2 to 8 V) was 20 µN/µm, having a 41% absolute error.

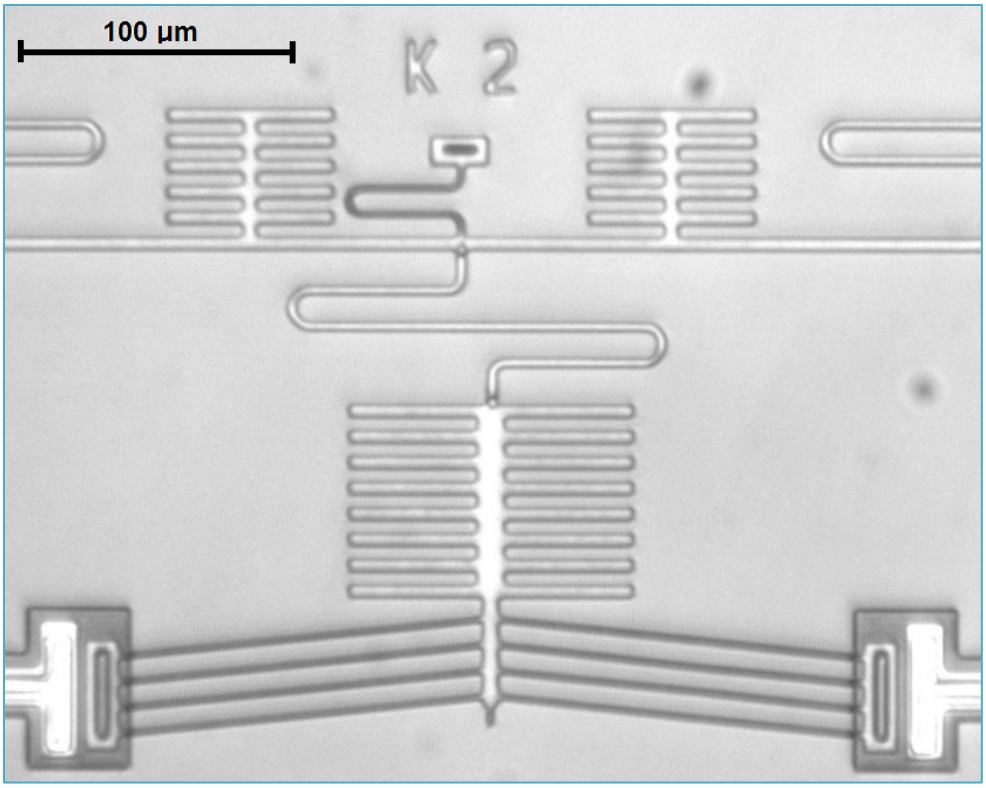

Figure 8.3.5: CS4 (Double Height with Spring K=15 µN/µm and U-Spring 29=µN/µm)

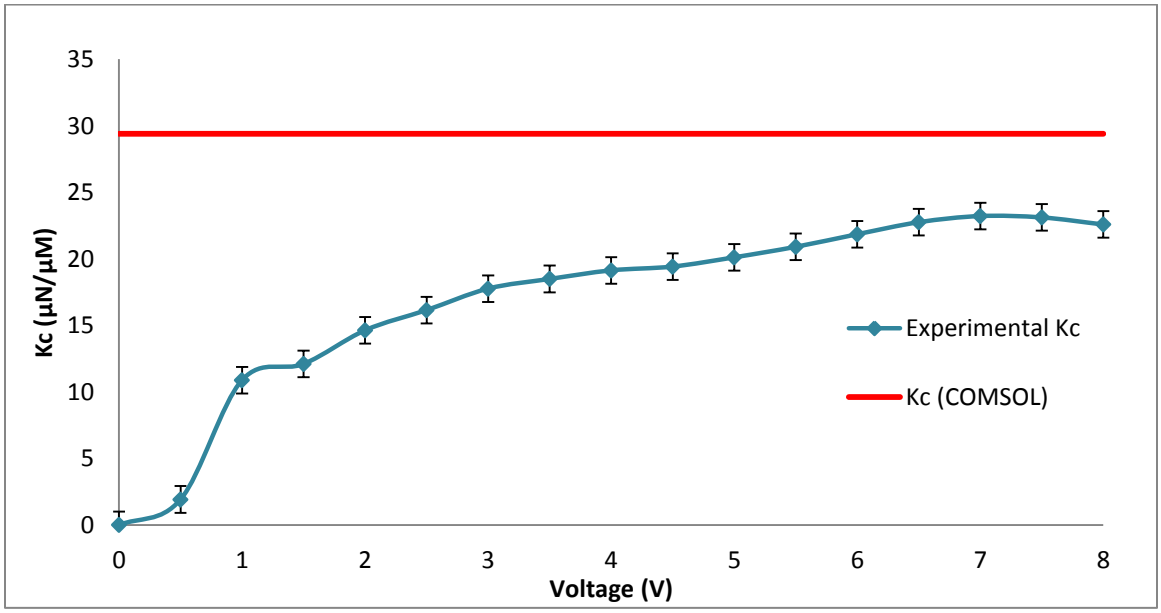

Figure 8.3.6: CS4 (Double Height with Spring K=15 µN/µm and U-Spring 29=µN/µm): Kc vs Voltage (Experimental and COMSOL Kc)

The second case was for the U-spring of 103 μN/μm (Figure 8.3.7). Data was collected from 6 chips. Each chip was tested 3 times, and each set of data analysed for 3 different ROIs resulting in 54 values for each data point (Figure 8.3.8). The calculated value of stiffness (averaged from 2 to 8 V) was 103 μN/μm.

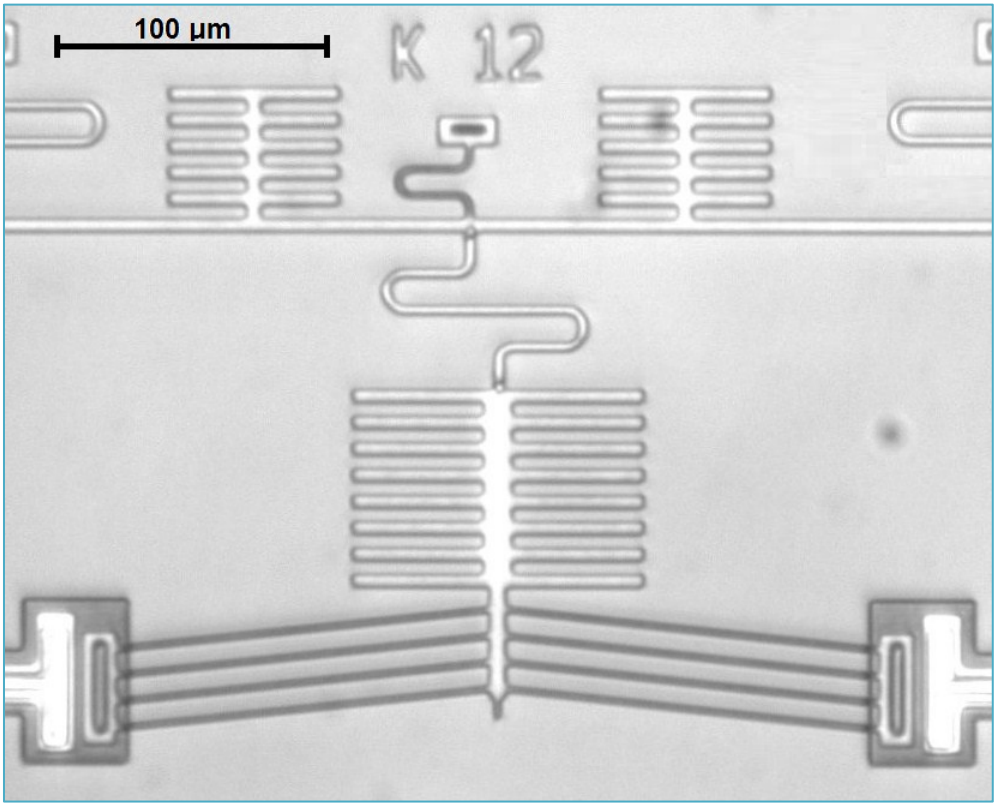

Figure 8.3.7: CS4 (Double Height with Spring K=83 μN/μm and U-Spring 104=μN/μm)

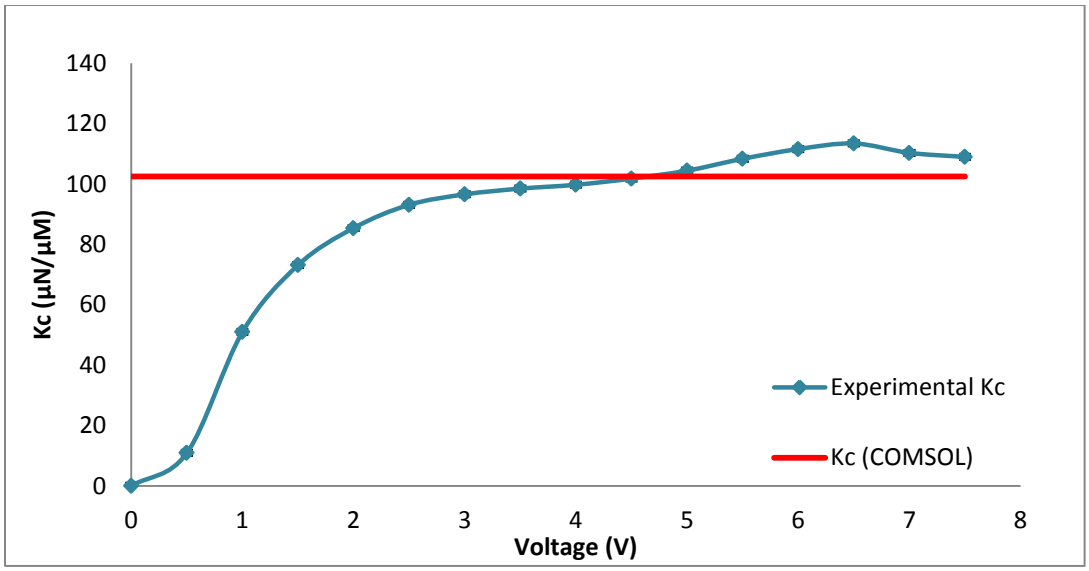

Figure 8.3.8: CS4 (Double Height with Spring K=83 µN/µm and U-Spring 104=µN/µm): Kc vc Voltage (Experimental and actual Kc)

Chapter 9: Cell Testing with CS4

9.1 Scope of Cell Testing

Based on exploration of the CS designs on CS4, it was determined that the double height Type B structures were the most suitable for cell testing. Successful cell testing was performed with B Type designs on 4 different chips. As the forces applied were at or near the chevron force limit, many tests were disregarded as a result of chevron buckling at high voltages (Figure 9.1.1).

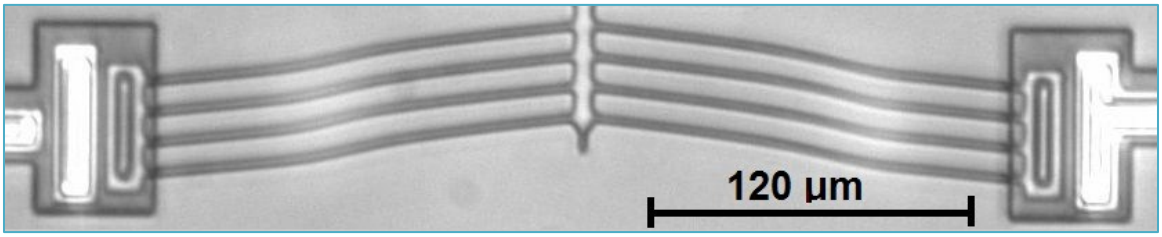

Figure 9.1.1: Buckled Chevron

9.2 Cell Preparation and Placement Method

Cell placement was performed using the well-established technique of the glass capillary micropipette. As the cell testing is being performed as a proof of concept, processing of large number of single cells was not performed. This means costly, automated systems for cell manipulation can be avoided.

9.2.1 Yeast Preparation

Baker's yeast, *Saccharomyces cerevisiae,* was used for cell testing as it is readily available, robust, and does not require an ethics procedure to use in the lab. The yeast was prepared according to manufacturer's instructions. Fleischmann's Active Dry Yeast was used. The yeast was mixed with 38ºC

water, and sugar at ratios of 11:50:5 respectively. The mixture was left to stand for 10 minutes, at which point the mixture doubles in size. Small amounts of the mixture are diluted with 38ºC water for viewing under the microscope.

9.2.2 Hardware

The cell pick and place system made use of the Wentworth™ Probestation Model 901 microscope, an additional side-mounted light source, a micropipette mounted on a 3 degree of freedom Wentworth™ probe station (Model PRO195LH), Polytetrafluroethylene tape by Seal Tape, Inc., 1.40 mm inner diameter and 1.80 mm outer diameter polyethylene capillary tubing, a 10 µL syringe, and the high resolution camera by Point Grey™. A schematic of this system is presented in Figure 9.2.1 [8] and the implemented system is presented in Figure 9.2.2 and Figure 9.2.3.

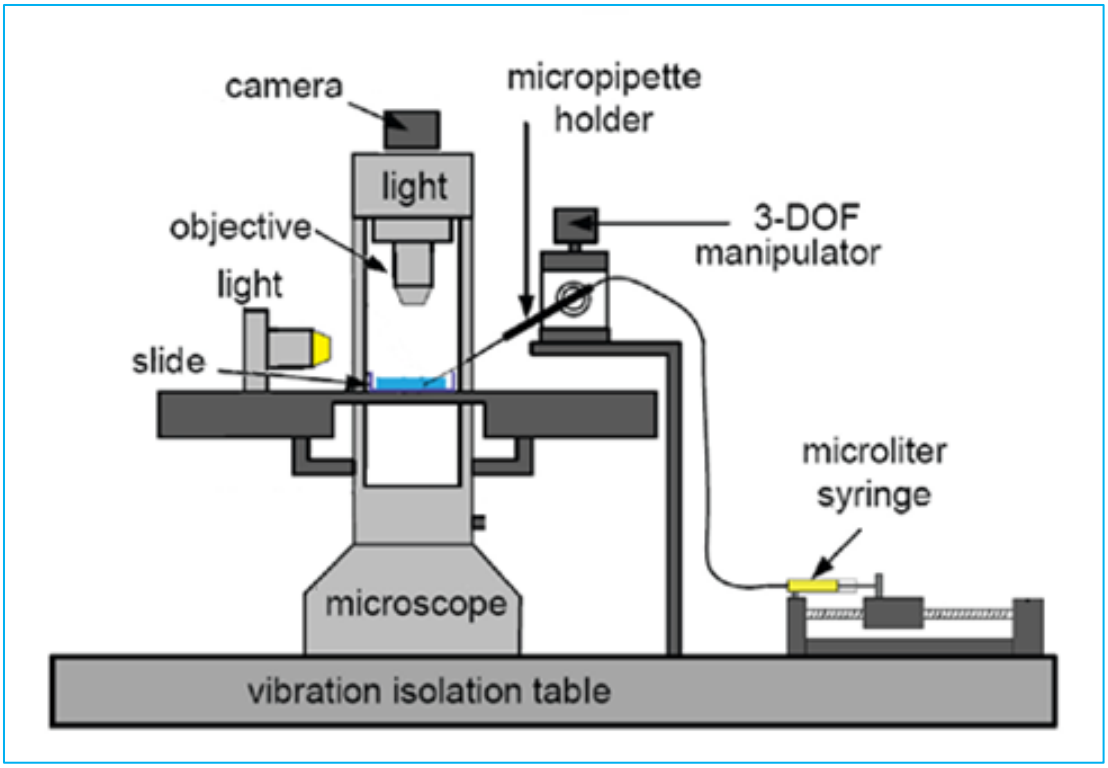

Figure 9.2.1: Cell Placement System Schematic (Adapted from [8])

The micro-pipette was created using a standard glass capillary tube by Kimble Glass Inc.. The initial tube had an inner diameter of 0.8 mm, outer diameter of 1.10 mm, and length of 100 mm. The tip was drawn to diameters ranging from 4 to 8 μm using a KOPF Model 730 Needle/Pipette Puller. Two pulls with settings of heat 1=20 and heat 2=11 were performed to draw the tips. The wide end of the micro pipette was inserted into the pipette holder, to prevent damage to the tip. A tight seal was insured by wrapping Teflon tape around the pipette prior to insertion into the tubing. The micropipette holder was mounted on the 3 degree of freedom probe station and connected to the tubing. The capillary tube was sealed to the 10 μL syringe with epoxy, and both the syringe and tubing were filled with vegetable oil. The use of vegetable oil in the system prevented

compression of the air pockets within the syringe and tubing, providing constant suction.

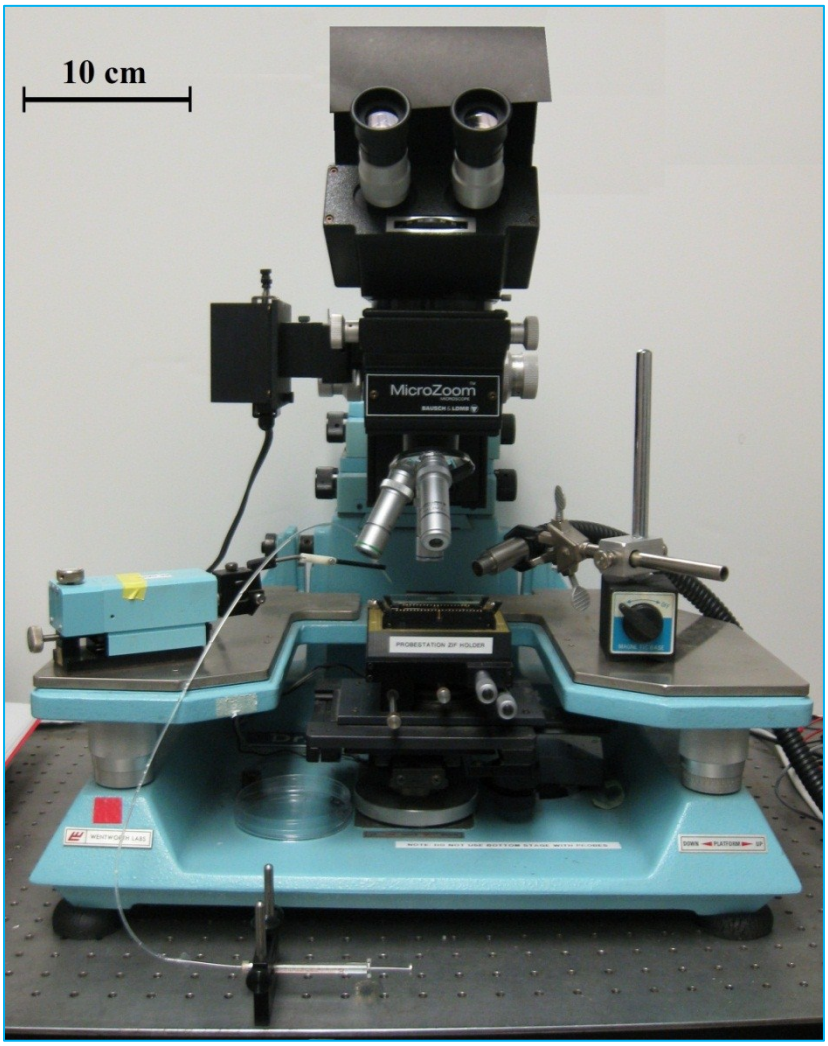

Figure 9.2.2: Cell Placement System

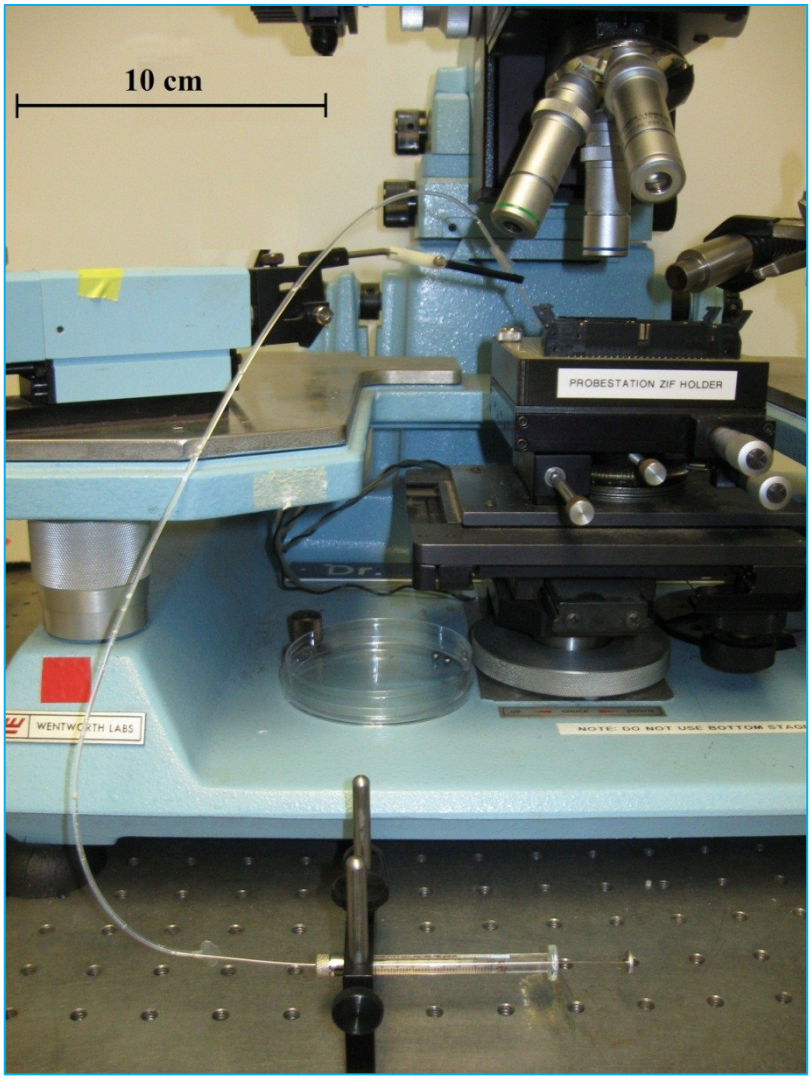

Figure 9.2.3: Cell Placement System Close-up (Syringe Capillary Tubing and Micropipette)

9.2.3 Procedure

A slide with a drop of water containing active yeast is mounted on the ZIF socket under the microscope. A target cell is chosen, and the tip of the micropipette is moved using the probe station until it is touching the cell. Negative pressure was applied to the capillary tube by drawing the stopper out of the syringe, controlling the aspiration of a desired cell. The cell is held with negative pressure to the tip of the micropipette (Figure 9.2.4).

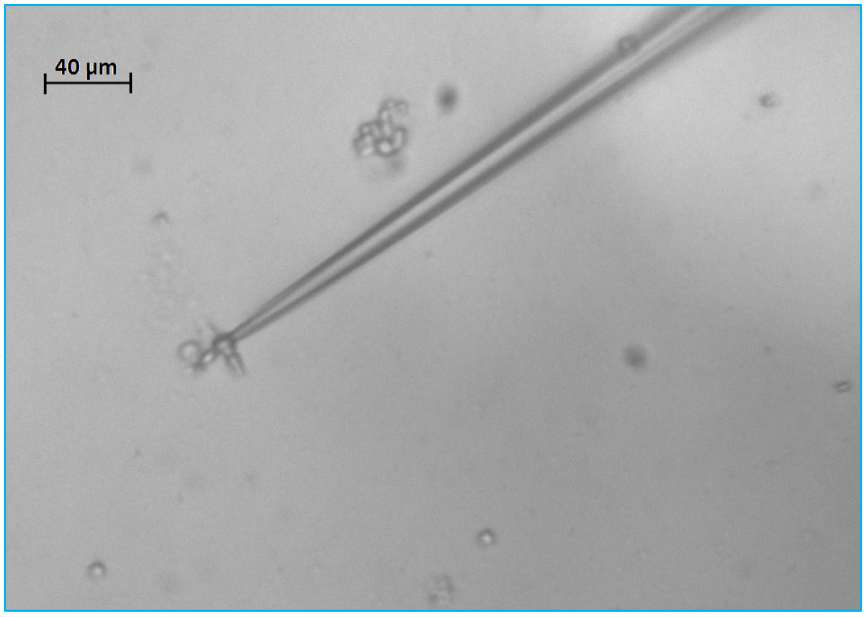

Figure 9.2.4: Cell Capture

The probe station with 3 degrees of freedom is used to manually manipulate the micropipette and control its tip position. The micropipette is then lifted from the slide so the CS4 chip can be mounted in the ZIF socket. The cell is lowered and positioned between the jaws of the desired gripper (Figure 9.2.5).

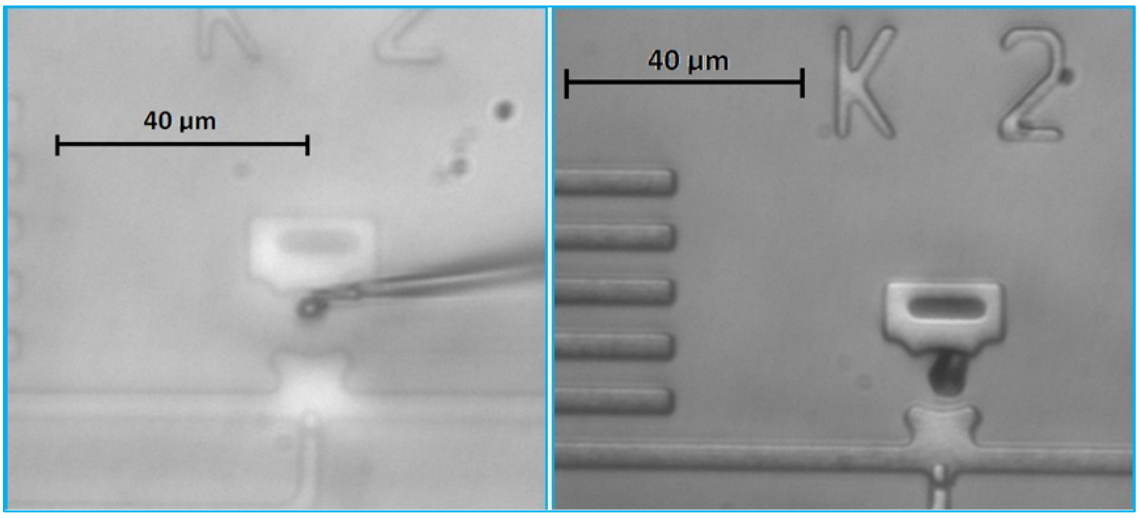

Figure 9.2.5: Initial Cell Placement

A few Pascals of positive pressure are created by pushing the stopper of the micro-syringe a small amount, releasing the cell in the desired location (Figure 9.2.6).

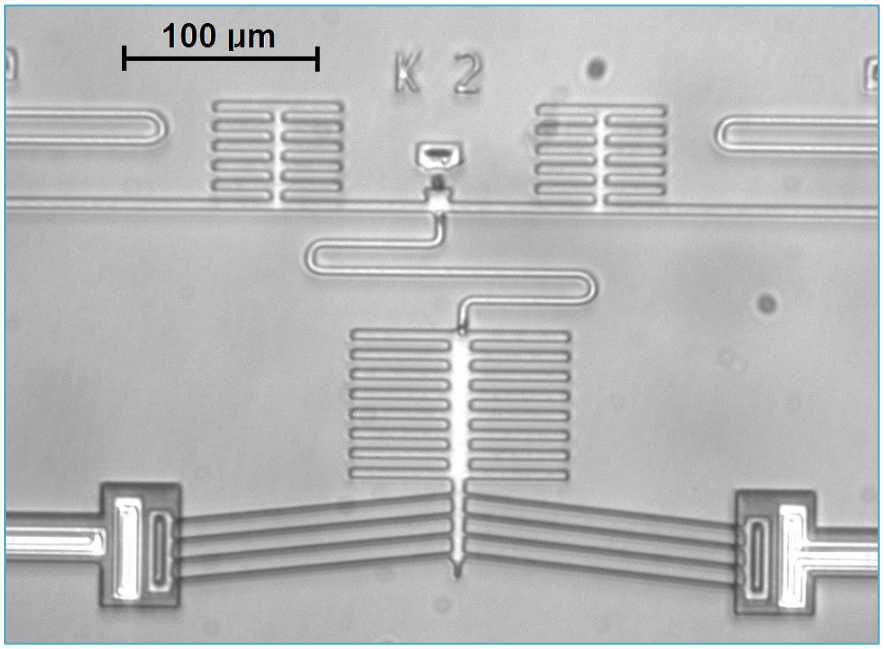

Figure 9.2.6: Final Cell Placement

During this process some problems were encountered. The first main problem involved cell capture. When using the micropipette to lift the cell out of the solution, the negative pressure was often not adequate to overcome the surface tension at the surface of the solution. This was overcome by allowing the fluid to evaporate to approximately the surface of the cell, thus breaking the surface of the fluid. The cell could then be easily lifted from the substrate. The next issue was the positioning of the cell within the jaw of the gripper. It was very difficult to lower to cell to the appropriate depth. Overshooting resulted in breaking the pipette, and rupturing the cell. The pipette had to been brought into focus

approximately 20 μm above the gripper. Then the focal plane was lowered about a micron at a time with the fine adjustment knob. The cell and pipette were then lowered into the focal plane. This prevented the pipette from inadvertently being forced into the substrate.

9.3 Sample Cell Testing Results - CS4BP1P2K83 Cell 1

This section will outline sample results for testing performed on Cell 1 (

Figure 9.3.1). Data was collected three times for squeezing of the cell in 0.5 V increments from 0 to 8 V.

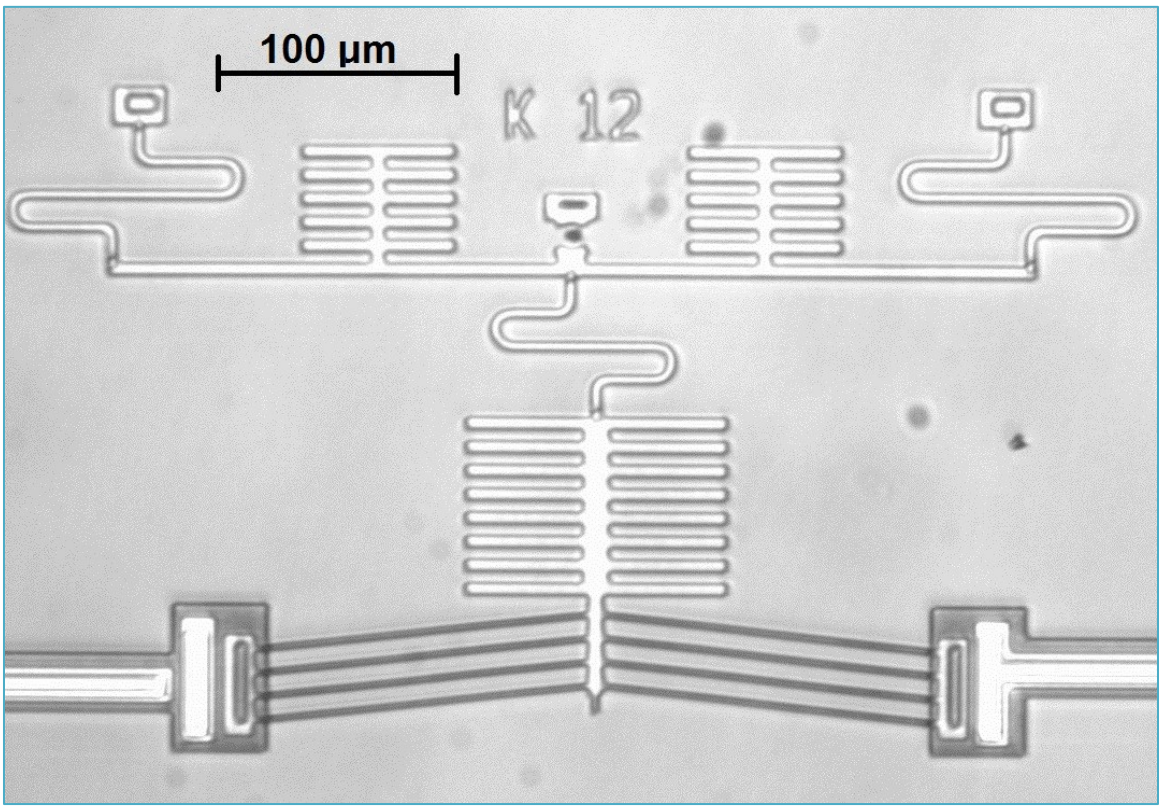

Figure 9.3.1: Testing with Cell 1: CS4 (Double Height K=104 µN/µm)

The three data sets were each analyzed with three different regions of interest selected for the Yamahata analysis. This results in data points representing 9 values. Error bars for each point in the graphs are the standard deviations of nine samples: 3 different trials, each first averaged over 3 ROIs. In the case of calculated values such as force and stress where multiple measurements are

combined, the standard additive and multiplicative formulas for combining errors were used e.g.

if $A = B+C \rightarrow \Delta A = \Delta B + \Delta C$,

if $A = B*C \rightarrow (\Delta A/A)^2 = (\Delta B/B)^2 + (\Delta C/C)^2$,

if $A = \lambda B, \Delta A = \lambda \Delta B$).

The resultant stiffness versus voltage curve is displayed in Figure 9.3.2. The calculated cell stiffness for Cell 1 is 18.4 μN/μm, based on an average of Kc from 4 to 8 V.

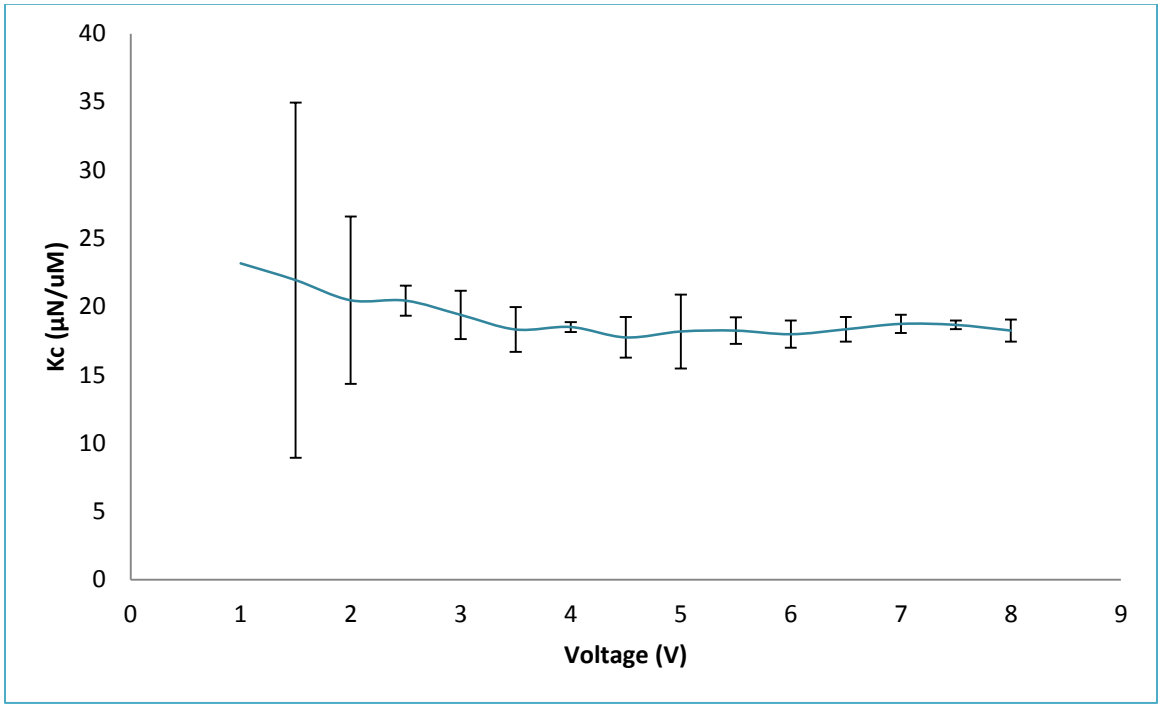

Figure 9.3.2: Cell 1 - Stiffness vs Voltage

The force versus displacement curve is presented in Figure 9.3.3.The calculated stiffness from the slope is 18.4 μN/μm, same as before.

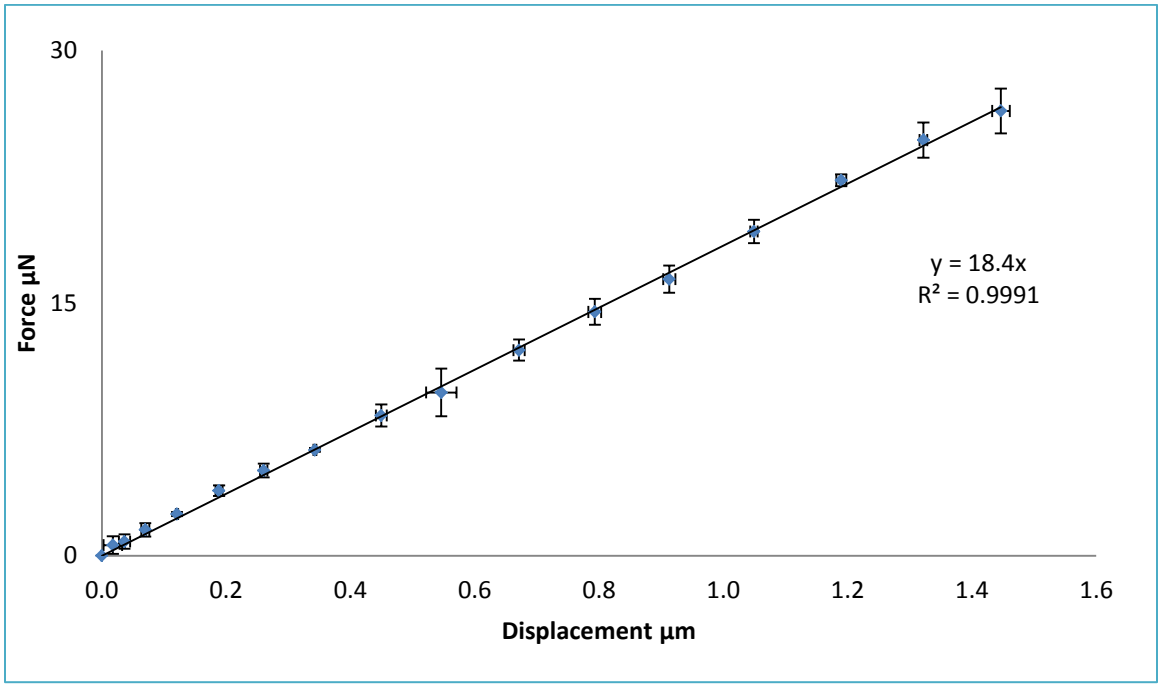

Figure 9.3.3: Cell 1 - Force vs Displacement

The stress versus strain curve for Cell 1 is presented in Figure 9.3.4. This calculation is based on a constant area of contact, 4 μm^2, the face of the gripper. The strain, ε, is calculated as the change in diameter of the cell divided by the original diameter of the cell (as described in Chapter 4).

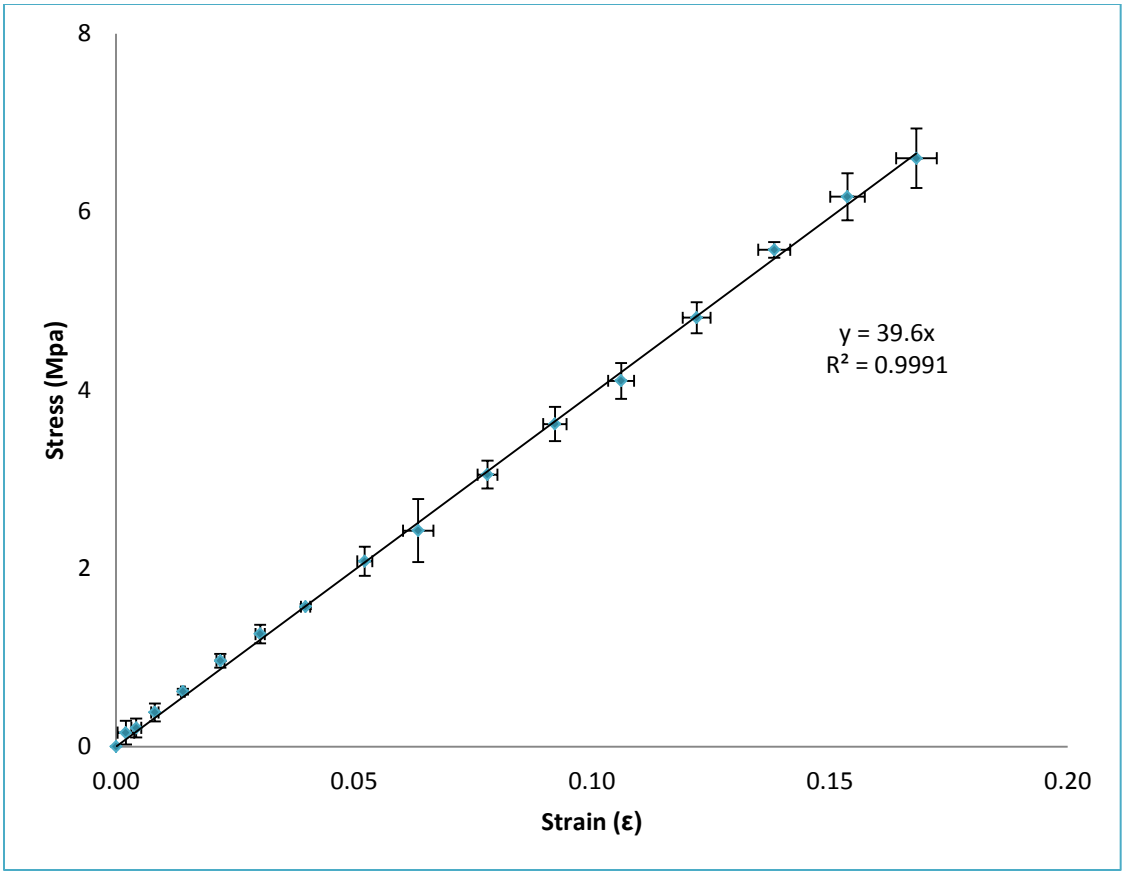

Figure 9.3.4: Cell 1 - Stress vs Strain

9.4 Yeast Cell Testing Result Cells 1,3,5,6,

Cell testing was successfully performed on four different yeast cells: Cells 1, 3, 5 & 6. The numbers are not consecutive because some cells (2, 4 & 7) were failed test attempts (cells stuck to jaw, buckled chevrons, etc.). Cell stiffness and Young's modulus we calculated in each case (Table 9.4.1). The force versus displacement curves and the stress versus strain curves from which the stiffness and Young's moduli were determined are presented in Figure 9.4.2 and Figure 9.4.2.

Table 9.4.1: Experimental Cell Properties

	Diameter (μm)	Stiffness (μN/μm)	Young's Modulus (Mpa)
Cell 3	**5.0± 0.2**	**6.5 ± 3.3**	**13.9 ± 7.1**
Cell 5	**8.5± 0.2**	**17.0 ± 3.1**	**36.52 ± 6.7**
Cell 1	**8.6 ± 0.2**	**18.4 ± 1.0**	**39.6 ± 2.2**
Cell 6	**9.0± 0.2**	**19.0 ± 1.2**	**40.8 ± 2.7**

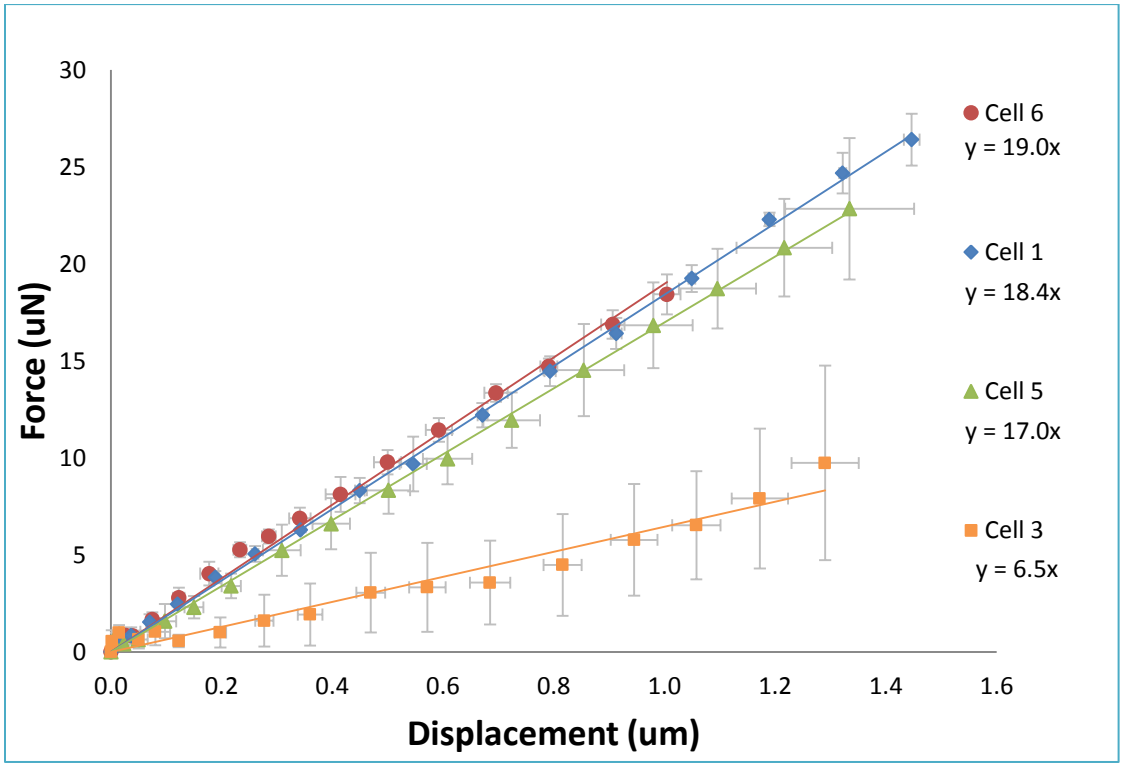

Figure 9.4.1: Force versus Displacement for 4 Yeast Cells

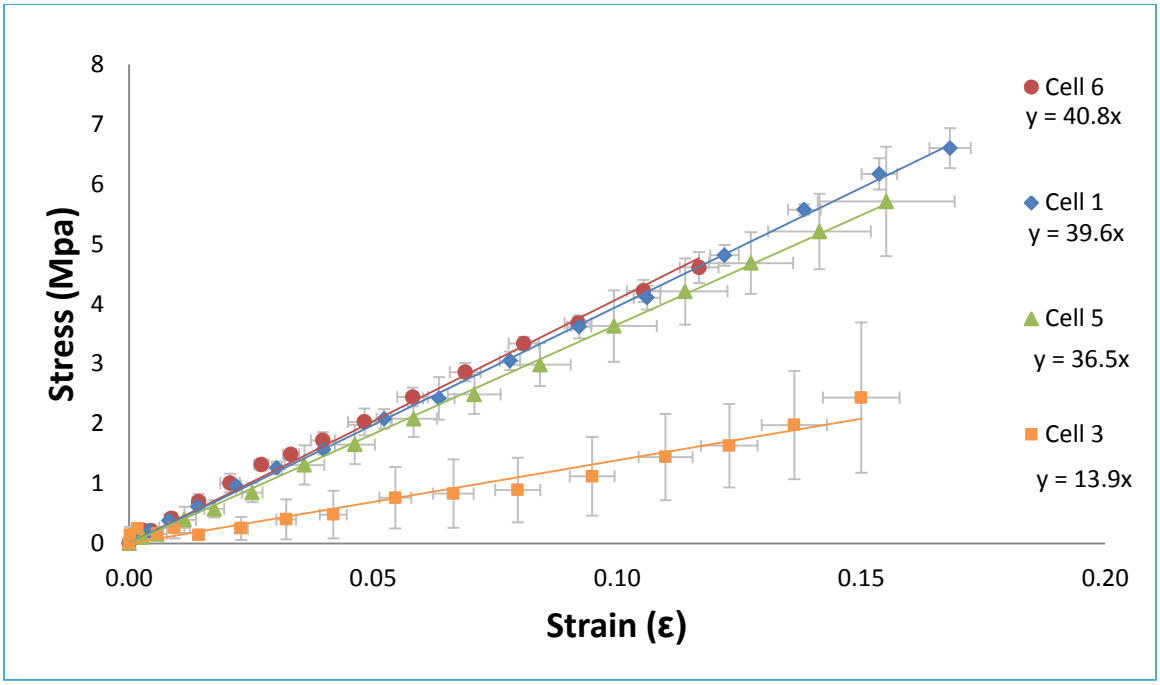

Figure 9.4.2: Stress versus Strain for 4 Yeast Cells

The Young's moduli of the four cells range from 13.9- 40.8 MPa, and the stiffnesses ranged from 6.5 - 19.0 μN/μm. It is hard to establish a trend with respect to cell diameter will such a small sample size, but it appears that stiffness and Young's Modulus increase with increasing cell diameter (see Figure 9.4.3).

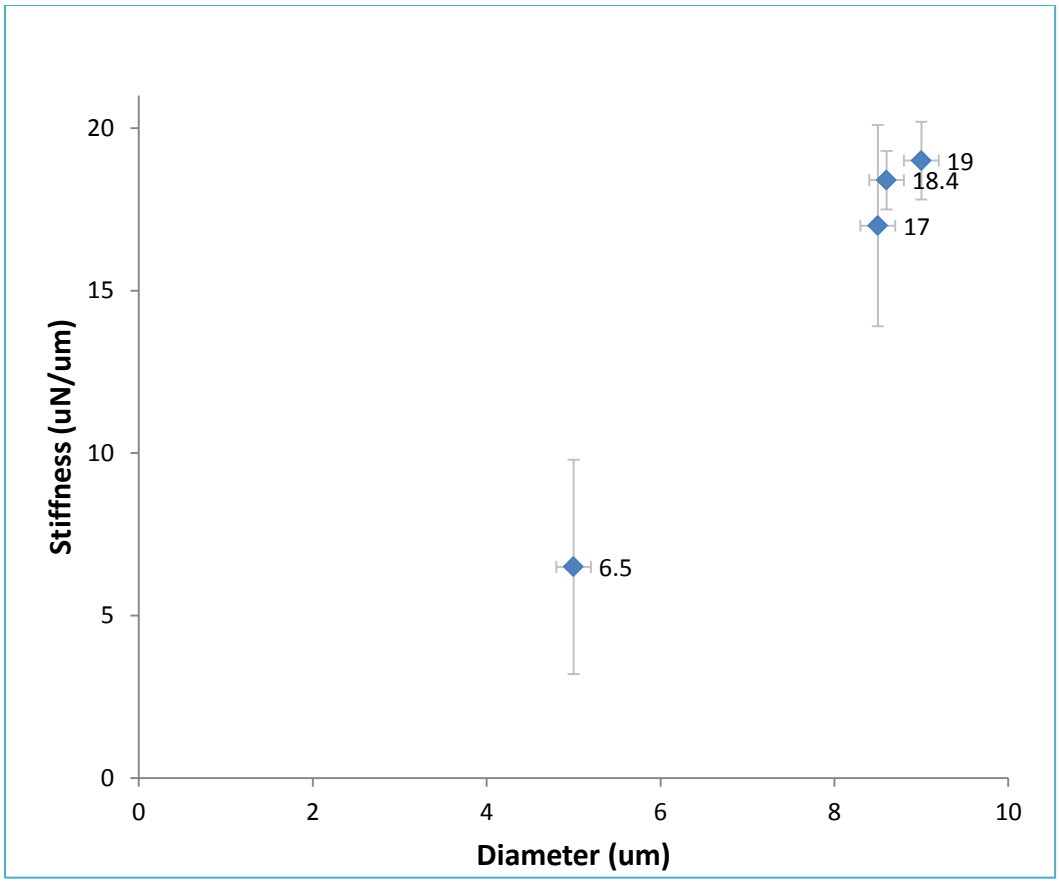

Figure 9.4.3: Stiffness versus Diameter for 4 Yeast Cells

Chapter 10: Discussion

The experimental results of this work will be discussed with respect to previous experimental testing performed on yeast, and possible sources of error will be outlined.

10.1 Comparison to Existing Literature

In order to compare the experimental results of this research to existing work, a small literature review was performed. Work by teams investigating the mechanical properties of yeast is presented in Table 10.1.1.

Table 10.1.1: Yeast Cell Mechanical Properties. Highlighted Entries: Large Cell Deformation (*Max Indentation Values Were Interpreted from Graphs and Figures As Not Explicitly Stated in Literature)

Stiffness (μN/μm)	Young's Modulus (Mpa)	Technique	Max Indentation (μm)*	Source
-	0.6	Nano-indentation Technique Aquatic Test	~0.055	Touhami et al, 2003 [20]
	0.73	Nano-indentation and Oscillation Aquatic Test	~0.007	Pelling et al, 2004 [32]
-	2.0	Nano-indentation Technique Aquatic Test	~0.06	Lanero et al, 2006 [33]
~1	3.24	Nano-indentation Technique		Fukuda, Nakajima, and Ahmad, 2011 [18]
~1	3.53	Nano-indentation Technique	1	Ahmad et al, 2008 [34]
6-19	**27**	**MEMS Cell Squeezer (This Work)**	**~5**	**Schwartz, 2012**
-	29	Pressurised Elastic Shell Model	NA	Vella et al, 2011 [22]
~11	112	Optic Fiber Probe Compression Aquatic Test	~4	Smith et al, 2009 [19]

Some different experimental techniques were employed by the different teams. Optic fiber probe compression techniques used large cell indentation, on the order of microns, and allowed global cell properties to be determined. Nano-indentation techniques reviewed used small cell indentations, on the order of nanometers. The large discrepancy between data obtained for local versus global techniques indicates that different aspects of the cell elasticity are being explored by the two approaches [33]. “Further progress is restricted by the lack of fundamental understanding and characterization of the mechanical properties of the yeast cell wall.” [38]

A team lead by Vella modeled the yeast cell as a pressurized elastic shell, performing an analytical study of the associated shell equations with finite element modeling and macroscopic experiments [22].This work indicated that there are two linear regimes in the force versus displacement curve for yeast; one for small indentations (smaller than the membrane thickness), and one for large indentations (larger than the membrane thickness). This means there are two separate linear stiffnesses, one associated with each regime [22].

Nano-indentation techniques may not represent actual global cell stiffness as extra dissipation force may be included in the measurement for the global spring [18].

This cell squeezing technique used in this thesis work was large cell indentation. As ‘whole cell’ squeezing is being performed, the mechanical properties determined are global.

The stiffnesses determined in this work ranged from 7 – 19 μN/μm. Smith used a similar cell squeezing technique, finding a cell stiffness of 11 μN/μm [19]. The values determined in this work are of the same order of magnitude, but slightly higher. This is likely a result of the testing environment. Smith's tests were performed in an aqueous environment, where this work was performed on a dry chip. Also, different strains of yeast were used. The values of cell stiffness reported for nano-indentation techniques was much lower, around 1 μN/μm. It is possible that these techniques are measuring a localized stiffness.

The range of Young's modulus determined in this work ranged from 14 to 41 MPa. This most closely resembles the results found by Vella (2011) where the predicted range for Young's modulus of yeast was from 12 to 46 MPa. The experimental measure of Young's modulus in this work is an approximation based on simplification of the contact area, while the stiffness is a pure measure, based only on cell deformation.

10.2 Sources of Error

10.2.1 Cell Effects

There are many possible sources for error in the developed measurement system. This section will address the main sources including: yeast cell testing in non-aqueous environment, the two- dimensional approximation for stress and strain calculations, possible cell hardening due to micro-pipette aspiration and

residual stress inherent in the device which affects measurements at low displacements (below 0.2 μm).

The cellular spring constant has been shown to depend on the extracellular osmotic pressure [21]. For this reason, most yeast test procedures described in literature employ an aqueous test environment. Due to large time requirements and increased complexity for an aqueous test device, initial test devices were designed to be tested dry. Cell drying prior to testing likely resulted in cell stiffening, resulting in measured cell stiffnesses higher than those reported in other literature.

It has been shown that micropipette aspiration can cause cell hardening [39]. It is possible that there is some residual cell hardening prior to testing as a result of cell placement.

10.2.2 Measurements at Small Displacements

As seen in Figure 9.3.2, at small displacements 0.22 um the stiffness measurements (0 to 4 V) are different than at high displacement. There are a number of hypotheses for why this is:

1) The assumption of constant area not accurate. At low displacements the contact area is small similar to AFM, while at high displacements, the contact is large similar to micro-plate compression

The measurement technique developed uses an assumed area of 4 μm^2. The calculated value of Young's modulus is dependent on this value. In reality the cell is deforming during squeezing, so the cell cross sectional area is increasing. This

would result in a non-linear stress strain relationship. The area of 4 μm^2 is equivalent to the cross sectional area of the cell at a midway point where the diameter is 2.25 μm. The calculated stress strain relationship is therefore linear about this chosen midway point.

2) The above hypothesis explains low stiffness values at low displacements; however some had low stiffness at high displacement.

Another possible explanation is that measurements at small displacements are negatively influenced by residual preloads existing in the springs (See Appendix H). Assuming a preload on the order of .2 um, this would produce a 100% error at .2 μm, but only a 4 - 7% error at 5 um.

3) The system is not able to account for cell deformation during squeezing, so the resultant stress strain is a linear approximation of a more complex process.

Whatever the cause of these problems, the developed system should not be used as a measurement tool for displacements smaller than 0.2 - 0.3 μm. The maximum displacement measured was approximately 2 μm. Therefore the system can only be used for the determination of global cell stiffness, and cannot be used to measure localized stiffnesses.

Chapter 11: Future Investigation

Determination of mechanical properties of the yeast cell is a complex problem. The layered structure of the yeast cell wall adds complexity as not all layers contribute equally to its mechanical strength [22].

There are many avenues for further research in this area. These include; fatigue testing, vibration testing, testing of the cell in the various growth phases, electrical shocking of the cell, comparison of cell indenter designs, and testing of various types of cells.

Mechanical stimulation in the form of low magnitude, high frequency (LMHF) vibration of cells has recently been shown to have positive effects on the skeletal system [40]. Osteocytes, the cells comprising bone, are hypothesized to be the mechanosensor which detects vibration stimulus [40]. Vibration can be used to sensitize bone cells and improve their osteogenic, or bone building, response to mechanical loading [41]. High frequency vibration has also been shown to have an osteogenic, effect on the early stages of cell differentiation in stem cells [42]. Currently testing on osteocytes has been performed in gel cultures. This device can perform vibration on a single cell sample in order to investigate the difference in cell response when not in a culture.

Continuation of this thesis work should include the implementation of an aqueous test environment (Figure 10.2.1). Initial designs have been completed, and will be tested in the future. The device designed will be used to separate an individual cell from a microorganism community. A fluid sample will be in injected into the

system, and using optical microscopy the cell of interest will be detected and clamped between the two grippers [43].

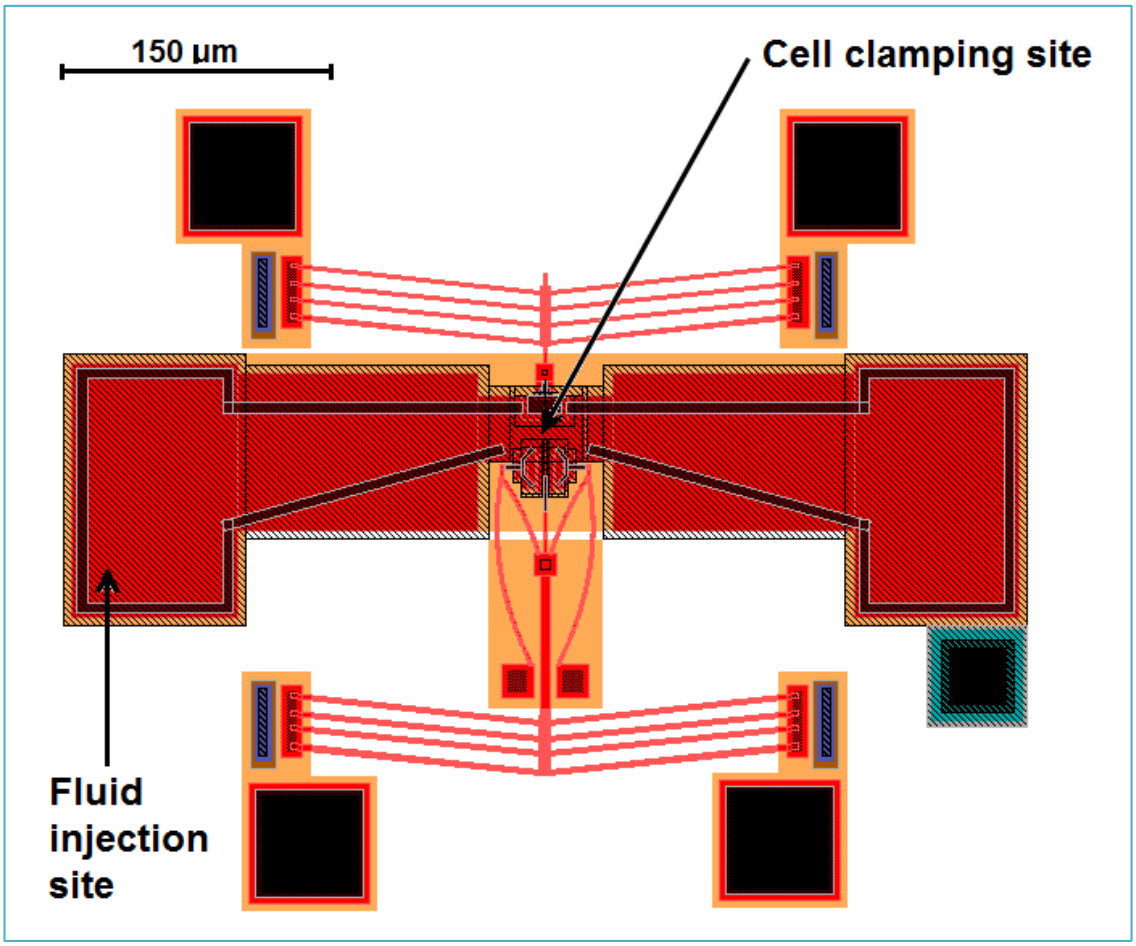

Figure 10.2.1: Implementation of Fluid Channel for Cell Testing [43]

Devices enabling electric potential to be applied across the cell have also been designed (Figure 10.2.2). It has been shown that electrical potential can influence the structure and function of the cell membrane compartments, proteins, and lipid bilayer [44].

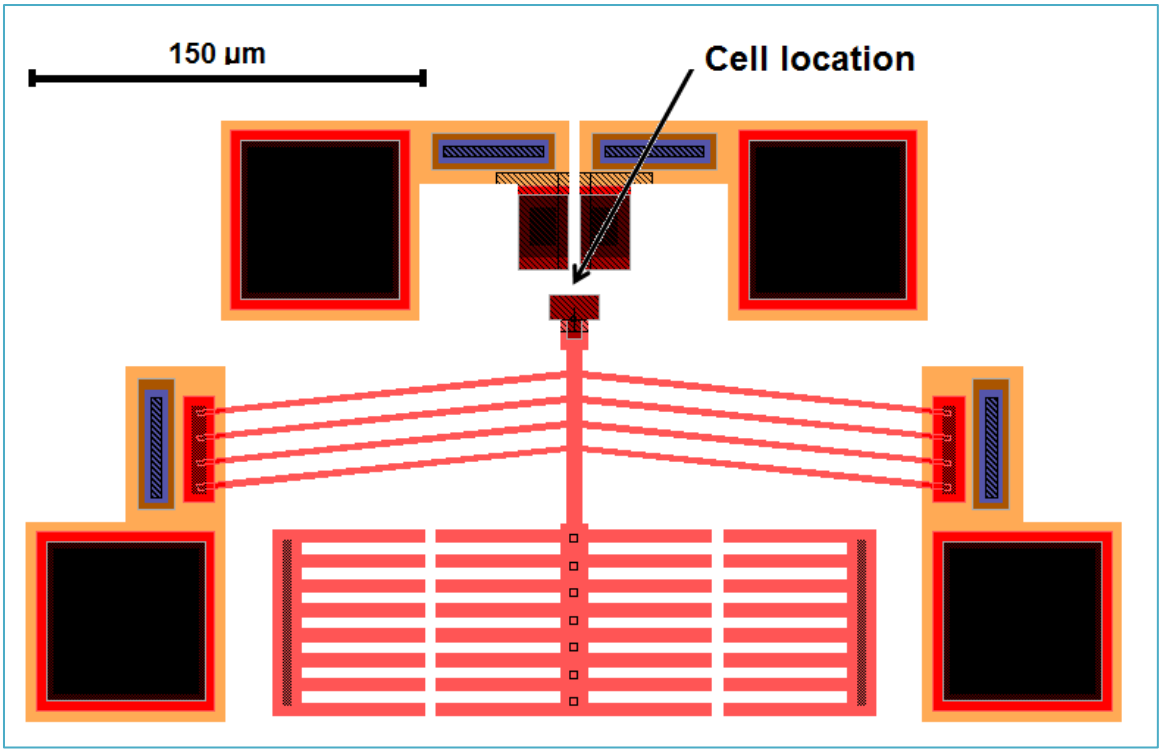

Figure 10.2.2: Implementation of Applied Electric Potential for Cell Testing [43]

Variations on the jaw designs have also been implemented (Figure 10.2.3). This will allow for comparison of the different indenter geometries on cell response.

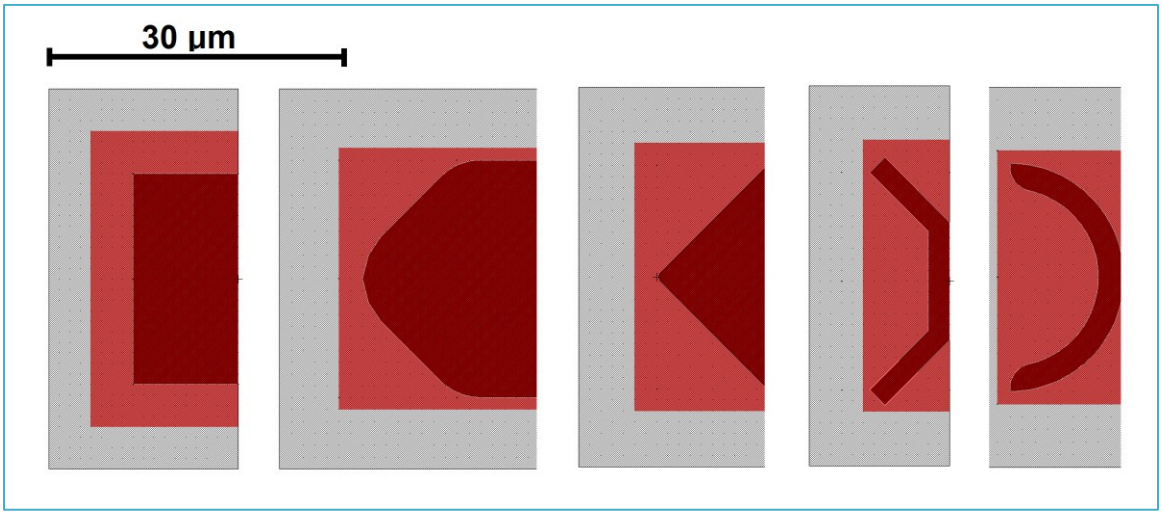

Figure 10.2.3: Jaw Design Variations [43]

Research of a theoretical nature is also required to better interpret the results of experimental cell testing. A quote from Arfsten sums this up:

"… the cellular spring constant is not solely a function of the cell wall mechanical behavior but also of the cellular interior. That means that the cell stiffness is not an intrinsic cell mechanical parameter. Moreover, it becomes clear that further studies of a theoretical nature as well as experimental nature are required to better understand the cell mechanical meaning of the obtained cell mechanical parameter." [21]

Chapter 12: Conclusions

In conclusion, the objectives of the thesis work have been met. A device capable of determining cell mechanical properties such as stiffness and Young's modulus has been designed, tested, and improved.

The first chip, IMUDTCS2 was implemented to test the appropriate pitch for periodic displacement measuring structures, and test a Type A gripper design. The appropriate pitch, 10 μm was determined and employed in the following designs. Stiction problems with the first Type A gripper lead to the modification and enhancement of the following designs.

The second chip, IMUDTCS4 incorporated Type B gripper designs which were modified so not to be cantilevered. All designs were also enhanced with periodic structures with a pitch of 10 μm, and with the incorporation of double height spring to increase stiffness in the vertical direction, helping to prevent stiction.

Double height Type B grippers were used for cell testing as they were able to measure the stiffness of a pseudo cell with great accuracy. Four cells were successfully tested, with their stiffnesses ranging from 14 - 40 μN/μm, and with Young's modulus ranging from 15 - 58 MPa, supporting the results of Vella [22]. As expected, these results fall in between the ranges experimentally determined for nanoindentation techniques and micro-plate compression which had complementary cell contact areas and cell deformation.

This work has established a starting point for future investigation in the Dalhousie MEMS Research Group. It also adds to the literature base for the measurement

of whole cell mechanical properties, as the majority of yeast cell testing studies were performed using nano-indentation.

Appendix A: PolyMUMPs™ Process Steps [4]

FIGURE 1.2. The surface of the starting n-type (100) wafers are heavily doped with phosphorus in a standard diffusion furnace using a PSG film as the dopant source. After removal of this PSG film, a 600 nm blanket layer of low stress silicon nitride (Nitride) is deposited followed by a blanket layer of 500 nm polysilicon (Poly 0). The wafers are then coated with UV-sensitive photoresist.

FIGURE 1.3. The photoresist is lithographically patterned by exposing it to UV light through the first level mask (POLY0) and then developing it. The photoresist in exposed areas is removed leaving behind a patterned photoresist mask for etching.

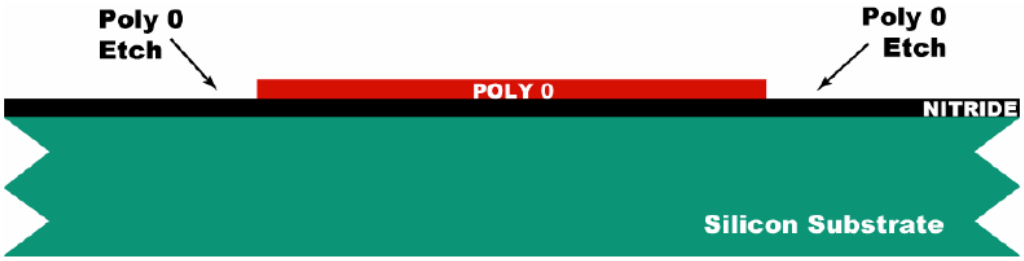

FIGURE 1.4. Plasma etching is used to remove the unwanted polysilicon. After the etch, the photoresist is chemically stripped in a solvent bath. This method of patterning the wafers with photoresist, etching and stripping the remaining photoresist is used repeatedly in the PolyMUMPs process.

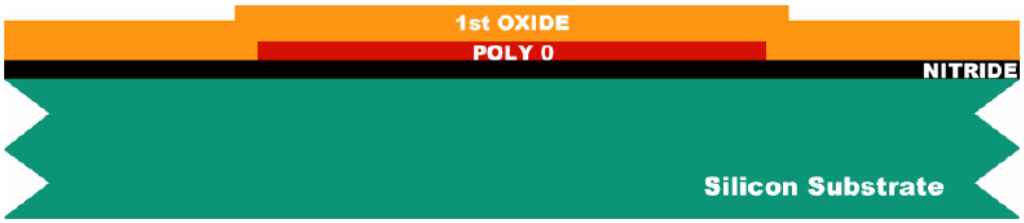

FIGURE 1.5. A 2.0 μm layer of PSG is deposited on the wafers by low pressure chemical vapor deposition (LPCVD). This is the first sacrificial layer.

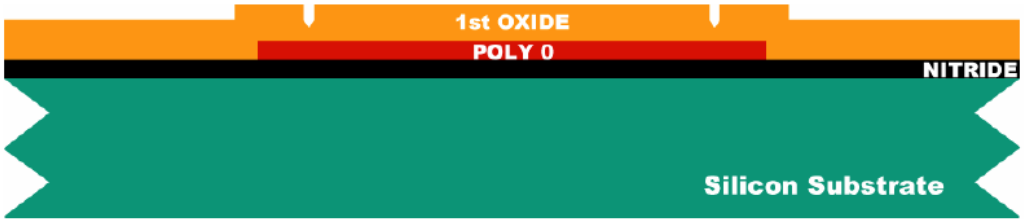

FIGURE 1.6. The wafers are coated with photoresist and the second level (DIMPLE) is lithographically patterned. The dimples, 750 nm deep, are reactive ion etched (RIE) into the first oxide layer. After the etch, the photoresist is stripped.

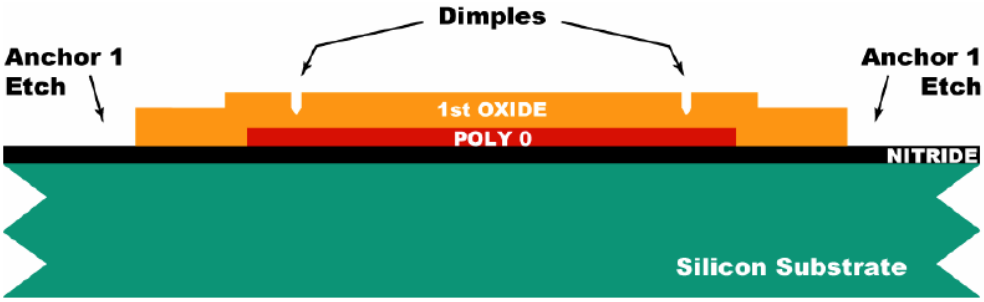

FIGURE 1.7. The wafers are re-coated with photoresist and the third level (ANCHOR1) is lithographically patterned. The unwanted oxide is removed in an RIEprocess and the photoresist is stripped.

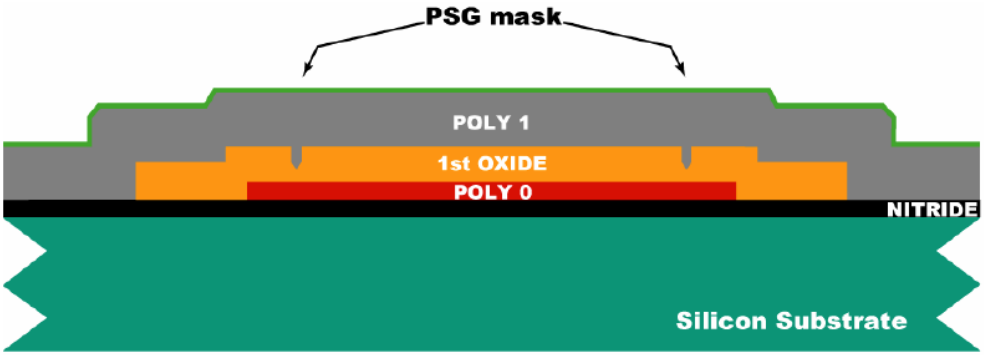

FIGURE 1.8. A blanket 2.0 μm layer of un-doped polysilicon is deposited by LPCVD followed by the deposition of 200 nm PSG and a 1050°C/1 hour anneal. The anneal serves to both dope the polysilicon and reduce its residual stress.

FIGURE 1.9. The wafer is coated with photoresist and the fourth level (POLY1) is lithographically patterned. The PSG is first etched to create a hard mask and then Poly 1 is etched by plasma processing. After the etch is completed, the photoresist and PSG hard mask are removed.

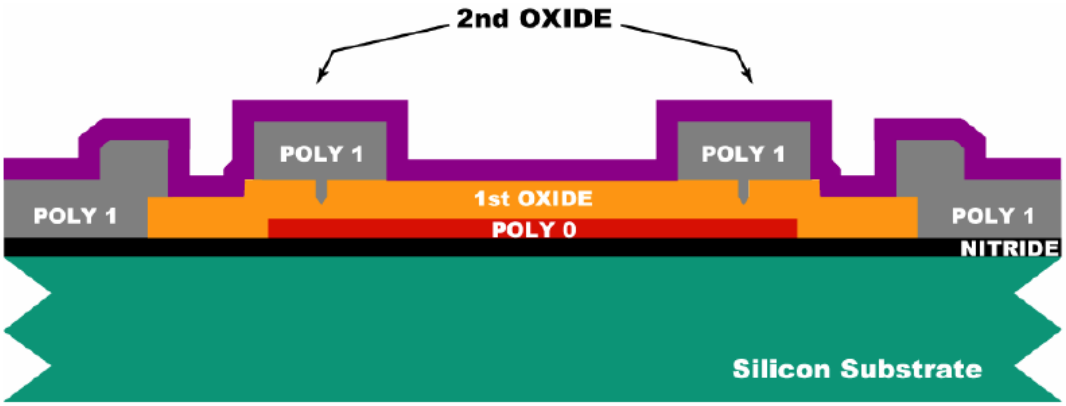

FIGURE 1.10. The Second Oxide layer, 0.75 µm of PSG, is deposited on the wafer. This layer is patterned twice to allow contact to both Poly 1 and substrate layers.

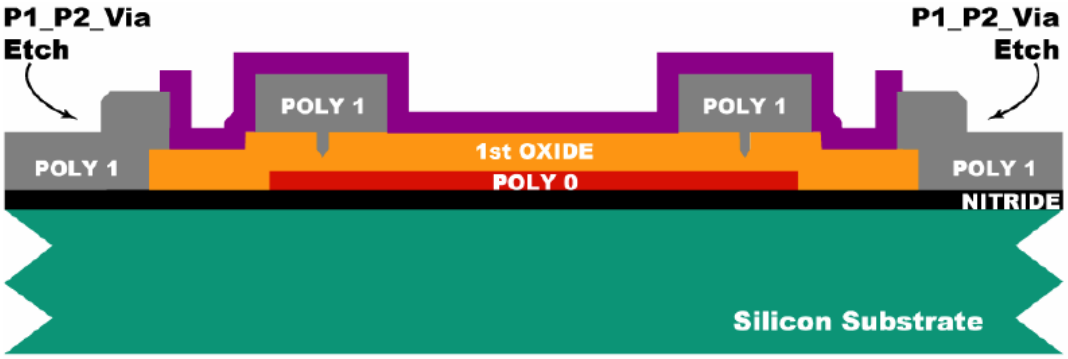

FIGURE 1.11. The wafer is coated with photoresist and the fifth level (POLY1_POLY2_VIA) is lithographically patterned. The unwanted Second Oxide is RIE etched, stopping on Poly 1, and the photoresist is stripped.

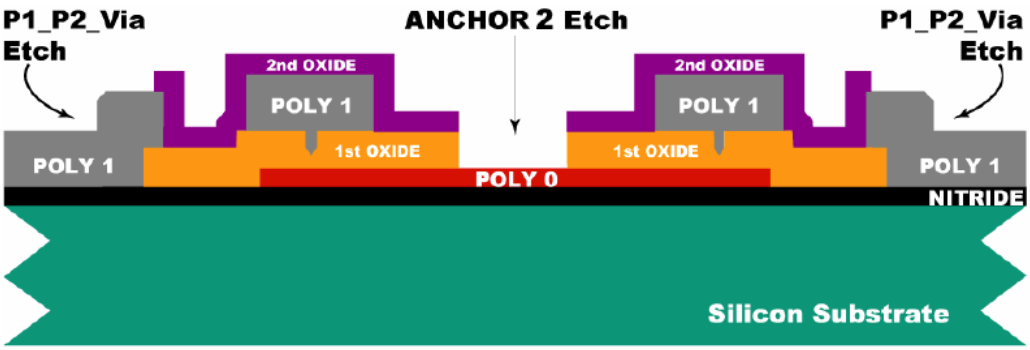

FIGURE 1.12. The wafer is re-coated with photoresist and the sixth level (ANCHOR2) is lithographically patterned. The Second and First Oxides are RIE etched, stopping on either Nitride or Poly 0, and the photoresist is stripped. The ANCHOR2 level provides openings for Poly 2 to contact with Nitride or Poly 0.

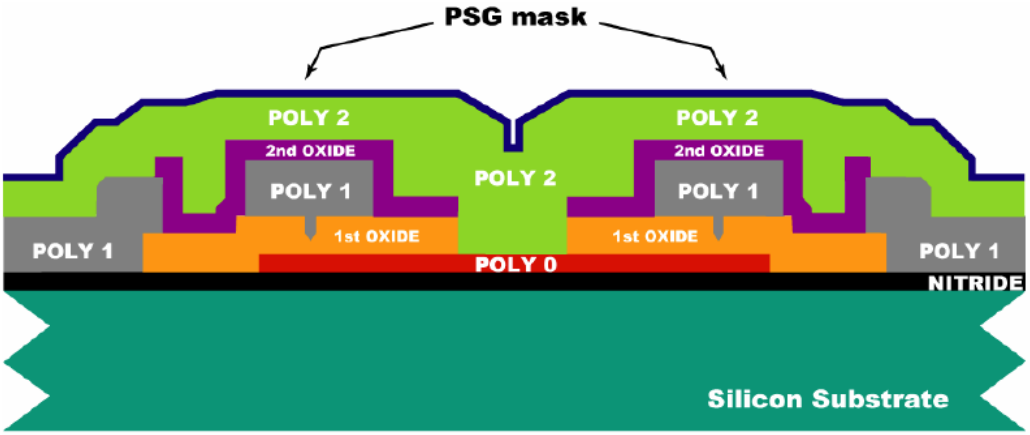

FIGURE 1.13. A 1.5 μm un-doped polysilicon layer is deposited followed by a 200 nm PSG hardmask layer. The wafers are annealed at 1050°C for one hour to dope the polysilicon and reduce residual stress.

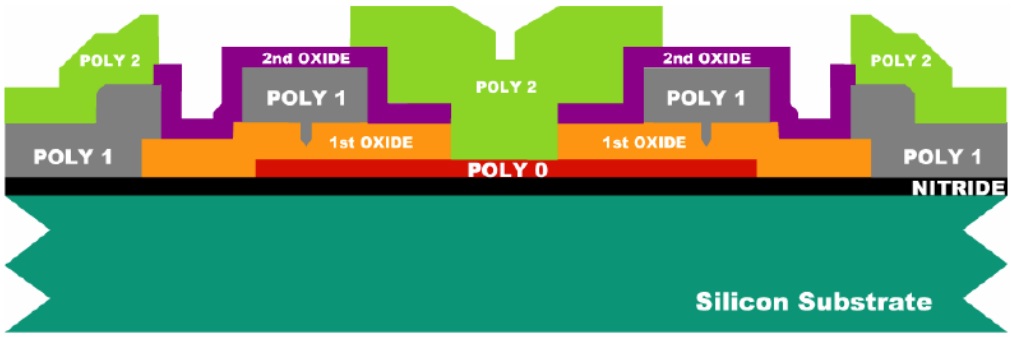

FIGURE 1.14. The wafer is coated with photoresist and the seventh level (POLY2) is lithographically patterned. The PSG hard mask and Poly 2 layers are etched and the photoresist and hard mask are removed. All mechanical structures have now been fabricated. The remaining steps are to deposit the metal layer and remove the sacrificial oxides.

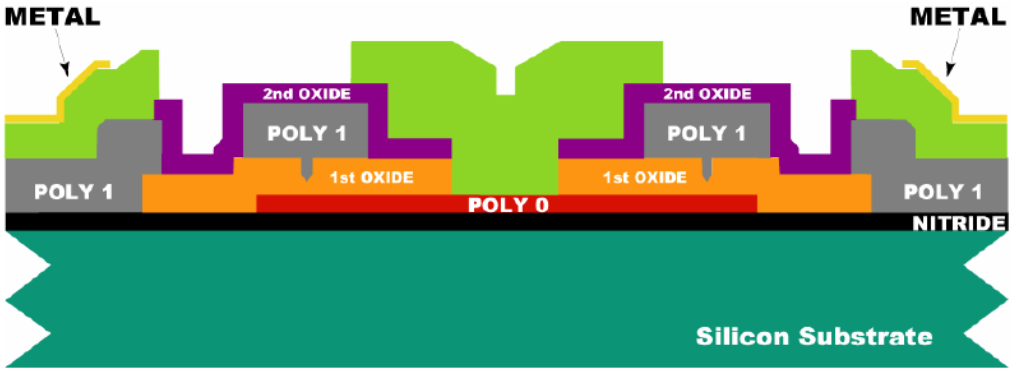

FIGURE 1.15. The wafer is coated with photoresist and the eighth level (METAL) is lithographically patterned. The metal (gold with a thin adhesion layer) is deposited by lift-off patterning which does not require etching. The side wall of the photoresist is sloped at a reentrant angle, which allows the metal to be deposited on the surfaces of the wafer and the photoresist, but provides breaks in the continuity of the metal over the photoresist step. The photoresist and unwanted metal (atop the photoresist) are then removed in a solvent bath. The process is now complete and the wafers can be coated with a protective layer of photoresist and diced. The chips are sorted and shipped.

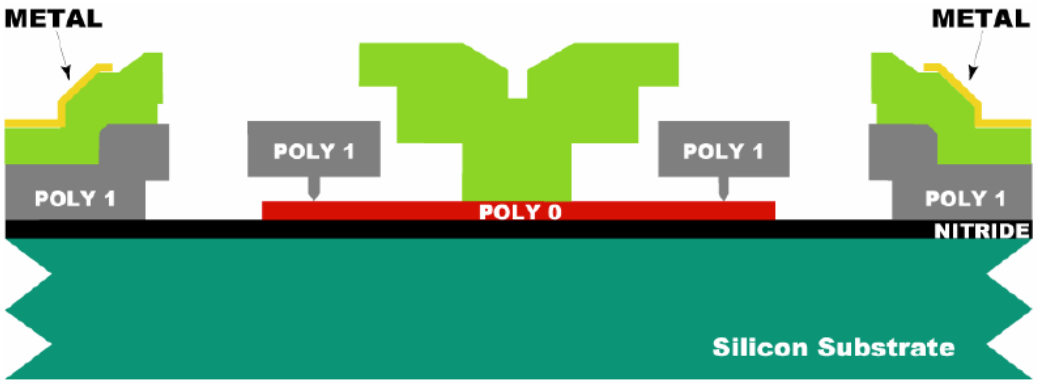

FIGURE 1.16. The structures are released by immersing the chips in a 49% HF solution. The Poly 1 "rotor" can be seen around the fixed Poly 2 hub. The stacks of Poly 1, Poly 2 and Metal on the sides represent the stators used to drive the motor electrostatically.

Appendix B: COMSOL Multiphysics Model Validation Geomtery [44]

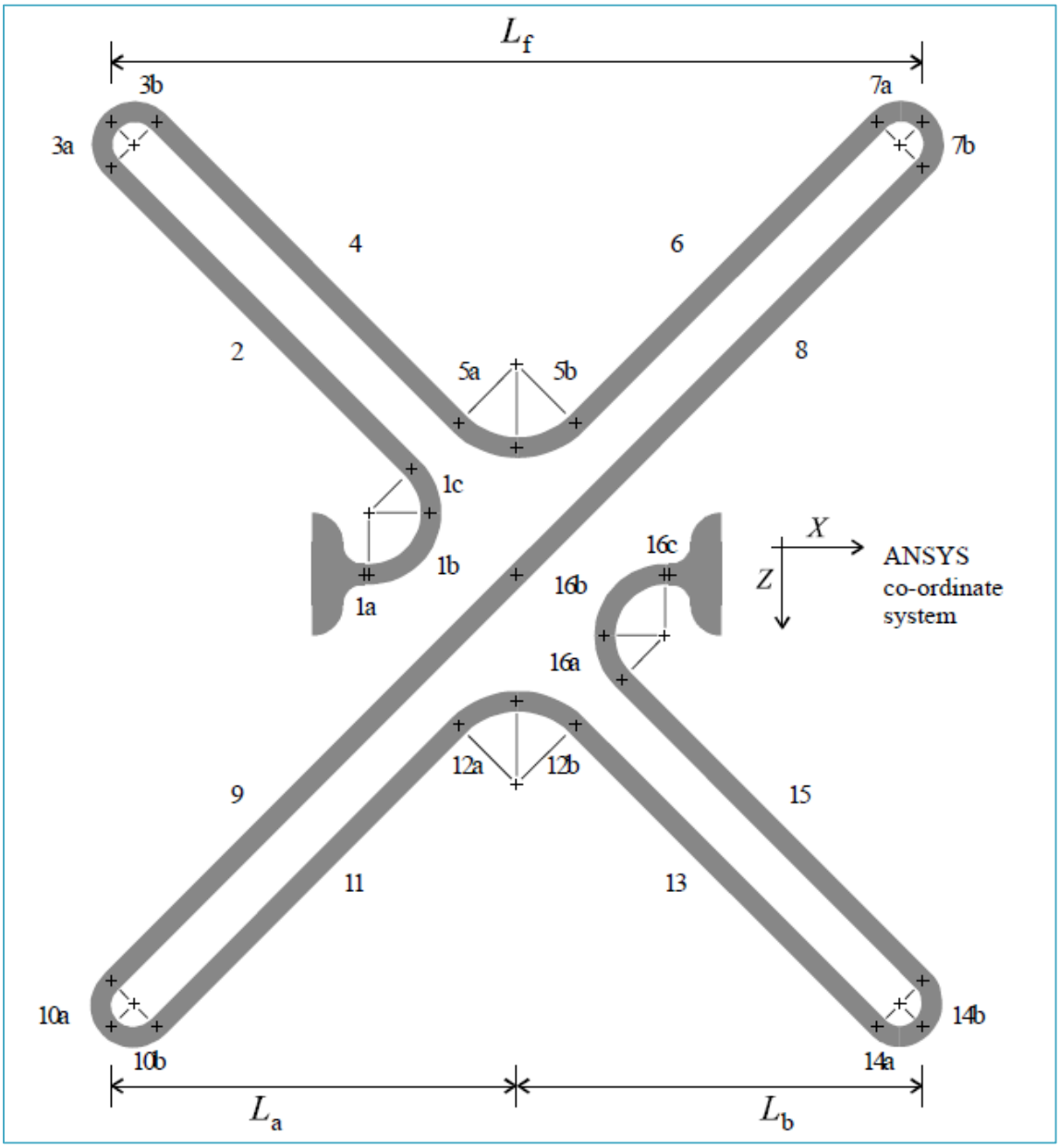

Figure 1: Geometric Layout of an X-Joint [44]

Table 1: X-Joint Variations [44]

Variation	Folded Length [µm]			Unfolded Length [µm]	Segments 2 µm wide	Segments 4 µm wide
	L_f	L_a	L_b			
X_std_01	79.5	39.75	39.75	458	1-16	
X_std_02	44.5	22.25	22.25	260	1-16	
X_std_03	26.5	13.25	13.25	158	1-16	
X_std_04	62	31	31	359	1-16	
X_std_05	37.5	17.75	17.75	209	1-16	
X_var_01	79.5	39.75	39.75	458	1-3, 7-10, 14-16	4-6, 11-13
X_var_02	79.5	39.75	39.75	458	1-7, 10-16	8-9
X_var_03	79.5	39.75	39.75	458	1, 3, 5, 7, 10, 12, 14, 16	2, 4, 6, 8, 9, 11, 13, 15
X_var_04	79.5	39.75	39.75	458	1-5, 10-13	5-8, 12-16
X_var_05	62	39.75	22.25	359	1-16	

Table 2: Joint Segments of an S-Joint [44]

Joint Segment	Point (X, Z) [µm]			Angle		Radius [µm]
	Start	End	Centre	Start	End	
1a	-15, 0	-14.5, 0				
1b	-14.5, 0	-9.5, -6	-14.5, -6	-90°	0°	6
1c	-9.5, -6	-10.25, -10.25	-14.5, -6	0°	45°	6
2	-10.25, -10.25	$-L_a$, $-L_a$				
3a	$-L_a$, $-L_a$	$-L_a$, $-L_a$-4.5	$-L_a$+2.25, $-L_a$-2.25	225°	135°	3.18
3b	$-L_a$, $-L_a$-4.5	$-L_a$+4.5, $-L_a$-4.5	$-L_a$+2.25, $-L_a$-2.25	135°	45°	3.18
4	$-L_a$+4.5, $-L_a$-4.5	-5.75, -14.75				
5a	-5.75, -14.75	0, -12.37	0, -20.5	225°	270°	8.13
5b	0, -12.37	5.75, -14.75	0, -20.5	270°	315°	8.13
6	5.75, -14.75	L_b-4.5, $-L_b$-4.5				
7a	L_b-4.5, $-L_b$-4.5	L_b, $-L_b$-4.5	L_b+2.25, $-L_b$-2.25	135°	45°	3.18
7b	L_b, $-L_b$-4.5	L_b, $-L_b$	L_b+2.25, $-L_b$-2.25	45°	-45°	3.18
8	L_b, $-L_b$	0, 0				
9	0, 0	$-L_a$, L_a				
10a	$-L_a$, L_a	$-L_a$, L_a+4.5	$-L_a$+2.25, L_a+2.25	135°	225°	3.18
10b	$-L_a$, L_a+4.5	$-L_a$+4.5, L_a+4.5	$-L_a$+2.25, L_a+2.25	225°	315°	3.18
11	$-L_a$+4.5, L_a+4.5	-5.75, 14.75				
12a	-5.75, 14.75	0, 12.37	0, 20.5	135°	90°	8.13
12b	0, 12.37	5.75, 14.75	0, 20.5	90°	45°	8.13
13	5.75, 14.75	L_b-4.5, L_b+4.5				
14a	L_b-4.5, L_b+4.5	L_b, L_b+4.5	L_b+2.25, L_b+2.25	225°	315°	3.18
14b	L_b, L_b+4.5	L_b, L_b	L_b+2.25, L_b+2.25	-45°	45°	3.18
15	L_b, L_b	10.25, 10.25				
16a	10.25, 10.25	9.5, 6	14.5, 6	225	180	6
16b	9.5, 6	14.5, 0	14.5, 6	180	90	6
16c	14.5, 0	15, 0				

Appendix C: IMUDTCS2 Schematic

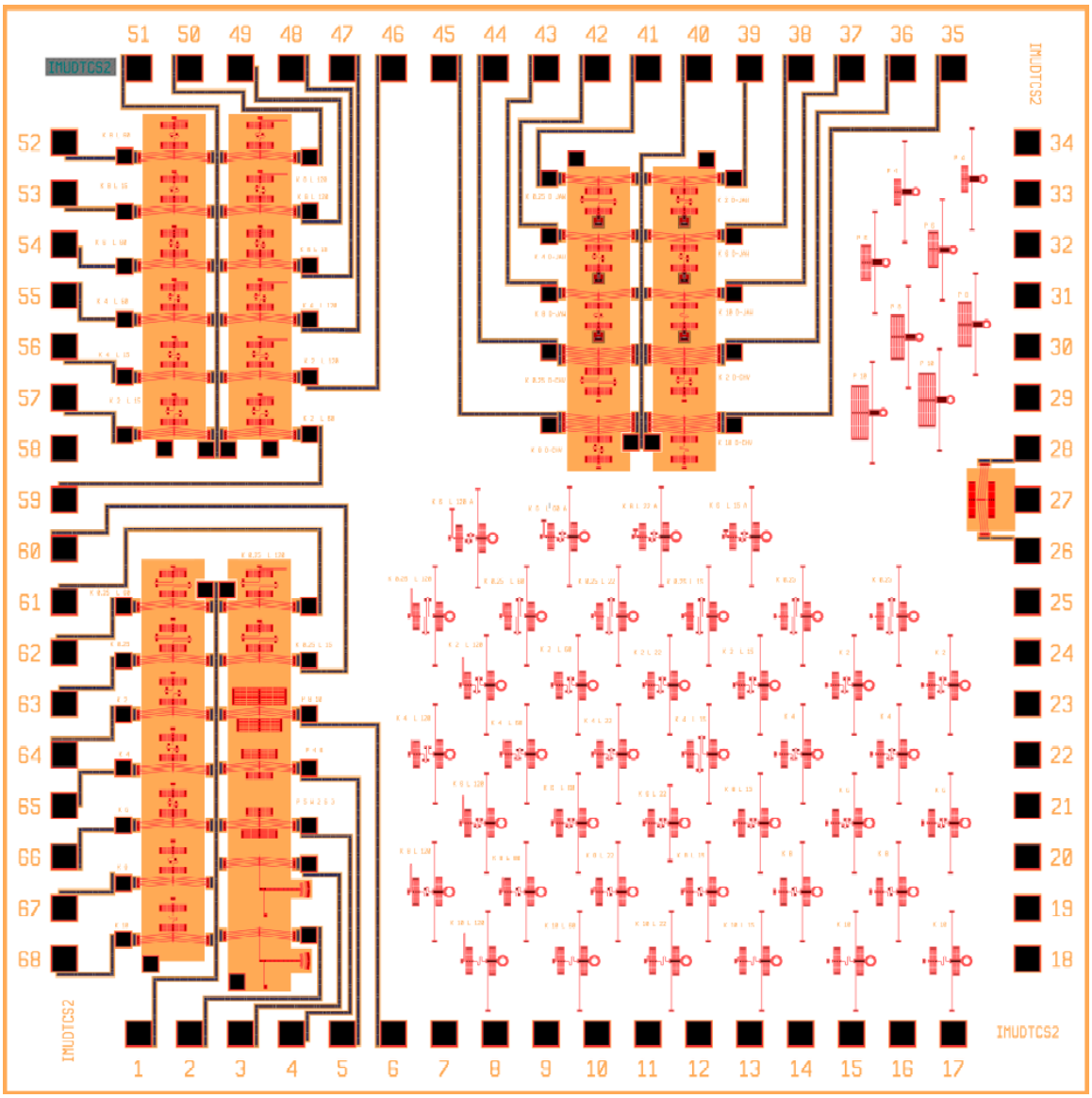

Appendix D: IMUDTCS2 Summary

P = pitch of comb (μm) K= Spring stiffness (μN/μm) L= length of 'U=spring' (μm)							
Chevron Driven				Probe Driven			
Yamahata	Pseudo Cell		Test Cell	Yamahata	Pseudo Cell		Test Cell
(2X) P=8, P=10	K=4.1 P=2	L=15 L=60 L=120	K=4.1 P=2	(2X) P=4	K=4.1 P=2	L=15 L=22 L=60 L=120	(6X) K=4.1 P=2
(2X) P=4, P=6	K=40 P=2	L=15 L=60 L=120	K=40 P=2	(2X) P=6	K=40 P=2	L=15 L=22 L=60 L=120	(6X) K=40 P=2
Rotational	K=91 P=2	L=15 L=60 L=120	K=91 P=2	(2X) P=8	K=91 P=2	L=15 L=22 L=60 L=120	(6X) K=91 P=2
	K=140 P=2	L=15 L=60 L=120	K=140 P=2	(2X) P=10	K=140 P=2	L=15 L=22 L=60 L=120	(6X) K=140 P=2
	K=154 P=2	L=15 L=60 L=120	K=154 P=2		K=154 P=2	L=15 L=22 L=60 L=120	(6X) K=154 P=2
			K=175 P=2		K=175 P=2	L=15 L=22 L=60 L=120	(6X) K=175 P=2

Appendix E: IMUDTCS4 Schematic

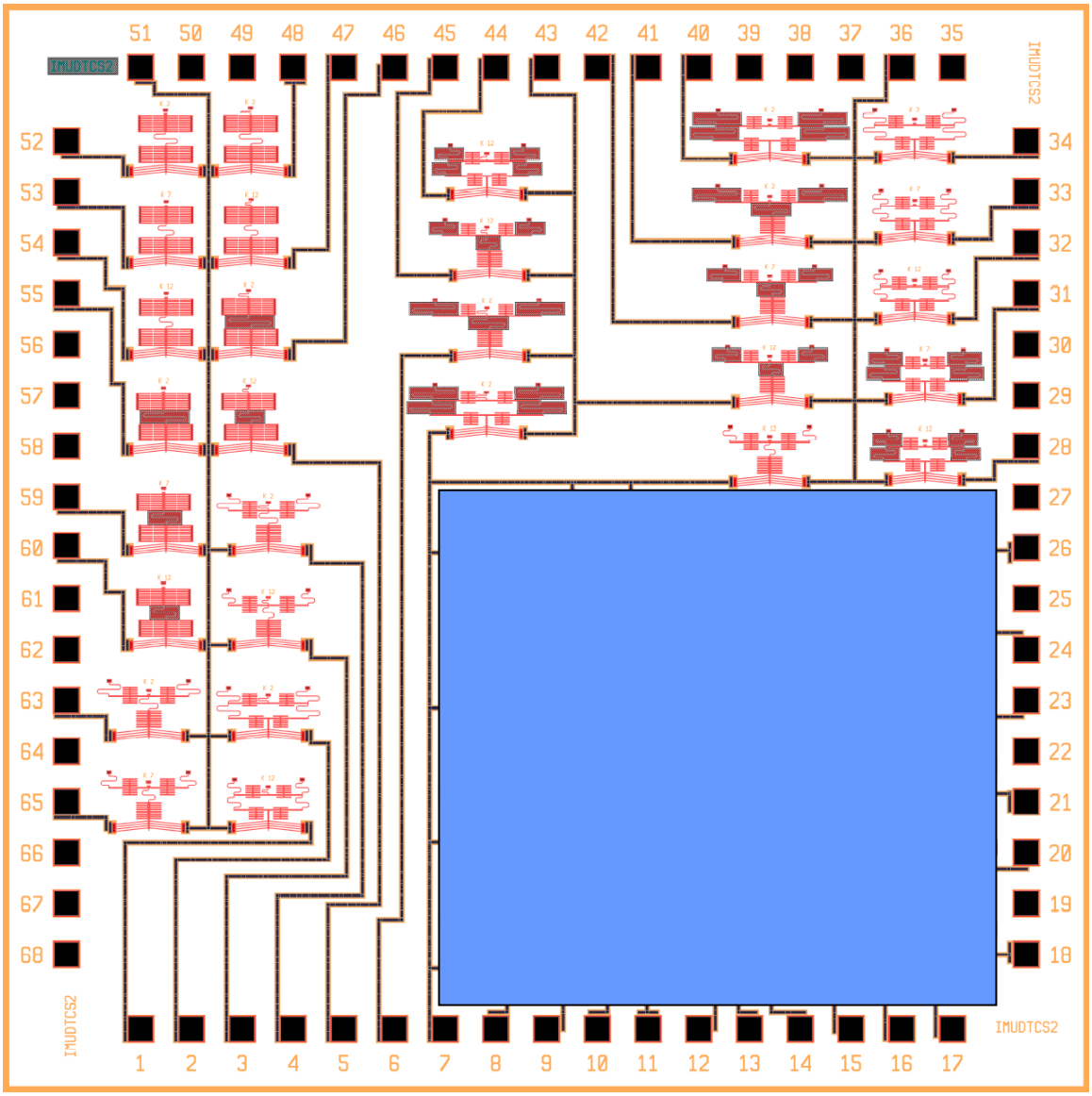

Appendix F: IMUDTCS4 Summary

Design		Stiffness (μN/μm)	Stiffness (μN/μm)	Stiffness (μN/μm)
		2.0	7.0	12.0
A	P1	44	134	203
	P1-P2	8.1	27	46
B	P1 k1	44	134	203
	k2	82	203	294
	P1-P2 k1	8.1	27	46
	k2	15.4	51.3	83.4
C	P1	44	134	203
	P1-P2	8.1	27	46

Appendix G: IMUDTCS4 Test Report

X	Not working														
✓	Working	Chip #													
B	Broken	1	2	3	4	5	6	7	8	9	10	11	12	13	14	15
Working Devices (%)		34	30	2	43	38	15	23	32	45	45	53	51	30	15	26
A	P1NCK2	X	X	X	✓	X	X	X	X	X	X	X	✓	X	X	B
	P1NCK7	X	X	X	X	X	X	X	X	X	X	X	X	X	X	B
	P1NCK12	X	X	X	X	X	X	X	X	X	X	X	X	X	B	B
	P1CK2	X	X	X	X	X	X	X	X	X	X	X	✓	X	X	B
	P1CK12	X	X	X	X	X	X	X	X	✓	X	X	✓	✓	✓	B
	P1P2NCK2	X	✓	X	X	X	X	X	X	✓	X	X	X	X	B	B
	P1P2NCK7	X	✓	X	X	X	X	X	✓	✓	✓	X	X	X	B	✓
	P1P2NCK12	X	✓	X	X	X	X	X	✓	✓	✓	✓	X	X	B	✓
	P1P2CK2	X	✓	X	X	X	X	X	✓	✓	✓		X	X	B	B
	P1P2CK12	X	✓	X	X	X	✓	X	✓	✓	✓	✓	X	✓	B	✓
B	P1NCK2	X	X	X	X	X	B	X	X	X	X	✓	X	X	B	X
	P1NCK7	X	X	X	X	X	B	X	X	X	X	X	X	X	B	X
	P1NCK12	X	✓	X	X	X	X	X	X	X	X	X	X	X	X	X
	P1CK2	B	X	X	X	X	X	X	X	X	X	✓	X	X	B	X
	P1CK12	X	X	X	✓	X	✓	X	X	✓	X	✓	X	X	B	X
	P1P2NCK2	X	✓	X	✓	X	X	X	X	✓	✓	✓	✓	X	✓	X
	P1P2NCK7	✓	✓	X	✓	✓	X	X	X	✓	✓	✓	X	X	✓	✓
	P1P2NCK12	✓	✓	X	✓	✓	X	X	X	✓	✓	✓	✓	X	✓	✓
	P1P2CK2	✓	✓	X	X	✓	X	X	X	✓	✓	✓	✓	X	✓	✓
	P1P2CK12	✓	✓	X	✓	✓	X	X	X	✓	✓	✓	✓	✓	✓	✓
C	P1NCK2	X	X	X	X	X	X	X	X	X	X	X	X	X	X	B
	P1NCK7	X	X	X	X	X	X	X	X	X	X	X	X	X	X	X
	P1NCK12	X	X	X	X	X	X	X	X	X	X	X	X	X	X	X
	P1CK2	X	X	X	✓	X	B	X	X	X	X	✓	X	X	X	X
	P1CK12	X	X	X	X	X	B	X	X	X	X	X	X	X	X	X
	P1P2NCK2	X	X	X	X	X	X	X	X	X	X	X	X	X	X	X
	P1P2NCK7	X	X	X	X	X	X	X	X	X	X	X	X	X	X	X
	P1P2NCK12	X	X	X	X	X	X	X	X	X	X	X	✓	X	X	X
	P1P2CK2	X	X	X	X	X	B	X	X	X	X	X	X	X	X	X
	P1P2CK12	X	X	X	X	X	X	X	X	X	X	X	X	X	X	B

Appendix H: Residual Stress Hypothesis

1] Theory: Preload from fabrication in the springs

Consider:

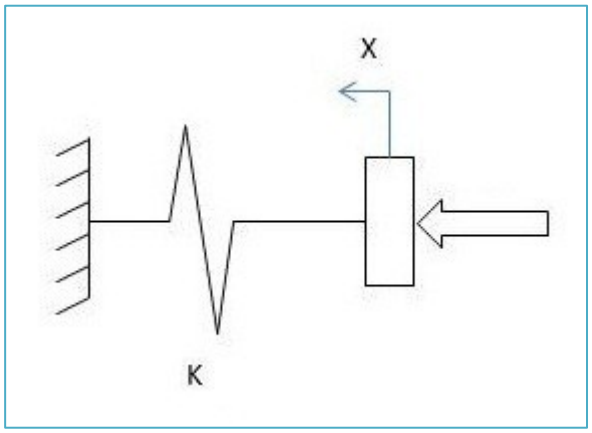

A spring 'K' with some existing compression of 'x'

A] Compress the spring an additional 'x'

Actual

$$k_{act} = \frac{F}{(x+x)} = \frac{F}{2x}$$

Measured

$$k_{meas} = \frac{F}{(x)}$$

Stiffness measured is twice the actual design stiffness. This is an error of 100%.

B] Compress the spring an additional 10 'x'

Actual

$$k_{act} = \frac{F}{(x+10x)} = \frac{F}{11}$$

Measured

$$k_{meas} = \frac{F}{(10x)}$$

Stiffness measured is 1.1 times the actual design. In this case, because the displacement is much larger than the preload compression, the error is lower; 10%.

Application to Experimental Results:

A] Pseudo cells

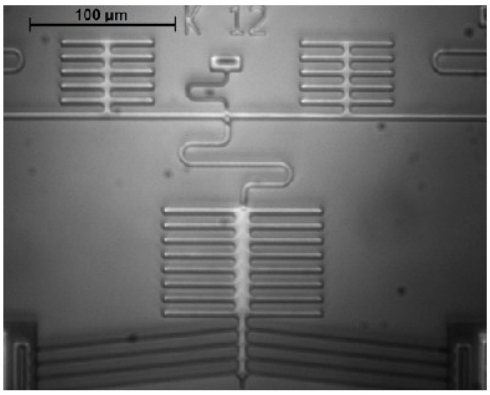

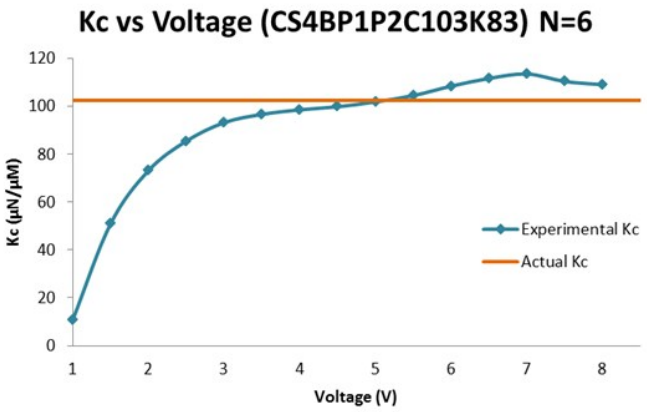

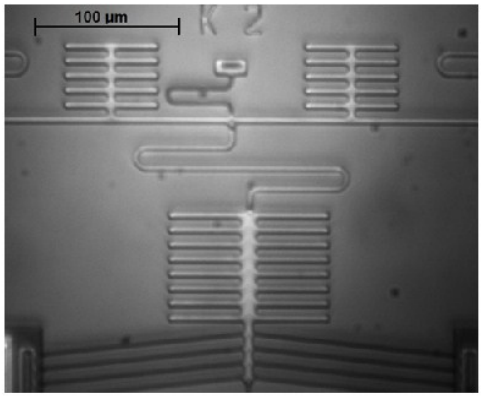

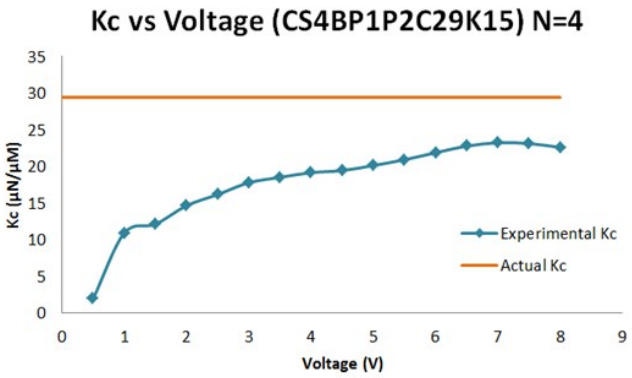

The springs in the designs implemented with pseudo cells (U-springs) appear to have been under existing extension loads. This would cause the initial measurements of cell stiffness to be less than the actual stiffness.

B] Cell Testing

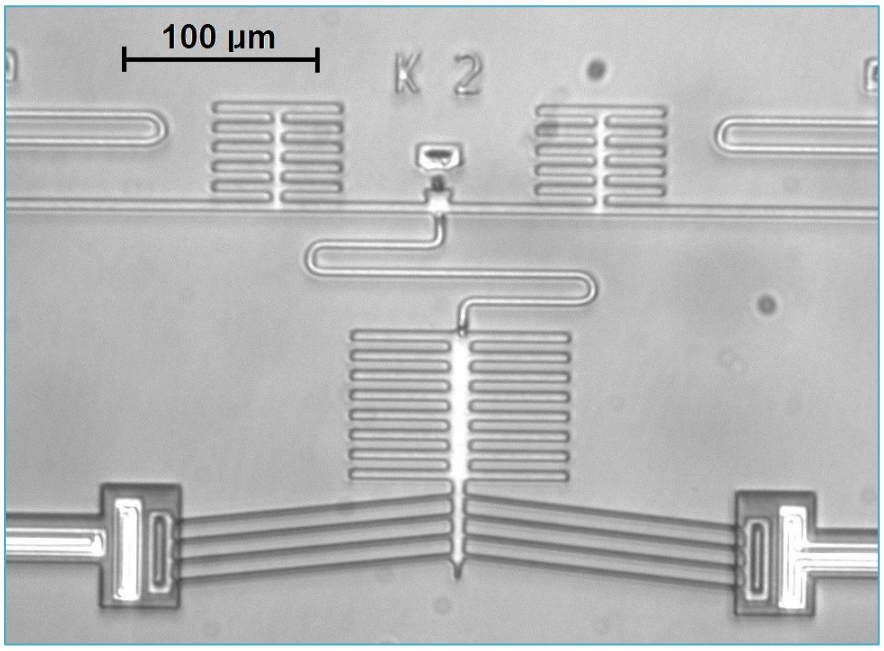

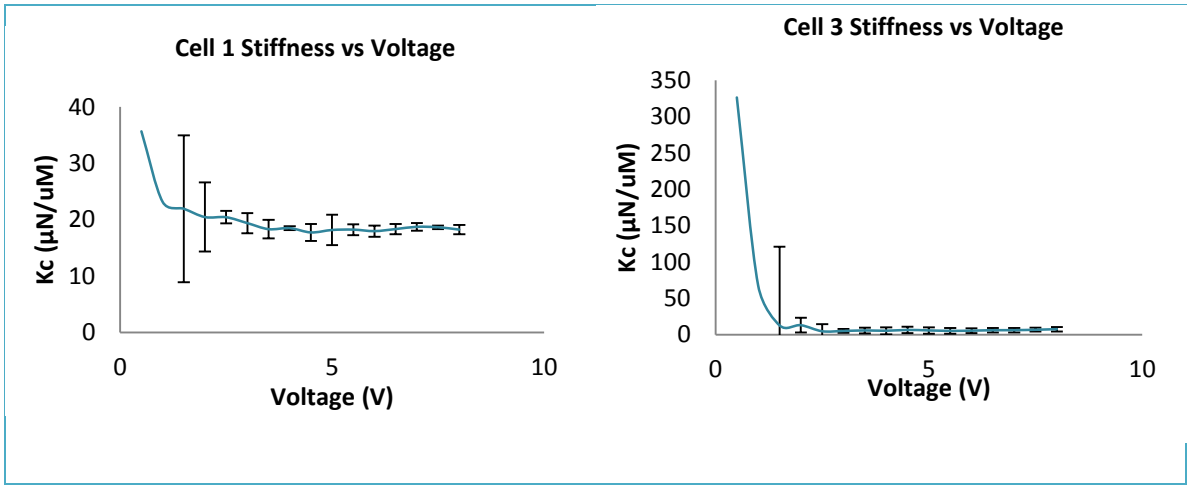

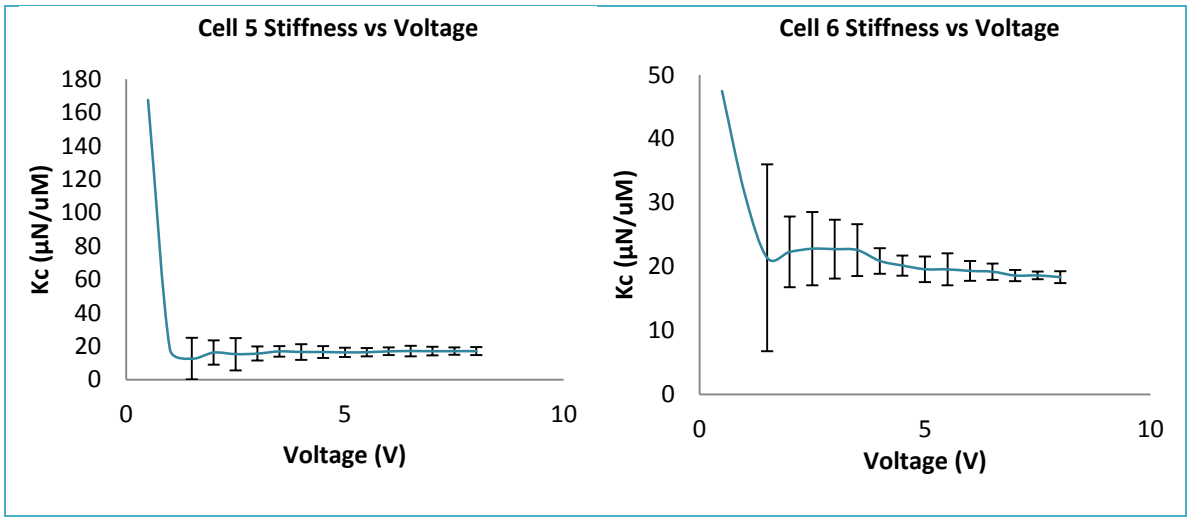

The results of cell testing indicate that the springs in the cell testing devices were under some initial compression, inflating initial measured values for cell stiffness.

The final step in the MEMS fabrication process is a baking cycle which is implemented to reduce any residual stresses present, but it is not 100% effective.

The case for Cell 1 reached a steady value for cell stiffness at 2.5 volts, a displacement of 0.188 µm. At this point the preload was overcome. The final cell displacement was 1.447 µm. The final measured value for cell stiffness would therefore be approximately12% greater than the actual stiffness.

Appendix I: Copyright Permissions for Image from Sinauer [13]

SINAUER ASSOCIATES, Inc. • Publishers • P.O. Box 407 • Sunderland, MA 01375-0407

Telephone: (413) 549-4300
Fax: (413) 549-1118
E-mail: orders@sinauer.com

PERMISSIONS AGREEMENT

October 31, 2012

Permission granted to:
Rachael Schwartz
30 Tremont Street
Dartmouth, NS
CANADA B2Y 1X3

FAX: 902-423-6711

Material to be reproduced:
Purves et al: *Life: The Science of Biology, Sixth Edition*
Figure 4.7 (enlarged line drawing of an animal cell), page 60

To be reproduced in the work:
Rachael Schwartz's Master's Thesis entitled "Development of a MEMS Device for the Determination of Cell Mechanics" to be published by Dalhousie University

Sinauer Associates owns copyright to the material described above and hereby grants permission for the one-time use of the material as specified, and for nonexclusive world rights provided that full and appropriate credit is given to the original source and that the work is for NON-COMMERCIAL use only. Please request permission for further use in subsequent editions, translations, or revisions of the work.

[redacted]

October 31, 2012
Date

Sherri L. Ellsworth
Permissions Coordinator

Please acknowledge your acceptance of these terms by signing one copy of this form and returning it to Sinauer Associates. Permission Agreement is not valid until signed by applicant and received by Sinauer Associates.

[redacted]

NOVEMBER 5, 2012
Date

Signature of Applicant

Received Time Nov. 2. 2012 4:50PM No. 1221

Appendix J: Copyright Permissions for Images from Loh et al [5]

SPRINGER LICENSE
TERMS AND CONDITIONS

Oct 30, 2012

This is a License Agreement between Rachael Schwartz ("You") and Springer ("Springer") provided by Copyright Clearance Center ("CCC"). The license consists of your order details, the terms and conditions provided by Springer, and the payment terms and conditions.

All payments must be made in full to CCC. For payment instructions, please see information listed at the bottom of this form.

License Number	3018320022789
License date	Oct 29, 2012
Licensed content publisher	Springer
Licensed content publication	Experimental Mechanics
Licensed content title	The Potential of MEMS for Advancing Experiments and Modeling in Cell Mechanics
Licensed content author	O. Loh
Licensed content date	Feb 1, 2009
Volume number	49
Issue number	1
Type of Use	Thesis/Dissertation
Portion	Figures
Author of this Springer article	No
Order reference number	
Title of your thesis / dissertation	The potential of MEMS for Advancing Experiments and Modeling in Cell Mechanics
Expected completion date	Dec 2012
Estimated size(pages)	150
Total	0.00 CAD
Terms and Conditions	

Introduction

The publisher for this copyrighted material is Springer Science + Business Media. By clicking "accept" in connection with completing this licensing transaction, you agree that the following terms and conditions apply to this transaction (along with the Billing and Payment terms and conditions established by Copyright Clearance Center, Inc. ("CCC"), at the time that you opened your Rightslink account and that are available at any time at http://myaccount.copyright.com).

Example 1: Springer Science + Business Media makes no representations or warranties with respect to the licensed material.

Example 2: Springer Science + Business Media makes no representations or warranties with respect to the licensed material and adopts on its own behalf the limitations and disclaimers established by CCC on its behalf in its Billing and Payment terms and conditions for this licensing transaction.

Indemnity
You hereby indemnify and agree to hold harmless Springer Science + Business Media and CCC, and their respective officers, directors, employees and agents, from and against any and all claims arising out of your use of the licensed material other than as specifically authorized pursuant to this license.

No Transfer of License
This license is personal to you and may not be sublicensed, assigned, or transferred by you to any other person without Springer Science + Business Media's written permission.

No Amendment Except in Writing
This license may not be amended except in a writing signed by both parties (or, in the case of Springer Science + Business Media, by CCC on Springer Science + Business Media's behalf).

Objection to Contrary Terms
Springer Science + Business Media hereby objects to any terms contained in any purchase order, acknowledgment, check endorsement or other writing prepared by you, which terms are inconsistent with these terms and conditions or CCC's Billing and Payment terms and conditions. These terms and conditions, together with CCC's Billing and Payment terms and conditions (which are incorporated herein), comprise the entire agreement between you and Springer Science + Business Media (and CCC) concerning this licensing transaction. In the event of any conflict between your obligations established by these terms and conditions and those established by CCC's Billing and Payment terms and conditions, these terms and conditions shall control.

Jurisdiction
All disputes that may arise in connection with this present License, or the breach thereof, shall be settled exclusively by arbitration, to be held in The Netherlands, in accordance with Dutch law, and to be conducted under the Rules of the 'Netherlands Arbitrage Instituut' (Netherlands Institute of Arbitration).***OR:***

All disputes that may arise in connection with this present License, or the breach thereof, shall be settled exclusively by arbitration, to be held in the Federal Republic of Germany, in accordance with German law.

Other terms and conditions:

v1.3

If you would like to pay for this license now, please remit this license along with your payment made payable to "COPYRIGHT CLEARANCE CENTER" otherwise you will be invoiced within 48 hours of the license date. Payment should be in the form of a check or money order referencing your account number and this invoice number RLNK500886353. Once you receive your invoice for this order, you may pay your invoice by credit card. Please follow instructions provided at that time.

Make Payment To:
Copyright Clearance Center
Dept 001
P.O. Box 843006
Boston, MA 02284-3006

For suggestions or comments regarding this order, contact RightsLink Customer Support: customercare@copyright.com or +1-877-622-5543 (toll free in the US) or +1-978-646-2777.

Gratis licenses (referencing $0 in the Total field) are free. Please retain this printable license for your reference. No payment is required.

Appendix K: Copyright Permissions for Images from Maksym et al [23]

References

[1] D.-H. Kim, P. K. Wong, J. Park, A. Levchenko and Y. Sun, "Microengineered Platforms for Cell Microbiology," *Annu. Rev. Biomed. Eng. Vol. 11,* pp. 203-233, 2009.

[2] C. Yamahata, E. Sarajlic, G. J. M. Krijnen and M. A. M. Gijs, "Subnanometer Translation of Microelectromechanical Systems Measured by Discrerte Fourier Analysis of CCD Images," *Journal of Microelectromechanical Systems, Vol. 19, No. 4,* pp. 1273-1275, 2010.

[3] J. G. Korvink and O. Paul, MEMS: a practical guide to design, analysis, and applications, Norwich, NY: William Andrew, Inc., 2006.

[4] J. Carter, A. Cowen, B. Hardy, R. Mahadevan, M. Stonefield and S. Wilcenski, "PolyMUMPs Design Handbook: a Mumps (R) process. Revision 11.0," MEMSCAP Inc., 2005.

[5] O. Loh, A. Vaziri and H. Esponosa, "The potential of MEMS for Advancing Experiments and Modeling in Cell Mechanics," *Experimental Mechanics Vol. 49,* pp. 105-124, 2009.

[6] N. Ellerington, "Macro Friction, Micro Friction and Stiction," Department of Mechanical Engineering, Dalhousie University, Halifax, 2009.

[7] Y. H. Anis, M. R. Holl and D. R. Meldreun, "Automated Selection and Placement of Single Cells Using Vision-Based Feedback Control," *IEEE Trransactions of Automated Science and Engineering, Vol. 7 No. 3,* pp. 598-606, 2010.

[8] Z. Lu, C. Moraes, G. Ye, C. A. Simmons and Y. Sun, "Single Cell Deposition and Patterning with a Robotic System," *PLos ONE 5 (10),* 2010.

[9] D. Sameoto, "Operation and Characterization of MUMPSs Produced Microactuators in a Water Environment," Dalhousie University, Halifax, 2004.

[10] R. Langlois, Interviewee, *Post Doc Researcher Dalhousie Oceanography.* [Interview]. 10 October 2012.

[11] C. Moraes, C. A. Simmons and Y. Sun, "Cell Mechanics Meets MEMS," *CSME Bulletin SCGM,* pp. 15-18, 2006.

[12] K. L. Billiar, "The Mechanical Environment of Cells in Collagen Gel Models: Global and local effecrs in three-dimensional biological hydrogels," *Stud Mechanobiol Tissue Eng Biomater Vol. 4,* pp. 201-245, 2011.

[13] I. Sinauer Associates, Artist, *Animal Cell.* [Art]. 2001.

[14] Wikimedia, "Fluorescent Cell," 2004.

[15] G. M. Walker, Yeast Physiology and Biotechnology, West Sussex: John Wiley & Sons Ltd., 1998.

[16] B. P. Curran and V. Bugeja, "Basic Investigations in Saccharomyces," in *Yeast Protocols: Methods in Molecular Biology*, Totowa, NJ, Humana Press, 2006, pp. 1-13.

[17] G. D. Najafpour, Biochemical Engineering and Biotechnology, Amsterdam: Elsevier B.V., 2007.

[18] T. Fukuda, M. Nakajima and M. R. Ahmad, "Nanorobotic Manipulation for a Single Biological Cell," in *Bioloigically Inspired Robotics*, CRC Press 2011, 2011, pp. 165-188.

[19] A. E. Smith, Z. Zhang, C. R. Thomas, K. E. Moxham and A. P. J. Middelberg, "The mechanical properties of Saccharomyces cerevisiae," *Proceedings of the National Academy of Sciences of the United States of America. Vol. 97, No. 18,* pp. 9871-9874, 2009.

[20] A. Touhami, B. Nysten and Y. F. Dufrene, "Nanoscale Mapping of the Elasticity of Microbial Cells by Atomic Force Microscopy," *Langmuir LangmuirLangmuir 19,* pp. 4539-4543, 2003.

[21] J. Arfsten, S. Leupold, C. Bradtmöller, I. Kampen and A. Kwade, "Atomic force microscopy studies on the nanomechanical properties of Saccharomyces cerevisiae," *Colloids and Surfaces B: Biointerfaces V79,* pp. 284-290, 2010.

[22] D. Vella, A. Ajdari, A. Vaziri and A. Boudaoud, "The indentation of pressurized elastic sheels: from polymeric capsules to yeast cells," *Journal of the Royal Society Interface,* pp. 1-8, 2011.

[23] M. A, T. G and W. Reichert, "Atomic force and total internal reflection fluoresence microscopy for the study of force transmission in endothelial cells.," *Biophys,* vol. 78, pp. 1725-1735, 2000.

[24] B. G. S. S. Van Vliet KJ, "The biomechanics toolbox: experimental approaches for living cells and biomolecules.," *Acta Mater,* vol. 51, pp. 5881-5905, 2003.

[25] H. RM, "Micropipette aspiration of living cells.," *J. Biomech,* vol. 33, pp. 15-22, 2000.

[26] S. Suresh, J. Spatz, M. A. D. M. Millls J, C. Lim, M. Beil and T. Seufferlein, "Connections between single-cell biomechanics and human disease states: gastrointestinal cancer and malaria," *Acta Biomaterialia,* vol. 1, pp. 15-30, 2005.

[27] M. Nollman, B. Z. Stone M, J. Gore, C. N, H. S. C, S. Mitelheiser, A. Maxwell, C. Bustamante and N. Cozzarelli, "Multiple modes of Escherichia coli DNA gyrase activity revealed by force and torque.," *Nature Structural and Molecular Biology,* vol. 14, pp. 264-271, 2007.

[28] G. N. Maksym, B. Fabry, J. P. Butler, D. Navajas, D. J. Tschumperlin, J. D. Laporte and J. J. Fredberg, "Mechanical properties of cultured human airway smooth muscle cells from 0.05 to 0.4 Hz," *J App lPhysiol,* p. 89:1619–1632, 2000.

[29] H. Mashmoushy, Z. Zhang and C. R. Thomas, "Micromanipulation measurements of the mechanical properties of baker's yeast cells," *Biotechnology Techniques. Vol. 12 No. 12,* pp. 925-929, 1998.

[30] J. C. Crocker, "Multiple Particle Tracking and Two-Point Microrheology in Cells," University of Pennsylvania ScholarlyCommons, 2007.

[31] Y. Zhao and X. Zhang, "Cellular mechanics study in cardiac myacytes using PDMS pillars array.," *Sens. Actuators,* vol. 125, no. A, pp. 398-404, 2006.

[32] B. Shay, "Cell Crushing Report," Dalhousie University, Mechanical Engineering Department, Halifax, Nova Scotia, 2007.

[33] J. Fraser, "Design, Fabrication and Characterization of Off-Chip Microgrippers," Dalhousie University, Mechanical Engineering, Halifax, Nova Scotia, 2006.

[34] R. Hickey, S. D. Kujath, Marek, T. Hubbard and M. Kujath, "Time and frequency respone of two-arm micromachine thermal actuators," *Journqal of Micromachines and Microengineering,* vol. 13, pp. 40-46, 2003.

[35] E. Rawashdeh, A. Karam and I. G. Fould, "Characterization of Kink Actuators as Compared to Traditional Chevron Shaped Bent-Beam Electrothermal Actuators," *Micromachines,* vol. 3, pp. 543-549, 2012.

[36] J. L. Luo, A. J. Flewitt, S. M. Spearing, N. A. Fleck and W. I. Milne, "Modeling of Microspring Thermal Actoator," *Dept. of Aeronautics & Astronautics. MIT. NSTI-Nanotech. Vol 1.,* 2004.

[37] B. Bschaden, Interviewee, *Personal Communication, Yamahata Technique.* [Interview]. 23 October 2012.

[38] C. Arthur, "MEMS Earthworm: The Design and Testing of a Bio-inspired High Precision, High Speed, Long Range Peristaltic Micro-Motor," Dalhousie University, Halifax, Nova Scotia, 2010.

[39] A. E. Pelling, S. Sehati, E. B. Gralla, J. S. Valentine and J. K. Gimzewsk, "Local Nanomechanical Motion of the Cell Wall of Saccharomyces cerevisiae," *Science V 305,* pp. 1147-1150, 2004.

[40] T. S. Lanero, O. Cavalleri and S. Krol, "Mechanical properties of single living cells encapsulated in polyelectrolyte matrixes," *Journal of Biotechnology,* 2006.

[41] M. R. Ahmad, M. Nakajima, S. Kojima, M. Homma and T. Fukuda, "In Situ Single Cell Mechanics Characterization of Yeast Cells Using Nanoneedles Inside Environmental SEM," *IEEE Transactions of Nanotechnology, Vol. 7, No. 5,* pp. 607-616, 2008.

[42] J. Schaber, M. A. Adrver, E. Eriksson, S. Pelet, E. Petelenz-Kurdziel, D. Klein, F. Posas, M. Goksor, M. Peter, S. Hohmann and E. Klipp, "Biophysical properties of Saccharomyces cerevisiae and their relationship with HOG pathway activation," *Eur Biophy,* vol. 39, pp. 1547-1556, 2010.

[43] Y. Lai, M. Kujath and T. Hubbard, "Modal Simulation and Testing of a Micro-Manipulator," *Journal of Dynamics Systems, Measurement and Control,* pp. 515-519, 2005.

[44] H. M. Fettig, "Design, Simulation and Testing of Micromachined Flexible Joints," Dalhousie University, Halifax, 2001.

[45] A. E. Smith, Z. Zhang and C. R. Thomas, "Wall material properties of yeast cells: Part 1. Cell measurements," *Chemical Engineering Science Vol.55,* pp. 2031-2041, 2000.

[46] A. J. Bibhendi and R. k. Korhonen, "A Finite Element Study of Micropipette Aspiration of Single Cells: Effect of Compressibility," *Computational and Mathematical Methods in Medicine,* p. ID 192618, 2012.

[47] E. Lau, S. Al-Dujaili, A. Guenther, D. Lui, L. Wang and L. You, "Effect of low-magnitude, high-frequency vibration on osteocytes in the regulation of osteoclasts," *Bone 46,* pp. 1508-1515, 2010.

[48] S. M. Tanaka, J. Li, R. L. Duncan, H. Yokota, D. B. Burr and C. H. Turner, "Effects of broad frequency vibration on cultured osteoblasts," *Journal of Biomechanics 36,* pp. 73-80, 2003.

[49] D. Pre, G. Ceccarelli, G. Gastaldi, A. Asti, E. Saino, L. Visai, F. Benazzo, M. Cusella De Angelis and G. Magenes, "The differentiation of human adipose-derived stem cells (hASCs) into osteoblasts promoted by low amplitude, high frequency vibration treatment," *Bone 49,* pp. 295-303, 2011.

[50] S. Warnat, Interviewee, *IMUDTSSY Design. Funded by the German Reserach Foundation. WA2982/2-1.* [Interview]. September 2012.

[51] D. Fologea, T. Vassu-Dimov, I. Stica, O. Csutak and M. Radu, "Increase of Sacchamoryces cerevisiae plating efficiency after treatment with bipolar eletric pulses," *Bioelectrochem. Bioenerg. Vol 46,* pp. 285-287, 1998.